TECHNISCHE UNIVERSITÄT WIEN

DIPLOMARBEIT

Algorithms for the Steady State Solution of Non-Linear Piezoelectric Systems

ausgeführt zum Zwecke der Erlangung
des akademischen Grades eines Diplom-Ingenieurs
unter der Leitung von

Univ.Ass. Dipl.-Ing. Dr.techn. Florian Toth
Univ.-Prof. Dipl.-Ing. Dr.techn. Manfred Kaltenbacher
Institut für Mechanik und Mechatronik, E325-A3

im Auftrag von und in Kooperation mit
USound GmbH

eingereicht an der Technischen Universität Wien
Fakultät für Maschinenwesen und Betriebswissenschaften
von

Alexander Papst
01228901
Sollgrabenstraße 103
2831 Warth

Wien, am 9. December 2020

Die approbierte gedruckte Originalversion dieser Diplomarbeit ist an der TU Wien Bibliothek verfügbar.
The approved original version of this thesis is available in print at TU Wien Bibliothek.
TU Bibliothek Your knowledge hub

Die approbierte gedruckte Originalversion dieser Diplomarbeit ist an der TU Wien Bibliothek verfügbar.
The approved original version of this thesis is available in print at TU Wien Bibliothek.

Ich nehme zur Kenntnis, dass ich zur Drucklegung dieser Arbeit nur mit Bewilligung der Prüfungskommission berechtigt bin.

Eidesstattliche Erklärung

Ich erkläre an Eides statt, dass die vorliegende Arbeit nach den anerkannten Grundsätzen für wissenschaftliche Abhandlungen von mir selbstständig erstellt wurde. Alle verwendeten Hilfsmittel, insbesondere die zugrunde gelegte Literatur, sind in dieser Arbeit genannt und aufgelistet. Die aus den Quellen wörtlich entnommenen Stellen, sind als solche kenntlich gemacht. Das Thema dieser Arbeit wurde von mir bisher weder im In- noch Ausland einer Beurteilerin/einem Beurteiler zur Begutachtung in irgendeiner Form als Prüfungsarbeit vorgelegt. Diese Arbeit stimmt mit der von den Begutachterinnen/Begutachtern beurteilten Arbeit überein.

Stadt und Datum Unterschrift

Die approbierte gedruckte Originalversion dieser Diplomarbeit ist an der TU Wien Bibliothek verfügbar.
The approved original version of this thesis is available in print at TU Wien Bibliothek.
TU Bibliothek Your knowledge hub WIEN

Contents

Table of contents **I**

Abstract **III**

Kurzfassung **IV**

1 Introduction **1**

2 Piezoelectric ceramics **3**

2.1 Polarization mechanism 4

2.2 Ferroelectricity and ferroelasticity 7

2.3 Observed behavior of piezoceramics 8

2.3.1 Electric loading 9

2.3.2 Mechanical loading 11

2.3.3 Mixed loading 13

3 Hysteresis models **17**

3.1 Ferroelectric hysteresis 17

3.2 Ferroelastic hysteresis 20

4 Piezoelectric-mechanical system **23**

4.1 Linear piezoelectric-mechanic coupled system 23

4.2 One dimensional piezoelectric coupled system 24

4.3 Nonlinear constitutive laws 28

5 Solution strategy **31**

5.1 Used methods 31

5.1.1 Multiharmonic ansatz 31

5.1.2 Harmonic balancing 34

5.1.3 Notation explanation 36

5.2 r-Approach (algorithm 1) 37

5.3 E-S-Approach (algorithm 2) 40

5.4 χ-Approach (algorithm 3) 42

Die approbierte gedruckte Originalversion dieser Diplomarbeit ist an der TU Wien Bibliothek verfügbar.
The approved original version of this thesis is available in print at TU Wien Bibliothek.
TU Bibliothek Your knowledge hub WIEN

6 Results and discussion **47**
6.1 Ferroelectric hysteresis . . . 47
6.1.1 Bipolar voltage excitation . . . 47
6.1.2 Bipolar increasing voltage excitation . . . 48
6.1.3 Unipolar increasing voltage excitation . . . 49
6.2 Ferroelastic hysteresis . . . 50
6.3 Physical behavior of the coupled system . . . 51
6.3.1 General behavior . . . 52
6.3.2 Bipolar charge excitation . . . 54
6.3.3 Unipolar charge excitation . . . 56
6.3.4 Constant charge excitation . . . 57
6.3.5 Showcases of the E-S-approach and χ-approach . . . 60
6.4 Comparison of the physical behavior of all three approaches . . . 61
6.4.1 Used Showcase . . . 61
6.4.2 Comparision . . . 62
6.5 Performance of the approaches . . . 65
6.6 Influence of considered harmonics . . . 67

7 Summary **71**

Bibliography **V**

List of figures **VII**

A Appendix **XI**
A.1 Parameters for simulation . . . XI
A.2 Addition physical behavior plots . . . XIII
A.2.1 Physical behavior of the r-approach . . . XIII
A.2.2 Physical behavior of the E-S-approach . . . XVII
A.2.3 Physical behavior of the χ-approach . . . XX
A.3 Reference case . . . XXIII
A.4 Comparison for various cases . . . XXIV

Die approbierte gedruckte Originalversion dieser Diplomarbeit ist an der TU Wien Bibliothek verfügbar.
The approved original version of this thesis is available in print at TU Wien Bibliothek.
TU WIEN Bibliothek Your knowledge hub

Abstract

Piezoelectric materials have a wide range of applications and are used in actuators as well as in sensors. The materials have a non-linear material behavior, which are often modeled linearly. The range of applicability for linear models is limited due to the actual nonlinear behavior of the material. The goal of this thesis is to develop an algorithm that can find the steady state solution of a nonlinear one dimensional piezoelectric system.

The nonlinear behavior of piezoelectric ceramics is described by highlighting important results from literature review and various polarisation mechanisms are presented. The interaction between the polarization and the electric field results in a typical hysteresis. For modeling the polarization hysteresis the domain wall model is used, which is based on the Jiles-Artherton model for magnetization.

Starting from the linear three dimensional constitutive equations, suitable assumptions are made to derive the one dimensional piezoelectric system. The one dimensional system gets extended with the nonlinear polarization behavior using the domain wall model.

With the use of the multiharmonic approach and the harmonic balance method, the system is solved for quasi-static steady state solutions. The nonlinear polarization is evaluated in the time domain and transformed into the frequency domain, where the system is solved via fix point iteration. Three different fix point iterations (r-approach, E-S-approach and χ-approach) are introduced.

With the help of these approaches, the system gets solved for various load cases and the results are compared. The E-S-approach does not converge for every case and the χ-approach is slow and not very accurate compared to the r-approach. The best results are obtained with the r-approach. This approach is very robust and is the only approach that handles bipolar loading cases well. Furthermore the r-approach converges to the correct solution even when considering only a few harmonics. With a larger number of considered harmonics the solution can be approximated more accurately, at the expense of greater numerical effort.

Die approbierte gedruckte Originalversion dieser Diplomarbeit ist an der TU Wien Bibliothek verfügbar.
The approved original version of this thesis is available in print at TU Wien Bibliothek.
TU Bibliothek WIEN Your knowledge hub

Kurzfassung

Piezoelektrische Materialien besitzen ein breites Anwendungsspektrum und werden in Aktoren sowie in Sensoren eingesetzt. Das Material zeigt ein starkes nichtlineares Verhalten, welches meist nur linearisiert angenähert wird. Das Ziel dieser Studie ist einen Algorithmus zu entwickeln, der ein eindimensionales piezoelektrisches System inklusive Nichtlinearitäten im eingeschwungenen Zustand lösen kann.

Das nichtlineare Verhalten von piezoelektrischen Materialien, im speziellen piezoelektrischen Keramiken, wird mithilfe von wichtigen Erkenntnissen aus der aktuellen Literatur erläutert und verschiedene Polarisationsmechanismen kurz dargestellt. Die Polarisation wird unter Verwendung der Domain-Wall-Theorie modelliert, das auf dem Jiles-Atherton-Model für die magnetische Hysterese basiert. Die Interaktion zwischen der Polarisation und dem elektrischen Feld resultiert in einer typischen Hysterese.

Ausgehend von dem dreidimensionalen linearen piezoelektrischen System wird ein eindimensionales System, unter passenden Annahmen, hergeleitet. Das eindimensionale System wird mithilfe des Domain-Wall-Model um das nichtlineare Polarisationsverhalten erweitert.

Durch den multiharmonischen Ansatz und Harmonic-Balance-Methode wird das System für eingeschwungene Zustände gelöst. Die nichtlineare Polarisation wird im Zeitbereich mit dem Domain-Wall-Model berechnet und anschließend in den Frequenzbereich transformiert. Im Frequenzbereich wird das System durch drei verschiedene Fixpunkt-Iterationen (r-Ansatz, E-S-Ansatz und χ-Ansatz) gelöst.

Mithilfe dieser Ansätze wird das eindimensionale System für verschiedene Lastfälle gelöst und die Resultate miteinander verglichen. Der E-S-Ansatz konvergiert nicht immer und der χ-Ansatz ist im Vergleich zu den anderen Ansätzen ungenau. Die besten Ergebnisse werden mit dem r-Ansatz erzielt. Dieser ist sehr robust und kann als einziger Algorithmus mit bipolaren Lastfällen umgehen. Zudem konvergiert der r-Ansatz auch mit wenigen Termen des multiharmonischen Ansatzes zur richtigen Lösung. Des weiteren wird mit einer höheren Anzahl an Termen wird die Lösung besser approximiert.

Die approbierte gedruckte Originalversion dieser Diplomarbeit ist an der TU Wien Bibliothek verfügbar.
The approved original version of this thesis is available in print at TU Wien Bibliothek.
TU Bibliothek WIEN Your knowledge hub

Chapter 1

Introduction

Piezoelectric devices are indispensable in many fields. The applications of piezoelectric sensors and actuators are wide, ranging from consumer products (smartphones, loudspeaker [1]) over medicine to process measurement technology. Piezoelectric materials allow an efficient conversion from mechanical energy to electric energy and vice versa [2]. One big challenge of piezoelectric materials lies in its strong nonlinear behavior, resulting in a hysteresis between electrical and mechanical field quantities (electric field and mechanical stress). If the material behavior is approximated only linearly, linear models reach the limits of their applicability fairly fast, which might lead to bad accuracy, making linear models unusable for certain applications [3].

The need for a better constitutive law occurs. The nonlinear interaction of the mechanical and electric field needs to be described more accurately. These interactions are quite complex and there are many different approaches to describe the hysteresis behavior [4] [5]. Piezoelectric models can be classified either according to the considered length scale or describing approach. Both classifications overlap each other. Micro-mechanical models describe the behavior of single grains or crystals, whereas macro-mechanical models are based on a macroscopic view. One can distinguish between a physical-based approach or a pure mathematical approach. The most prominent mathematical model for hysteresis is the Preisach-model [6] [5], but others, like the Prandtle-Ishlinskii model [7] or network-based models [8] are used to model the hysteresis with high accuracy too. These models describe the behavior without considering physical laws and are often thermodynamically inconsistent.

Physical models are thermodynamically consistent, but include some phenomenological considerations, connecting the model to physical material parameter [9]. An energy-based domain wall model was presented by Smith and Hom [10], which has been derived from the Jiles-Artherton-model [11].

Both model-types (physical/phenomenological) have their advantages and disadvantages depending upon the operation regimes [12]. Most of the current models only take the ferroelectric or ferroeleastic behavior into account. In this thesis, the linear piezoelectric-

Die approbierte gedruckte Originalversion dieser Diplomarbeit ist an der TU Wien Bibliothek verfügbar.
The approved original version of this thesis is available in print at TU Wien Bibliothek.
TU Bibliothek Your knowledge hub WIEN

mechanical system will be extended by the ferroelectric behavior of the material, furthermore also ferroelastic behavior will be discussed briefly.

The three dimensional problem gets reduced to a one dimensional problem and three different solution approaches are introduced and compared to each other. Only steady state solutions are of interest in this thesis and with the use of a multiharmonic approach and harmonic balancing, the nonlinear piezoelectrical coupled system is solved. All of the approaches converge to the exact result in most cases. There are performance and converging differences, which will be discussed too. The multiharmonic approach and harmonic balancing reduces the computational effort significantly for periodic solutions.

The long term goal is to implement a non-linear material model in the open source finite element software (www.opencfs.org [13]), in order to simulate specific piezoelectric coupled problems with high precision.

Die approbierte gedruckte Originalversion dieser Diplomarbeit ist an der TU Wien Bibliothek verfügbar.
The approved original version of this thesis is available in print at TU Wien Bibliothek.
TU WIEN Bibliothek Your knowledge hub

Chapter 2

Piezoelectric ceramics

This section is meant as a short summary of the characteristics and mechanisms appearing in piezoelectric ceramics. There are two other materials showing piezoelectric behavior, namely single crystals and polymers [14]. Some typical piezoceramics are lead zirconate titanate (PZT) or barium titanate ($BaTiO_3$), used for actuators and sensors. Quartz single crystals (SiO_2) are the most prominent piezoelectric crystals for measuring devices. The first piezoelectric polymer - polyvinilidene fluoride (PVDF) - was first discovered in 1969. Since that time many more piezoelectric polymers were discovered [3]. Single crystals and polymers show a weak piezoelectric effect and are therefore mainly used in sensors. Piezoceramics on the other hand show a strong coupling behavior, making them most prominent for various applications, such as actuators [14]. In this thesis we are interested to model actuators, therefore only piezoelectric ceramics are considered.

Crystalline ceramics Piezoelectric ceramics are crystalline ceramics, which means that the material exhibits long range order. Long range order requires atoms, that are arrayed in a repeating three dimensional pattern. The smallest unit is a cell unit. These unit cells are arranged in a certain crystal lattice. One characteristic property from piezoelectric ceramics is their polarization ability [15]. $BaTiO_3$ and PZT are materials with a Perovskite structure [3]. Materials with Perovskite structure have four different phases. A paraelectric cubic phase above the Curie temperature, and three ferroelectric phases. The most important ferroelectric phase of $BaTiO_3$ is the tetragonal phase between 5 and 120° C [3].

Spontaneous polarization If an external electric field is applied, the material polarizes. A macroscopically directed polarization occurs and the polarization vector follows the direction of the applied external electric field. Even after the external field is gone, the material stays polarized. In Fig. 2.1 two phases of $BaTiO_3$ are shown. A paraelectric cubic phase (non polarized) and a ferroelectric tetragonal phase (polarized). The polarization in the tetragonal phase is permanent, even no external electric field is applied.

Die approbierte gedruckte Originalversion dieser Diplomarbeit ist an der TU Wien Bibliothek verfügbar.
The approved original version of this thesis is available in print at TU Wien Bibliothek.
TU WIEN Bibliothek Your knowledge hub

Due to the tetragonal structure of the $BaTiO_3$ unit cell, six possible directions of the polarization vectors are possible as shown in Fig. 2.6 [3] [16].

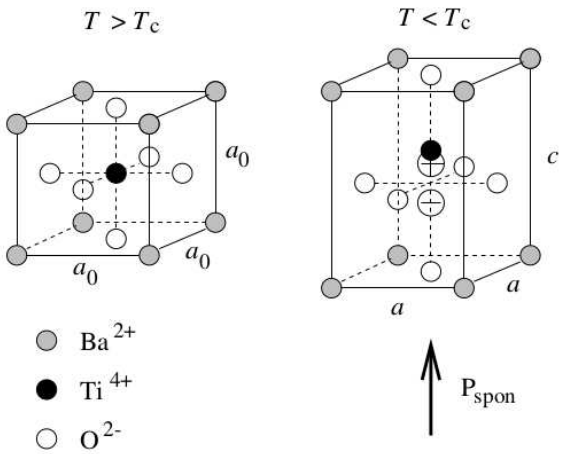

Figure 2.1: Left: Paraelectric phase of $BaTiO_3$. The titanium ion is placed in the center of the unit cell (non-polarized and symmetric). Right: Ferroelectric tetragonal phase of $BaTiO_3$. The titanium ion is shifted in one direction, producing a polarization (polarized and asymmetric); Figure from [15].

Virgin state A freshly produced piezoelectric ceramic is in the so called virgin state. In this state, the overall macroscopic net polarization is zero. The unit cells have spontaneous polarization, but they are oriented randomly, thus canceling each other out, resulting in a overall net polarization of zero.

2.1 Polarization mechanism

There are four different mechanisms that can cause polarization [16],

- Electronic polarization P_{el},
- Ionic polarization P_{io},
- Dipolar polarization P_{di},
- Space charge polarization P_{sc}.

The total polarization is the sum of all

$$P_{\mathrm{total}} = P_{\mathrm{el}} + P_{\mathrm{io}} + P_{\mathrm{di}} + P_{\mathrm{sc}}. \tag{2.1}$$

Electronic polarization and ionic polarization are only prominent at high frequencies ($> 10^{10}$Hz) [16] and can thus be neglected for most actuator applications. Space charge

Die approbierte gedruckte Originalversion dieser Diplomarbeit ist an der TU Wien Bibliothek verfügbar.
The approved original version of this thesis is available in print at TU Wien Bibliothek.
TU Bibliothek Your knowledge hub WIEN

polarization plays a minor role in ceramics and can be neglected too. Therefore, in this case eq. (2.1) simplifies to

$$P_{\text{total}} = P_{\text{di}}. \tag{2.2}$$

For the sake of completeness all of the above mentioned polarization mechanism will be explained in the following.

Electronic polarization Electronic polarization occurs in every material, since the effect comes from electrons. In a non-polarized atom, the probability of the electron position in the orbit, is the same for every possible location. If a external electric field is applied, the probability shifts and the charges will swing with the frequency of the electric field. At very high frequencies (10^{15}Hz), the electrons cannot keep up with the electronic field anymore, and the effect vanishes. At lower frequencies 10^{10} Hz the effect is typically neglected [16].

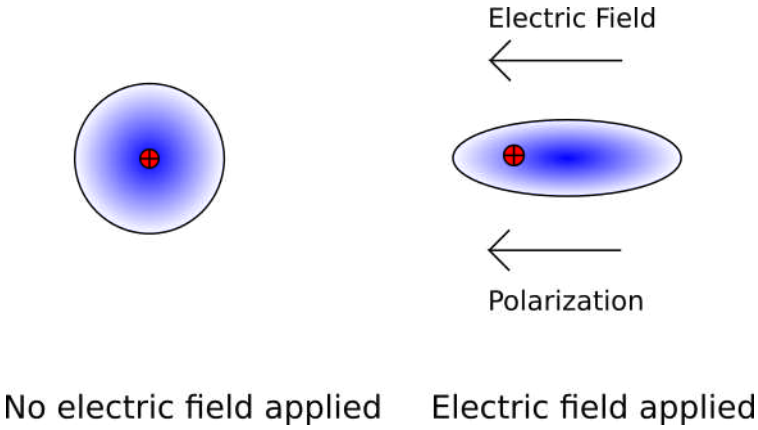

Figure 2.2: Left: Atom without applied electric field. Nucleus (red) in the center and probability of electron position is symmetric (blue). Right: Atom in applied electric field. The electric field shifts the probability field to one side, resulting in a polarization.

Ionic polarization In solid material with ionic bindings, the ionic charges also can contribute to the dielectric constant. The idea is displayed schematically in Fig. 2.3. The ions are located in fixed grids, positive and negative respectively. When applying an electric field, these grids move towards the negative and positive electrode, respectively. This occurs only in high frequency ranges (10^{12-13}Hz) [16].

Dipolar polarization In contrast to the previous polarization mechanisms, dipolar polarization occurs at low frequencies ($<10^{10}$ Hz) and vanishes at higher frequencies. Without an applied electric field, the probability which side is occupied by the ions is equal and therefore resulting in a overall net polarization of zero. If an electric field is applied, the probability will be shifted to one side, resulting in an overall polarization.

Die approbierte gedruckte Originalversion dieser Diplomarbeit ist an der TU Wien Bibliothek verfügbar.
The approved original version of this thesis is available in print at TU Wien Bibliothek.
TU Bibliothek WIEN Your knowledge hub

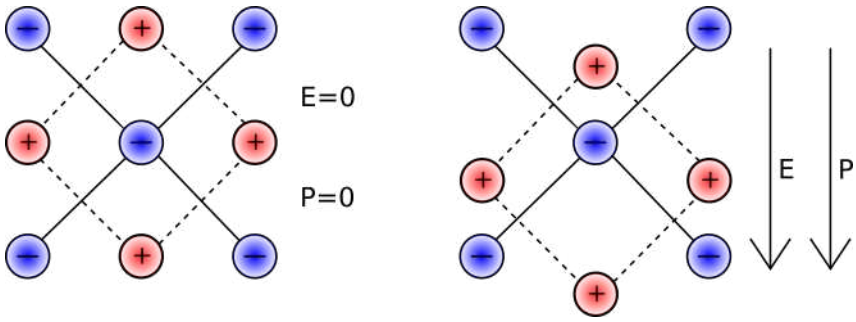

Figure 2.3: Left: No electric field applied. Ionic grid is neutral and no polarization occurs. Right: Electric field is applied, resulting in a shift of the ionic grid, which produces a polarization.

Even after the applied electric field vanishes, the polarization remains, since the ions are still on one side, and can not switch to the other side without input of additional energy to enable them to travel over the local maximum. This principle is displayed in Fig. 2.4.

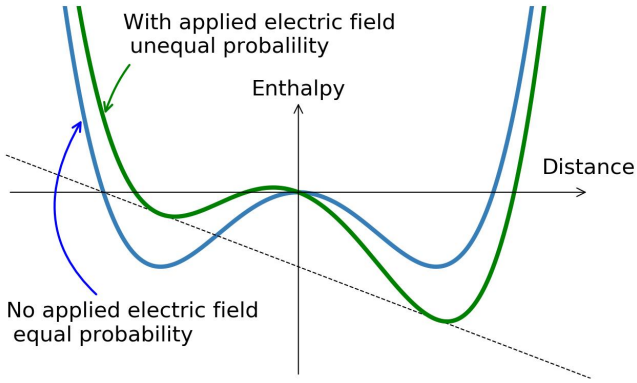

Figure 2.4: Influence of an electric field on the probability which side the ion occupies.

The blue graph shows the energy-potential over the space with no applied electric field. There one can see two minimums. The ions follow the principle of minimum energy, meaning to have as less enthalpy as possible. Thus if both minimums are the same, the probability that the ions choose one or the other side is the equal, and therefore a net polarization of zero occurs. The green curve shows the energy-potential function for a material under influence of an applied electric field. The electric field shifts the minimums. Therefore one minimum is now the only global minimum and the probability that ions will choose this side is higher. After the electric field vanishes the ion still stays on this side, because there is a activation energy needed to get to the other side. The macroscopic view of this effect is shown in Fig. 2.5, where the virgin state and a polarized state of the material are visualized. This mechanism is responsible for spontaneous polarization. Once an electric field is applied, the material experiences a polarization which stays even

Die approbierte gedruckte Originalversion dieser Diplomarbeit ist an der TU Wien Bibliothek verfügbar.
The approved original version of this thesis is available in print at TU Wien Bibliothek.
TU Bibliothek Your knowledge hub WIEN

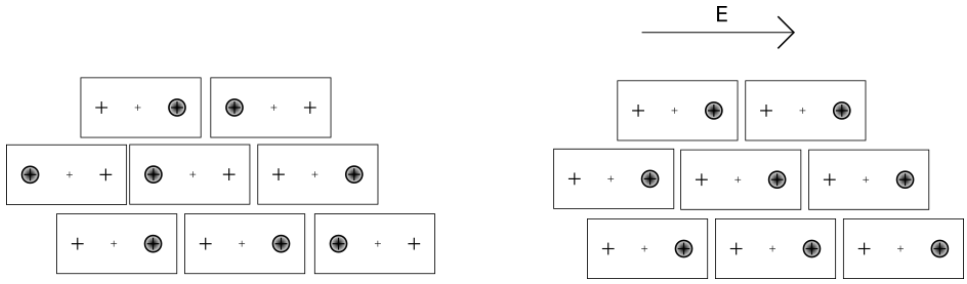

Figure 2.5: Left: If the material is in the virgin state, or completely depolarized, the overall polarization of the unit cell results in a net polarization of zero. Right: If an external field is applied, a overall polarization occurs. The same principle as displayed in Fig. 2.4.

after the external field is gone.

Space charge polarization This polarization occurs in heterogeneous materials or at the interface of two different materials with different permittivities and conductivities, where the free charges of the material build up the internal polarization. Since ceramics do not have any free charges, space charge polarization can be neglected and is not discussed any further.

2.2 Ferroelectricity and ferroelasticity

Ferroelectricity If a piezoelectric crystal with the ability of spontaneous polarization changes the direction of the polarization, due to an external electric field, the material is called ferroelectric. In a piezoelectric $BiTiO_3$-crystal the polarization has a maximum of 6 possible directions [3], as shown in Fig. 2.6. In the virgin state, there is no preferred polarization direction and the polarization of all unit cells are arranged randomly. If a high external electric field ($>$ coercive electric field strength E_c) is applied, the polarization vector switches in the direction of the electric field. Due to the switching of the unit cells, a volume change occurs [14]. This effect is responsible for the typical piezoelectric material behavior under electric load, which is discussed in section 2.3.1.

Ferroelasticity Mechanical stress interacts with the piezoelectric material too, this is called ferroelasticity. High mechanical stress fields can change the polarization direction of the unit cell, changing the volume and overall polarization of the material. In contrast to the electric field, mechanical stress can only depolarize the material [15]. Once the material is completely depolarized, it can only be polarized again by applying an electric field. This effect is displayed in the ferroelastic hysteresis, occurring during mechanical loading, discussed in section 2.3.2.

Die approbierte gedruckte Originalversion dieser Diplomarbeit ist an der TU Wien Bibliothek verfügbar.
The approved original version of this thesis is available in print at TU Wien Bibliothek.
TU Bibliothek Your knowledge hub WIEN

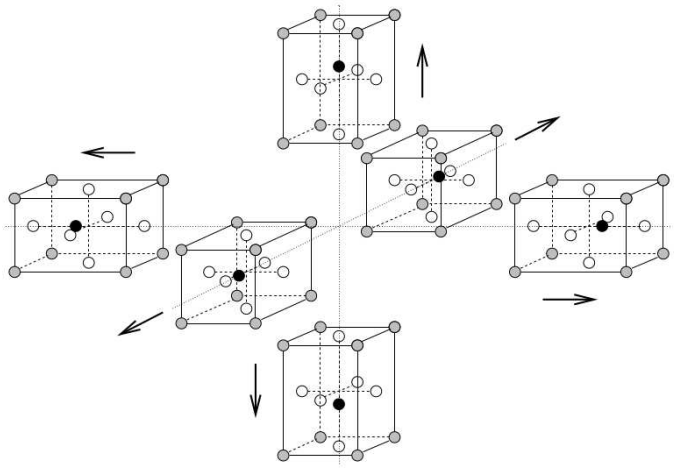

Figure 2.6: Possible polarization directions in a unit cell. Figure from [15].

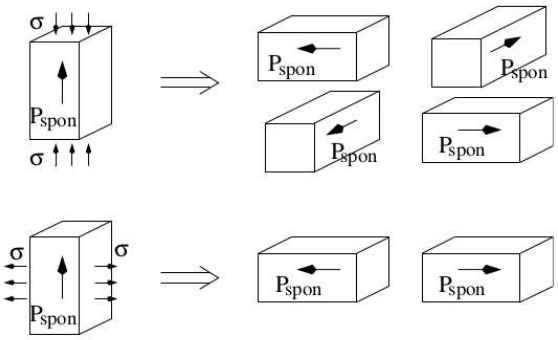

Figure 2.7: Response of a unit cell if mechanical stress is applied. Figure from [15].

2.3 Observed behavior of piezoceramics

In order to model piezoceramics in a sufficiently accurate way, one has to observe the behavior of the material first. In the previous sections the theory of polarization mechanism, ferroelectricity and ferroelasticity have been discussed briefly. In this section experiments, which displaying the piezoceramic material behavior are presented and discussed. Piezoceramics have strong nonlinear material behavior, which makes it a very complex topic. In reality only mixed loading cases occur, but for simplicity the loading cases can be split in three different cases:

- Pure electric loading: Electric field polarizes and depolarizes the material.
- Pure mechanic loading: High mechanical stress field depolarizes the material.
- Mixed loading: Combination of electric and mechanical loading.

Although mixed loading occurs all the time in reality, it is better for understanding and simplicity to neglect the influence of one part and only look into the single loading cases.

Die approbierte gedruckte Originalversion dieser Diplomarbeit ist an der TU Wien Bibliothek verfügbar.
The approved original version of this thesis is available in print at TU Wien Bibliothek.
TU Bibliothek Your knowledge hub WIEN

For some applications this is a sufficient approximation of the reality.

2.3.1 Electric loading

Applying an electric loading (external electric field) changes the properties of the material (due to the mechanism of dipolar polarization), namely the polarization and the accompanying volume change. Electric loading of piezoceramics is a special loading case, that considers only the ferroelectric effects of the material, ferroelastic behavior is neglected. Ferroelectric properties of piezoceramics are a topic of many research papers. Crack Lynch et al. [17] investigate the behavior of lead lanthanum zirconate-titanate ceramic (PLZT) under cyclic polarization switching. This results in cracking the ceramic and promotes crack growth. Therefore most piezoceramics are driven with unipolar cycles. Methee Promsawat et al. [18] looked into electrical fatigue behavior of PZT under different temperatures, which shows that piezoelectric properties are depending on temperature, as seen in Fig. 2.8. For simplicity those effects (temperature dependency, cracking) are not

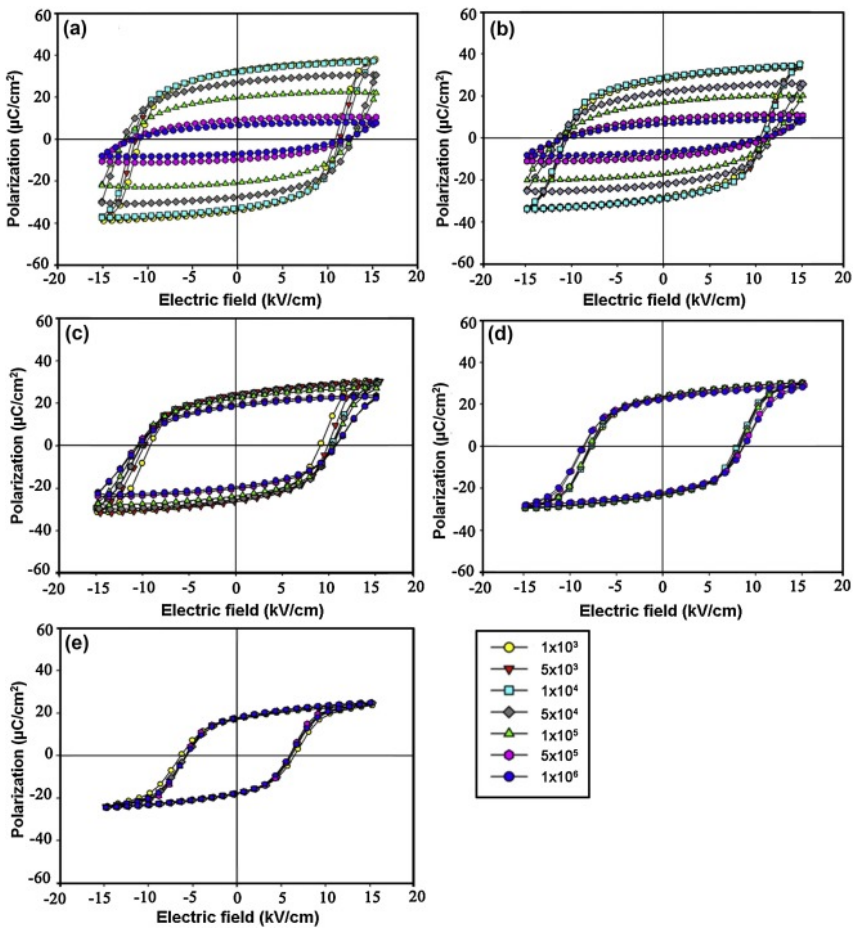

Figure 2.8: Hysteresis loops for different temperatures and electric loading cycles. (a) 25, (b) 50, (c) 100, (d) 150 and (e) 200°C. Figure from [18].

.

considered in this thesis, to keep the focus on qualitativly recreating the typical piezo-

Die approbierte gedruckte Originalversion dieser Diplomarbeit ist an der TU Wien Bibliothek verfügbar.
The approved original version of this thesis is available in print at TU Wien Bibliothek.
TU Bibliothek Your knowledge hub WIEN

electric hysteresis loop displayed in Fig. 2.9 and butterfly loop shown in Fig. 2.10 [15].

In Fig. 2.9 the material starts at virgin state (1), meaning no macroscopic net polarization is present. With an increasing electric field the polarization increases until a maximum is reached (2), meaning a further increase of the electric field does not result in a higher polarization. The polarization is saturated. Decreasing the applied electric field to zero a remnant polarization stays remnant (3), meaning the material is still polarized, even without an external electric field. Applying a negative electric field, the polarization will decrease and become zero at the coercive electric field strength E_c (4). When decreasing it further a negative polarization occurs, and finally reaching a negative saturation polarization (5). Without any electric field now a negative remnant polarization remains (6). Raising the electric field again, we pass the positive coercive electric field strength where the polarization is zero and ends up at (2) again. The initial polarization curve ((1) - (2)) only appears if the material is non-polarized. The second characteristic diagram

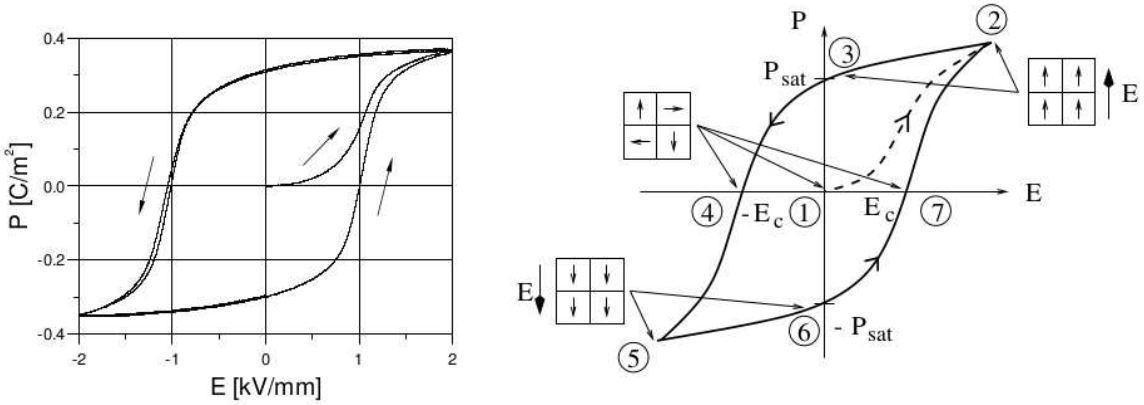

Figure 2.9: Typical hysteresis curve: polarization P over electric field E. On the left measurements of experiments are shown, and on the right the hysteresis is sketched schematically. Figure from [15].

for the electric loading case is the butterfly loop (Fig. 2.10). Starting from a unpolarized material (1), a rise of the external electric field increases the strain (2). Decreasing the electric field to zero (3) leaves a remnant strain, decreasing the electric field further into the negative, at coercive electric field strength (4) the strain becomes zero (at this electric field strength, the polarization is zero too). Decreasing it even more, let the material expands again, due to the fact that it gets polarized again (5). If then no electric field is applied, we end up at (3) with a remnant strain, caused by the remnant polarization. Figure 2.9 and Figure 2.10 show a major loop. With different excitation signals, different loops, the so called minior loops or inner hysteresis loops can occur. They can vary in shape, depending on the initial polarization and excitation. In Fig. 2.11 results of experiments are displayed [19]. Note that there are many different possible starting positions and excitation signals which all result in different hysteresis and butterfly loops.

Die approbierte gedruckte Originalversion dieser Diplomarbeit ist an der TU Wien Bibliothek verfügbar.
The approved original version of this thesis is available in print at TU Wien Bibliothek.
TU Bibliothek Your knowledge hub WIEN

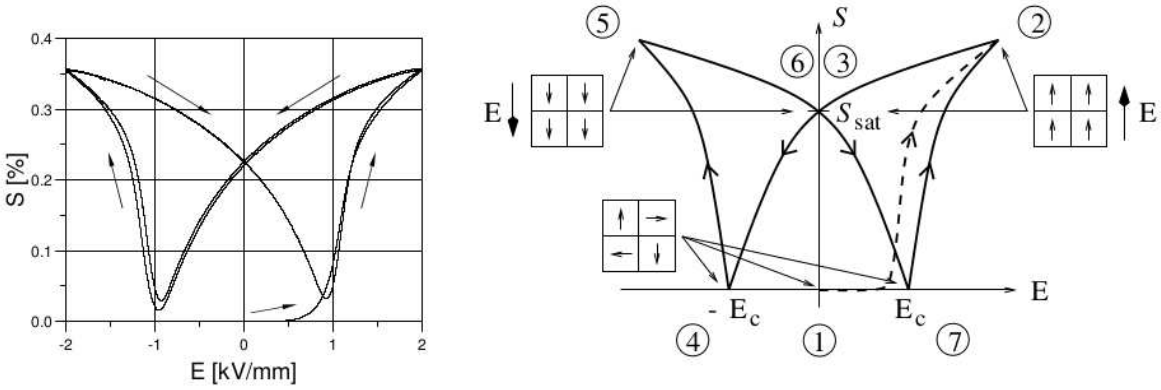

Figure 2.10: Butterfly loop: strain S over electric field E. On the left measurements of Experiments are shown, and on the right the butterfly loop is sketched schematically. Figure from [15].

2.3.2 Mechanical loading

Mechanical loading of piezoelectric ceramic (PZT) shows nonlinear behavior, as discussed in many papers ([20] [21] [22] [23]). If stress is applied on a unit cell, as shown in section 2.2, the polarization and the orientation of the unit cell switches at a certain threshold. For uni-axial stress there is no preferred new polarization direction, except the new orientation of the polarization must be orthogonal to the direction of the applied stress. Note that with a mechanical stress field one can only depolarize the material. Unpolarized piezoceramics in the virgin state experience an irreversible strain if mechanical stress is applied. In Fig. 2.12 a schematic stress-strain-curve is shown. Starting at the virgin state (1) mechanical stress is applied until (2) all unit cells are switched in the plane orthogonal to the stress direction. After releasing the stress, only the linear elastic contribution of the strain vanishes, leaving a irreversible strain (3). Polarization can vanish and/or decreases if mechanical stress is applied on polarized material [21]. In Fig. 2.13 the stress-strain curve of such an experiment is shown. The probe was polarized prior to the test. Applying stress to the probe causes a domain switching strain (domain switching strain was calculated from the total strain subtracting the linear elastic strain). Only a part of the domain switching strain will regress, leaving a permanent strain, although there was a considerable relaxation after unloading. The stress-strain-curve of polarized piezoceramics looks qualitatively the same as in Fig. 2.12. Experiments conducted by Mitsuhiro et al. [22] strongly suggest that the resulting remanent strain is the result of domain switching. When unloaded, only some of the domains switched back, but most remains in their state, as shown in Fig. 2.14. Yao et al. [20] investigated the fatigue behavior in PZT ceramics induced by cyclic mechanical loading, where it was shown that the the piezoelectric constant fatigues with cyclic loading.

Die approbierte gedruckte Originalversion dieser Diplomarbeit ist an der TU Wien Bibliothek verfügbar.
The approved original version of this thesis is available in print at TU Wien Bibliothek.
TU Bibliothek WIEN Your knowledge hub

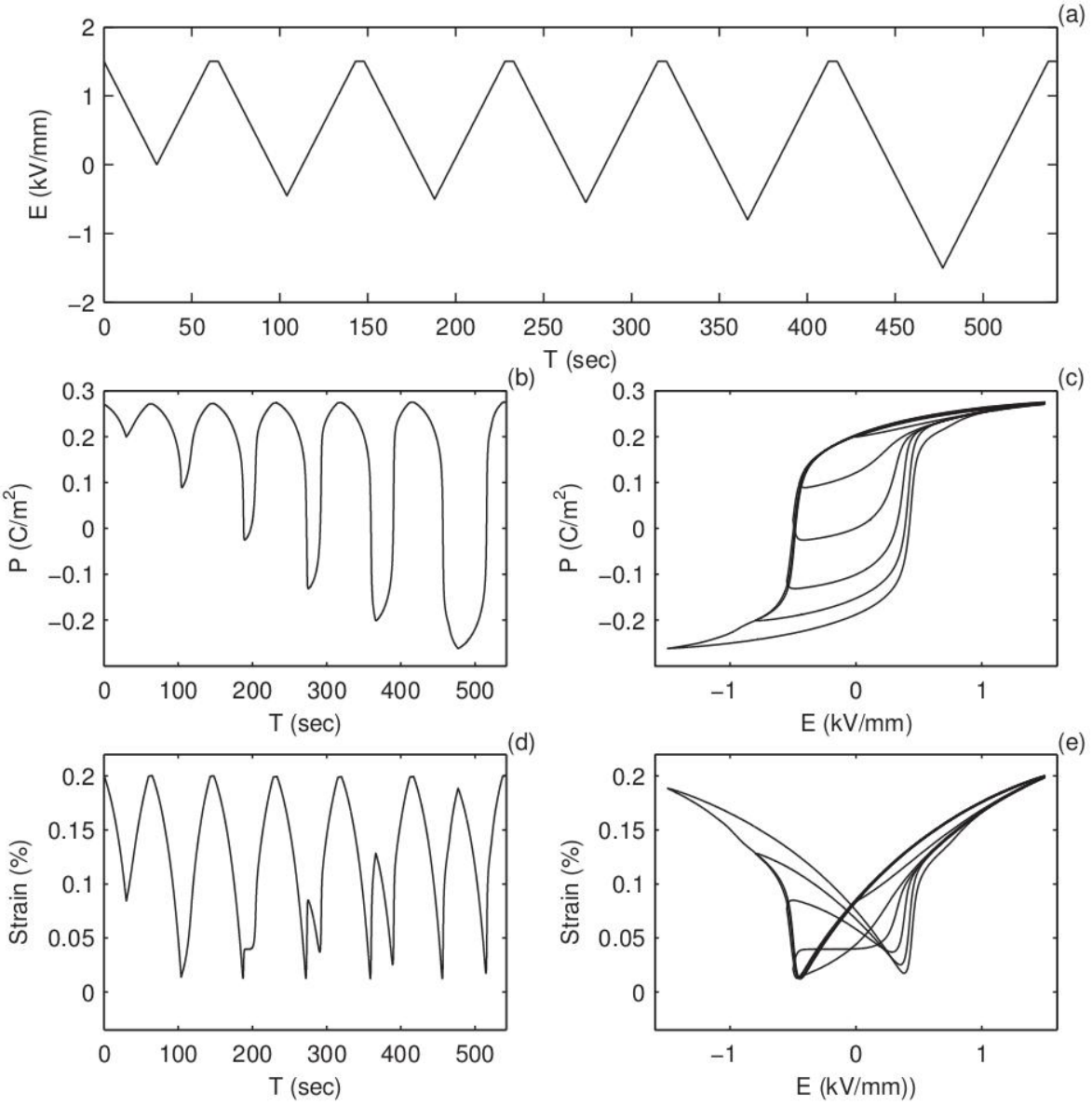

Figure 2.11: Minor loops of PZT. Figure from [19].

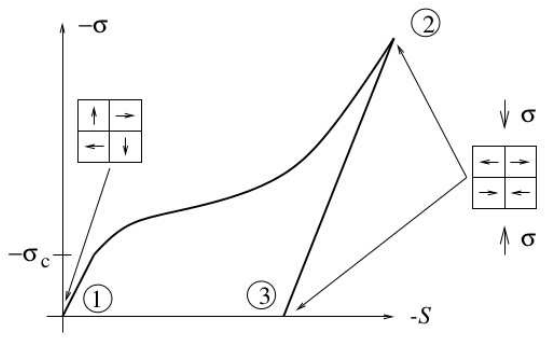

Figure 2.12: Schematic stress-strain-curve for unpolarized piezoceramic. Figure from [15].

Die approbierte gedruckte Originalversion dieser Diplomarbeit ist an der TU Wien Bibliothek verfügbar.
The approved original version of this thesis is available in print at TU Wien Bibliothek.

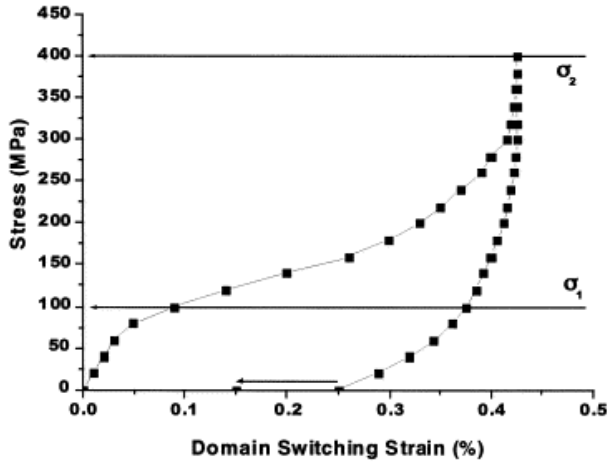

Figure 2.13: Stress-strain-curve for polarized piezoceramic. Figure from [21].

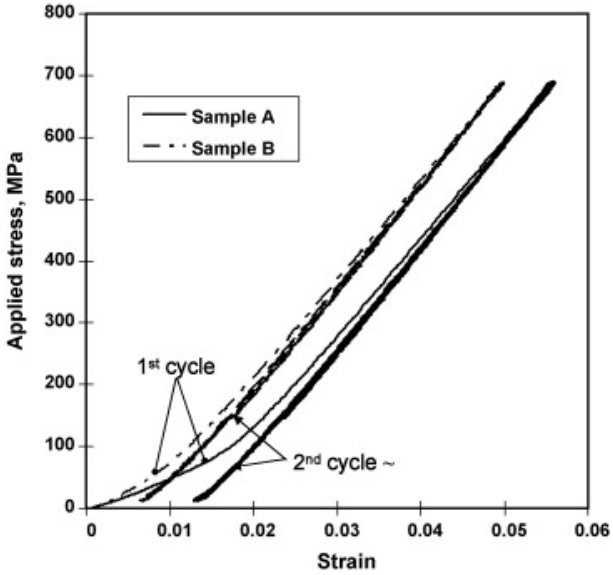

Figure 2.14: Stress-strain-curve for polarized piezoceramic, for two different materials and over two stress cycles. Figure from [22].

2.3.3 Mixed loading

The electro-mechanical response of piezoceramic including ferroelastic and ferroelectric effects are investigated in [24]. In this paper the effects of constant uni-axial stress and dynamic electric loading of PLZT is studied. The paper shows that mechanical depolarization begins at 5MPa indicating that constitutive modeling underlies some limitations.

In Figure 2.15 hysteresis loops (dielectric displacement D over electric field E) and in Fig. 2.16 the butterfly loops for certain uni-axial stress levels are displayed. Higher static stress applied results in less overall polarization, getting smaller butterfly and hysteresis loops. This is only meant as a short overview and only showcases one specific case.

There are much more possible loading cases, for example dynamic electric and me-

Die approbierte gedruckte Originalversion dieser Diplomarbeit ist an der TU Wien Bibliothek verfügbar.
The approved original version of this thesis is available in print at TU Wien Bibliothek.
TU Bibliothek WIEN Your knowledge hub

chanical loading. Currently no paper with experimental data for this case was found, therefore it will not be discussed in this thesis.

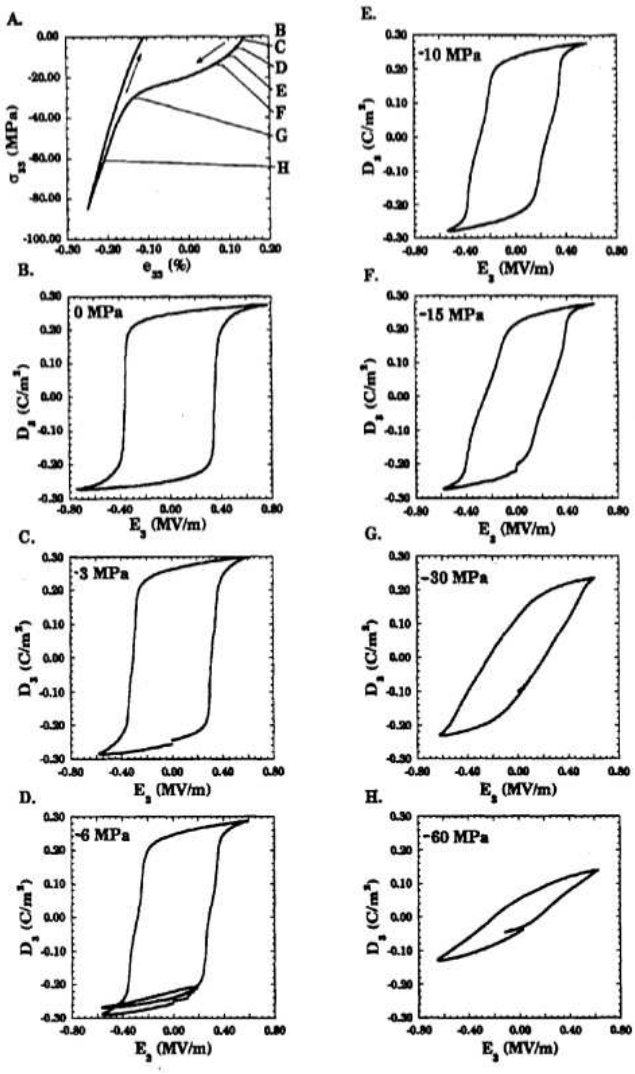

Figure 2.15: Mixed loading case: Polarization hysteresis under different constant mechanical stress. Figure from [24].

Die approbierte gedruckte Originalversion dieser Diplomarbeit ist an der TU Wien Bibliothek verfügbar.
The approved original version of this thesis is available in print at TU Wien Bibliothek.

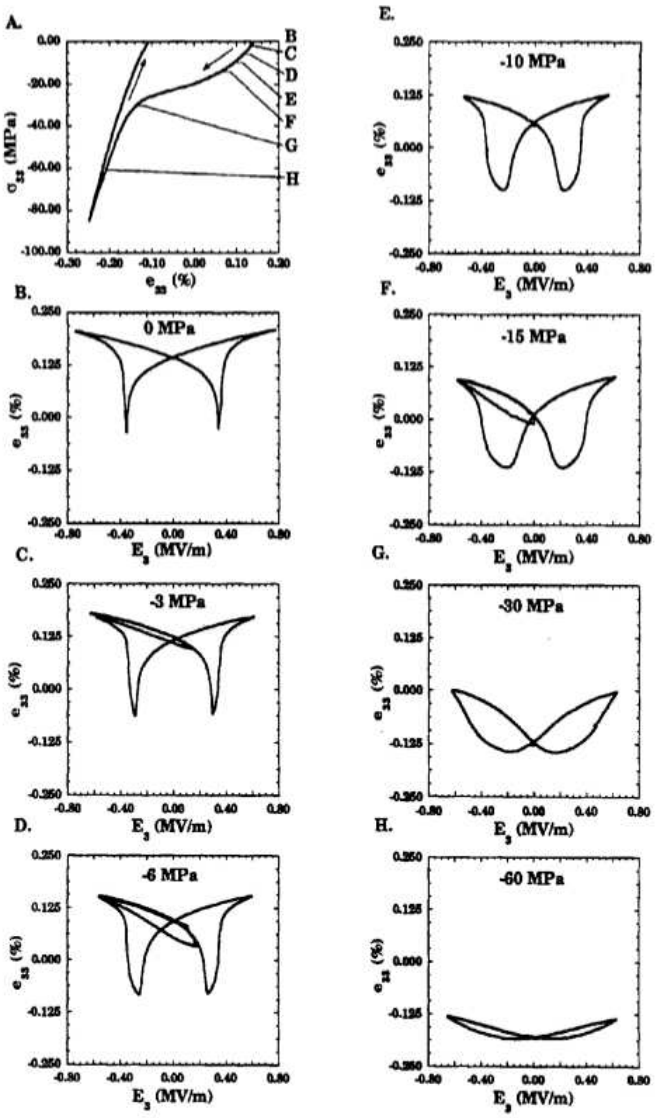

Figure 2.16: Mixed loading case: Butterfly loop under different constant mechanical stress. Figure from [24].

Die approbierte gedruckte Originalversion dieser Diplomarbeit ist an der TU Wien Bibliothek verfügbar.
The approved original version of this thesis is available in print at TU Wien Bibliothek.

Die approbierte gedruckte Originalversion dieser Diplomarbeit ist an der TU Wien Bibliothek verfügbar.
The approved original version of this thesis is available in print at TU Wien Bibliothek.

Chapter 3

Hysteresis models

Due to the piezoelectric material behavior of piezoelectric ceramics, two hystereses occur [15]. The ferroelectric hysteresis displays the interaction of the electric field and the polarization, and the ferroelastic hysteresis shows the interaction between the mechanical stress and polarization.

3.1 Ferroelectric hysteresis

The ferroelectric hysteresis describes the interaction between the electric field and the polarization, resulting in the typical polarization hysteresis and butterfly loop (displayed in Fig. 2.9 and Fig. 2.10). There are many different approaches for modeling this behavior. One of the first hysteresis model comes from Preisach [6] in 1935, initially meant for describing the magnetization hysteresis, but was later adopted for ferroelectric materials and used in many piezoelectric models [5] [7]. This model is purely phenomelogical, other models such as the Jiles-Artherton model (JA-model) [11], also first developed for magnetization. This model is derived from thermodynamic considerations and connects them to physical parameters. Based on the JA-model Ralph C. Smith introduced a domain wall model for piezoelectric material [10] [25], and in 2005 an energy based model [12]. Other hysteresis models are also used succesfully, such as the Prandtle-Ishlinskii model [7] and neural network model [8]. In this thesis the polarization model from Smith [25] is used.

Domain wall model for piezoelectric materials

This model is based on the domain wall theory [11] which is used by Jiles and Artherton in their model for ferromagnetic hysteresis. This theory was adopted in the paper of Smith et al. [25]. The underlying idea is that the polarization occurs in small domains within the material. However the domain walls cannot move freely, they are pinned. To change these domain walls and to change the direction of the polarization, a pinning energy is

Die approbierte gedruckte Originalversion dieser Diplomarbeit ist an der TU Wien Bibliothek verfügbar.
The approved original version of this thesis is available in print at TU Wien Bibliothek.
TU Bibliothek Your knowledge hub WIEN

needed to be overcome the pinning of the domain wall. This is similar to the concept of the dipolar polarization mechanism, where the ion needs an activation energy to switch sides as described in section 2.1. This pinning causes the hysteresis loop and is described with a differential equation. If no pinning would occur the polarization hysteresis would be the anhysteretic polarization. The basic shape of the hysteresis is described by the anhysteretic polarization

$$P_{\mathrm{an}}(t) = P_{\mathrm{s}} \left[\coth\left(\frac{E_{\mathrm{e}}(t)}{a}\right) - \left(\frac{E_{\mathrm{e}}(t)}{a}\right) \right]. \tag{3.1}$$

In this case a Langevin function serves as anhysteretic polarization curve, where P_{s} is the maximal achievable polarization, also called saturated polarization. Here a denotes a material parameter which needs to be fitted to experimental data. The effective electric field E_{e}

$$E_{\mathrm{e}}(t) = E(t) + \alpha P(t), \tag{3.2}$$

is composed of the applied electric field E and the total polarization of the material P, weighted with the parameter α, which needs to be fitted with experimental data too. The polarization can be split up into two parts

$$P(t) = cP_{\mathrm{an}}(t) + (1-c)P_{\mathrm{irr}}(t) \tag{3.3}$$

the anhysteretic part P_{an} and the irreversible polarization P_{irr}. The parameter c denotes the percentage of anhysteretic and irreversible portion of the polarization and may range from 0 to 1. The irreversible polarization is described by a differential equation of first order

$$\frac{\mathrm{d}P_{\mathrm{irr}}(t)}{\mathrm{d}E(t)} = \frac{\tilde{\delta}\left[P_{\mathrm{an}}(t) - P_{\mathrm{irr}}(t)\right]}{k\delta - \alpha\left[P_{\mathrm{an}}(t) - P_{\mathrm{irr}}(t)\right]}. \tag{3.4}$$

The switching parameter δ is dependent on the sign of the time derivative of the electric field and is weighted with the parameter k, which is connected the pinning energy needed to change the domain walls. If the electric field is rising δ may take the value 1 and -1 if the electric field is falling

$$\delta = \mathrm{sign}\left(\mathrm{d}E\right). \tag{3.5}$$

Without δ no hysteresis would occur. The other switching parameter $\tilde{\delta}$

$$\tilde{\delta} = \begin{cases} 0 \ \left[\mathrm{d}E > 0 \text{ and } P > P_{\mathrm{an}}\right] \text{ or } \left[\mathrm{d}E < 0 \text{ and } P < P_{\mathrm{an}}\right] \\ 1 \text{ , otherwise} \end{cases}, \tag{3.6}$$

prevents non physical behavior for some parameter sets, where the polarization could decrease even the electric field is still increasing. This is prevented by $\tilde{\delta}$ which does not allow a change of P_{irr} until the polarization crosses the anhysteretic curve.

Die approbierte gedruckte Originalversion dieser Diplomarbeit ist an der TU Wien Bibliothek verfügbar.
The approved original version of this thesis is available in print at TU Wien Bibliothek.
TU Bibliothek WIEN Your knowledge hub

Evaluation with the forward-difference-method

The equations (eq. (3.2) to eq. (3.6)) are solved in the time domain, since it is hard to find a closed analytic form for this partial differential equation (PDE) in the frequency domain. To solve them in the time domain a simple forward difference method is used. Therefore one needs to discretize the eq. (3.4),

$$\frac{{}^{n+1}P_{\text{irr}} - {}^{n}P_{\text{irr}}}{{}^{n+1}E - {}^{n}E} = \frac{{}^{n}\tilde{\delta}\left({}^{n}P_{\text{an}} - {}^{n}P_{\text{irr}}\right)}{k\,{}^{n}\delta - \alpha\left({}^{n}P_{\text{an}} - {}^{n}P_{\text{irr}}\right)}. \tag{3.7}$$

By rearranging equation eq. (3.7) we get an equation for the next irreversible polarization ${}^{n+1}P_{\text{irr}}$ based on the previous irreversible polarization ${}^{n}P_{\text{irr}}$ and the known electric field ${}^{n,n+1}E$. The index n denotes the current time step, and $n+1$ the next time step.

$${}^{n+1}P_{\text{irr}} = {}^{n}P_{\text{irr}} + \left({}^{n+1}E - {}^{n}E\right)\frac{{}^{n}\tilde{\delta}\left({}^{n}P_{\text{an}} - {}^{n}P_{\text{irr}}\right)}{k\,{}^{n}\delta - \alpha\left({}^{n}P_{\text{an}} - {}^{n}P_{\text{irr}}\right)} = f\left({}^{n+1}E, {}^{n}E, {}^{n}P_{\text{irr}}\right). \tag{3.8}$$

The anhysteretic polarisation P_{an} is evaluated by eq. (3.1) using known values from the previous time step, i.e.

$${}^{n}P_{\text{an}} = P_{\text{s}}\left(\coth\left(\frac{{}^{n}E + \alpha\,{}^{n}P}{a}\right) - \frac{a}{{}^{n}E + \alpha\,{}^{n}P}\right) = f\left({}^{n}E, {}^{n}P\right), \tag{3.9}$$

using the total polarization P computed with the same assumption by

$${}^{n}P = c\,{}^{n}P_{\text{an}} + (1-c)\,{}^{n}P_{\text{irr}} = f\left({}^{n}P_{\text{irr}}, {}^{n}P_{\text{an}}\right). \tag{3.10}$$

The parameters δ and $\tilde{\delta}$ are computed as

$${}^{n}\delta = \text{sign}\left({}^{n+1}E - {}^{n}E\right), \tag{3.11}$$

$${}^{n}\tilde{\delta} = \begin{cases} 0\,, \left[{}^{n+1}E - {}^{n}E > 0 \text{ and } {}^{n}P > {}^{n}P_{\text{an}}\right] \text{ or } \left[{}^{n+1}E - {}^{n}E < 0 \text{ and } {}^{n}P < {}^{n}P_{\text{an}}\right] \\ 1\,, \text{ otherwise} \end{cases}. \tag{3.12}$$

With a known $E(t)$ and a starting-point ${}^{0}P_{\text{irr}}$, one can use a forward difference scheme to evaluate the polarization $P(t)$. Due to the explicit nature of the forward difference scheme eq. (3.8) does not have to be iterated, but it is important that the discrete time steps are sufficiently small. If a implicit forward difference scheme eq. (3.13)

$${}^{n+1}P_{\text{irr}} = {}^{n}P_{\text{irr}} + \left({}^{n+1}E - {}^{n}E\right)\frac{{}^{n}\tilde{\delta}\left({}^{n}P_{\text{an}} - {}^{n+1}P_{\text{irr}}\right)}{k\,{}^{n}\delta - \alpha\left({}^{n}P_{\text{an}} - {}^{n+1}P_{\text{irr}}\right)} = f\left({}^{n+1}E, {}^{n}E, {}^{n+1}P_{\text{irr}}\right), \tag{3.13}$$

would be used, equilibrium iterations have to be done. The solution of this implicit scheme would be more robust, but it needs more computational effort.

Die approbierte gedruckte Originalversion dieser Diplomarbeit ist an der TU Wien Bibliothek verfügbar.
The approved original version of this thesis is available in print at TU Wien Bibliothek.
TU Bibliothek Your knowledge hub WIEN

3.2 Ferroelastic hysteresis

Mechanical stress interacts with polarization of the material too, resulting in a hysteresis [20] [21] [22], as shown in Fig. 2.12. As for the ferroelectric hysteresis there are many approaches to model this behavior. Hwang et. al. [23] uses a Preisach model, and in [24] a switching model was used. In a report from Smith [25], thermodynamic principles are deployed to quantify the anhysteretic behavior of the material, and energy relations are used to model the irreversible and reversible motion of domain walls, similar to the JA-model. For the mechanical hysteresis this paper uses the equations proposed in the work of Smith et. al. [25].

The hysteresis model used in this thesis is based on the domain wall model and is similar to the ferroelectric model, but with a different anhysteretic curve. The effective mechanical stress σ_e is composed of the applied mechanical stress σ and the strain S, weighted with the parameter α'.

$$\sigma_\mathrm{e} = \sigma + \alpha' S. \tag{3.14}$$

The effective mechanical stress is assumed as a polynomial function of the anhysteretic strain S_an

$$\sigma_\mathrm{e} = 2\alpha_1 S_\mathrm{an} + 4\alpha_2 S_\mathrm{an}^3 + 6\alpha_3 S_\mathrm{an}^5, \tag{3.15}$$

with $\alpha_{1,2,3}$ as fitting parameters. The irreversible strain is expressed with a similar differential equation as the irreversible polarization

$$\frac{\mathrm{d}S_\mathrm{irr}(t)}{\mathrm{d}\sigma} = \frac{S_\mathrm{an}(t) - S_\mathrm{irr}(t)}{k'\delta' - \alpha' \left[S_\mathrm{an}(t) - S_\mathrm{irr}(t)\right]}. \tag{3.16}$$

The switching parameter δ' is dependent of the slope of the mechanical stress

$$\delta' = \mathrm{sign}\left(\mathrm{d}\sigma\right), \tag{3.17}$$

and the total strain is

$$S = c' S_\mathrm{an}(t) - (1 - c') S_\mathrm{irr}(t). \tag{3.18}$$

The parameter c' describes the proportion of anyhsteretic and irreversible strain. The parameters α', k' and c' have to be fitted according to the material. Since the ferroelastic hysteresis is modeled with an equivalent model as the ferroelectric hysteresis, but with a other anhysteretic curve many parameters are denoted similarly. To prevent confusion, all similar parameters are denoted with a apostrophe $'$ for the ferroelastic hysteresis.

Evaluation of the ferroelasitic hysteresis

For the anhysteretic curve one simply combines eq. (3.14), eq. (3.15), eq. (3.18) and uses a root-finding algorithm to find the roots of S_an. The irreversible part is described by

Die approbierte gedruckte Originalversion dieser Diplomarbeit ist an der TU Wien Bibliothek verfügbar.
The approved original version of this thesis is available in print at TU Wien Bibliothek.
TU Bibliothek Your knowledge hub WIEN

a differential equation, similar to the one used for ferroelectric behavior. To solve the differential equation the forward difference method is used. Therefore the eq. (3.15) must be discretised. With the strain of the previous time step ${}^{n-1}S$ (or a start value ${}^{0}S = 0$) one can evaluate the current anhysteretic strain ${}^{n}S_{\text{an}}$ by finding the roots of eq. (3.15). The irreversible part of the strain ${}^{n+1}S_{\text{irr}}$ for the next step is described by a similar differential equation, as in section 3.1. With the current anhysteretic strain ${}^{n}S_{\text{an}}$ and irreversible strain ${}^{n}S_{\text{irr}}$ one can calculate the irreversible strain for the next step ${}^{n+1}S_{\text{irr}}$ by discretizing eq. (3.16)

$$ {}^{n+1}S_{\text{irr}} = {}^{n}S_{\text{irr}} + \left({}^{n+1}\sigma - {}^{n}\sigma\right) \frac{\left({}^{n}S_{\text{an}} - {}^{n}S_{\text{irr}}\right)}{k' \, {}^{n}\delta' - \alpha' \left({}^{n}S_{\text{an}} - {}^{n}S_{\text{irr}}\right)} = f\left({}^{n+1}\sigma, {}^{n}\sigma, {}^{n}S_{\text{irr}}\right). \tag{3.19} $$

The total strain is composed out of the weighted sum of ${}^{n}S_{\text{an}}$ and ${}^{n}S_{\text{irr}}$

$$ {}^{n}S = c' \, {}^{n}S_{\text{an}} + (1 - c') \, {}^{n}S_{\text{irr}} = f\left({}^{n}S_{\text{irr}}, {}^{n}S_{\text{an}}\right). \tag{3.20} $$

For the sake of completeness the parameter δ' for each step is stated

$$ {}^{n}\delta' = \text{sign}\left({}^{n+1}\sigma - {}^{n}\sigma\right). \tag{3.21} $$

Die approbierte gedruckte Originalversion dieser Diplomarbeit ist an der TU Wien Bibliothek verfügbar.
The approved original version of this thesis is available in print at TU Wien Bibliothek.
TU Bibliothek WIEN Your knowledge hub

Die approbierte gedruckte Originalversion dieser Diplomarbeit ist an der TU Wien Bibliothek verfügbar.
The approved original version of this thesis is available in print at TU Wien Bibliothek.

Chapter 4

Piezoelectric-mechanical system

In the previous chapter we discussed the material behavior and how one can model and evaluate it. In this chapter the coupled system will be presented. Starting from the linear system, we will implement the nonlinear material behavior via constitutive equations in the governing equations of the mechanical and electrical field.

4.1 Linear piezoelectric-mechanic coupled system

This chapter relies heavily on "Numerical Simulations of Mechatronic Sensors and Actuators" [14] and is only meant as a rough overview, as these equations are well established in literature. Starting from the balance of momentum

$$\boldsymbol{f}_{\mathrm{V}} + \nabla \cdot \underset{\sim}{\boldsymbol{\sigma}} = \rho \boldsymbol{a}, \tag{4.1}$$

where $\boldsymbol{f}_{\mathrm{V}}$, $\underset{\sim}{\boldsymbol{\sigma}}$ and $\boldsymbol{a}$ denote the volume force, Cauchy stress tensor and acceleration vector, respectively. While only static solutions are considered and no volume forces are taken into account, one will arrive at the simplified mechanical equilibrium equation,

$$\nabla \cdot \underset{\sim}{\boldsymbol{\sigma}} = \mathbf{0}. \tag{4.2}$$

The Gauss's law written in the differential form,

$$\nabla \cdot \boldsymbol{D} = q_e, \tag{4.3}$$

can be simplified by taking into account that piezoelectric ceramics are insulators and therefore the free electric charges are zero ($q_e = 0$) leading to the simplified electric governing equation

$$\nabla \cdot \boldsymbol{D} = 0. \tag{4.4}$$

Die approbierte gedruckte Originalversion dieser Diplomarbeit ist an der TU Wien Bibliothek verfügbar.
The approved original version of this thesis is available in print at TU Wien Bibliothek.
TU WIEN Bibliothek Your knowledge hub

The dielectric displacement field is denoted as $\boldsymbol{D}$. With constitutive relationship

$$\boldsymbol{\sigma} = \underset{\sim}{\boldsymbol{C}}\boldsymbol{S} - \underset{\sim}{\boldsymbol{e}}^T\boldsymbol{E}, \tag{4.5}$$

and

$$\boldsymbol{D} = \underset{\sim}{\boldsymbol{e}}\boldsymbol{S} + \underset{\sim}{\boldsymbol{\epsilon}}^S\boldsymbol{E}, \tag{4.6}$$

the electric and mechanical governing equation are coupled. In the material law the stress tensor is written in Voigt notation and denoted as $\boldsymbol{\sigma}$, $\underset{\sim}{\boldsymbol{e}}$ denotes the piezoelectric couple tensor between electric and mechanical field and $\underset{\sim}{\boldsymbol{C}}$ the stiffness tensor. The linear permittivity tensor is denoted as $\underset{\sim}{\boldsymbol{\epsilon}}^S$ and $\boldsymbol{E}$ is the electric field. By introducing the differential operator $\mathcal{B}$

$$\mathcal{B} = \begin{pmatrix} \frac{\partial}{\partial x} & 0 & 0 & 0 & \frac{\partial}{\partial z} & \frac{\partial}{\partial y} \\ 0 & \frac{\partial}{\partial y} & 0 & \frac{\partial}{\partial z} & 0 & \frac{\partial}{\partial x} \\ 0 & 0 & \frac{\partial}{\partial z} & \frac{\partial}{\partial y} & \frac{\partial}{\partial x} & 0 \end{pmatrix}^T, \tag{4.7}$$

the material law eq. (4.5) in Voigt notation can be inserted into the simplified balance of momentum eq. (4.2) leading to eq. (4.9). For the coupled electric partial differential equation, one inserts the material law for dielectrics eq. (4.6) into the electric equilibrium equation eq. (4.4) leading to

$$\nabla \cdot \left(\underset{\sim}{\boldsymbol{e}}\boldsymbol{S} + \underset{\sim}{\boldsymbol{\epsilon}}^S\boldsymbol{E}\right) = 0. \tag{4.8}$$

$$\mathcal{B}^T\boldsymbol{\sigma} = \mathcal{B}^T\left(\underset{\sim}{\boldsymbol{c}}\boldsymbol{S} - \underset{\sim}{\boldsymbol{e}}^T\boldsymbol{E}\right) = \boldsymbol{0}. \tag{4.9}$$

4.2 One dimensional piezoelectric coupled system

For this thesis, only a one dimensional case and static solutions are considered. This greatly simplifies the governing equations, since now the mechanical and electrical field quantities can be written as scalars, and due to the static viewpoint the acceleration vector vanishes, leading to a simplified mechanical and electrical differential equation.

Piezoelectric actuators can be driven via electric current $I = \mathrm{d}Q/\mathrm{d}t$ or voltage U. For a voltage driven applications the electrical field $E = U/d$ is known, due to the known electrode distance d and applied voltage U. If a piezoelectric system is current controlled (current excitation is equal to charge excitation), the charges Q and the dielectric displacement field $D = Q/A$ is known, where A denotes the electrode area and the electric field E is the unknown . Additionally the system can be excited with a mechanical force f, which results in a mechanical stress $\sigma = \mathrm{f}/A$. All in the following introduced systems are charge and force controlled and therefore the input quantities are the dielectric displacement field and mechanical stress.

To derive the one dimensional equations, suitable boundary conditions (BC) and assumptions have to be applied. We assume known BC for the mechanical stress and

Die approbierte gedruckte Originalversion dieser Diplomarbeit ist an der TU Wien Bibliothek verfügbar.
The approved original version of this thesis is available in print at TU Wien Bibliothek.
TU Bibliothek Your knowledge hub WIEN

dielectric displacement field, therefore the electric field and mechanic strain are the unknowns. Lets first introduce a Cartesian coordinate system built out of the three unit vectors $\boldsymbol{e_1}$, $\boldsymbol{e_2}$ and $\boldsymbol{e_3}$. The unit vectors are aligned to the orthogonal material axsis. In Fig. 4.1 one three dimensional piezoelectric element with the applied conditions is shown.

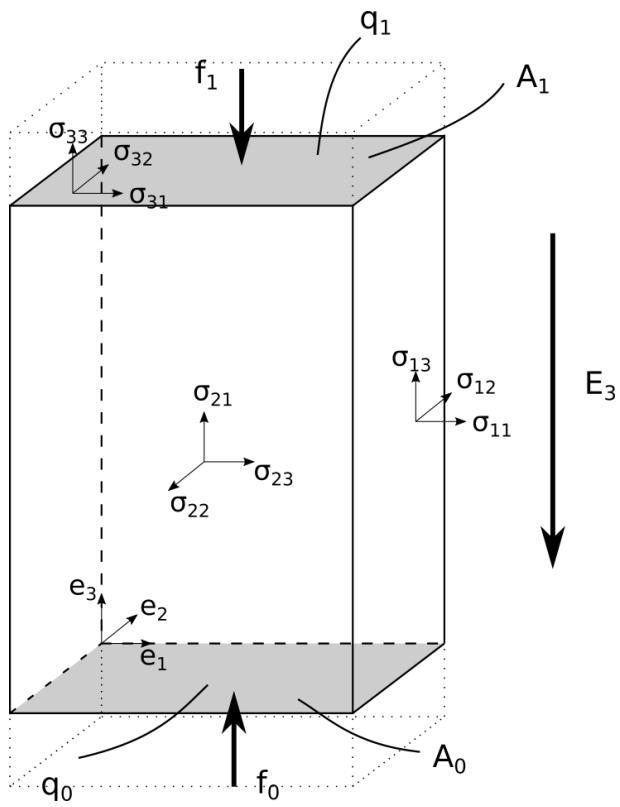

Figure 4.1: Applied Force and electric charges on A_0 and A_1 on a small piezoelectric element. Only A_0 and A_1 are allowed to displace in $\boldsymbol{e_3}$-direction, the dotted lines are indicating the allowed deformation. The electric field occurs only in $\boldsymbol{e_3}$-direction.

In a first step we assume that the charge densities $q_0 \neq q_1$ are constant over bottom and top boundary (A_0 and A_1). At the sides we assume $\boldsymbol{D} \cdot \boldsymbol{n} = 0$. Therefore no gradients arise in $\boldsymbol{e_1}$- and $\boldsymbol{e_2}$-direction. The vector $\boldsymbol{n}$ denotes the normal vector of a surface. The electric field occurs only in $\boldsymbol{e_3}$-direction and the electric field in $\boldsymbol{e_1}$- and $\boldsymbol{e_2}$-direction is zero

$$E_1 = E_2 = 0, \tag{4.10}$$

and only the electric equilibrium equation in $\boldsymbol{e_3}$-direction is of interest. Furthermore we demand that the material is a ideal homogeneous insulator. This results in an constant electric field

$$E_3 = \text{const.}\,, \tag{4.11}$$

and constant polarization

$$P_3 = \text{const.}\,. \tag{4.12}$$

Die approbierte gedruckte Originalversion dieser Diplomarbeit ist an der TU Wien Bibliothek verfügbar.
The approved original version of this thesis is available in print at TU Wien Bibliothek.
TU Bibliothek Your knowledge hub WIEN

along the $\boldsymbol{e_3}$-direction inside the material. The electric one dimensional equilibrium equation for electrostatic

$$\frac{\partial}{\partial z} D_3 = \frac{\partial}{\partial z} \epsilon_0 E_3 + \frac{\partial}{\partial z} P_3 = 0, \tag{4.13}$$

is therefore automatically fulfilled with the applied boundary conditions and assumptions. By only allowing a displacement of A_0- and A_1-boundary in $\boldsymbol{e_3}$-direction and demanding that the displacement on all other boundaries is zero

$$u_1 = u_2 = 0, \tag{4.14}$$

no gradient arises in $\boldsymbol{e_1}$- and $\boldsymbol{e_2}$-direction. Therefore only the balance of momentum in $\boldsymbol{e_3}$-direction is of interest. The simplified mechanical one dimensional governing equation

$$\frac{\partial}{\partial z} \sigma_{33} = 0, \tag{4.15}$$

is solved for every $\sigma_{33} = \text{const.}$. This is fulfilled with the applied boundary condition

$$\mathrm{f}_0 = \mathrm{f}_1, \tag{4.16}$$

leading to

$$\sigma_{33} = \frac{\mathrm{f}_1}{A_1} = \frac{\mathrm{f}_0}{A_0} = \text{const.}. \tag{4.17}$$

The displacement vector u is defined as

$$\boldsymbol{u} = \boldsymbol{X} - \boldsymbol{x} = \begin{pmatrix} u_1 \\ u_2 \\ u_3 \end{pmatrix} = \begin{pmatrix} X_1 \\ X_2 \\ X_3 \end{pmatrix} - \begin{pmatrix} x_1 \\ x_2 \\ x_3 \end{pmatrix}, \tag{4.18}$$

with X as the position of one point before the deformation and x is the position of the same point after the deformation. Because of eq. (4.14) and the definition of strain S_{ii} and shear strain S_{ij}

$$S_{ii} = \frac{\partial u_i}{\partial x_i}, \tag{4.19}$$

$$S_{ij} = S_{ji} = \frac{\partial u_i}{\partial x_j} + \frac{\partial u_j}{\partial x_i}, \tag{4.20}$$

no strain S_{ii} occurs in $\boldsymbol{e_1}$- and $\boldsymbol{e_2}$-direction and all shear strains are zero,

$$S_{11} = S_{22} = S_{12} = S_{13} = S_{23} = 0. \tag{4.21}$$

If eq. (4.10) and eq. (4.21) are inserted in the mechanical material law eq. (4.5) and orthotropic material behavior is assumed, one can rewrite it as a matrix-vector system

Die approbierte gedruckte Originalversion dieser Diplomarbeit ist an der TU Wien Bibliothek verfügbar.
The approved original version of this thesis is available in print at TU Wien Bibliothek.
TU Bibliothek WIEN Your knowledge hub

and obtain these set of equations,

$$\begin{pmatrix} \sigma_{11} \\ \sigma_{22} \\ \sigma_{33} \\ \sigma_{23} \\ \sigma_{13} \\ \sigma_{12} \end{pmatrix} = \begin{pmatrix} C_{11} & C_{12} & C_{13} & 0 & 0 & 0 \\ C_{12} & C_{22} & C_{23} & 0 & 0 & 0 \\ C_{13} & C_{23} & C_{33} & 0 & 0 & 0 \\ 0 & 0 & 0 & C_{44} & 0 & 0 \\ 0 & 0 & 0 & 0 & C_{55} & 0 \\ 0 & 0 & 0 & 0 & 0 & C_{66} \end{pmatrix} \begin{pmatrix} 0 \\ 0 \\ S_{33} \\ 0 \\ 0 \\ 0 \end{pmatrix} - \begin{pmatrix} 0 & 0 & e_{31} \\ 0 & 0 & e_{31} \\ 0 & 0 & e_{33} \\ 0 & e_{15} & 0 \\ e_{15} & 0 & 0 \\ 0 & 0 & 0 \end{pmatrix} \begin{pmatrix} 0 \\ 0 \\ E_3 \end{pmatrix}, \tag{4.22}$$

resulting in

$$\begin{pmatrix} \sigma_{11} \\ \sigma_{22} \\ \sigma_{33} \\ \sigma_{23} \\ \sigma_{13} \\ \sigma_{12} \end{pmatrix} = \begin{pmatrix} C_{13}S_{33} - e_{31}E_3 \\ C_{23}S_{33} - e_{31}E_3 \\ C_{33}S_{33} - e_{33}E_3 \\ 0 \\ 0 \\ 0 \end{pmatrix}. \tag{4.23}$$

Now the equations are decoupled. Only the third row of eq. (4.23) is of interest, where we get our one dimensional material law in $\boldsymbol{e_3}$-direction

$$\sigma_{33} = C_{33}S_{33} - e_{33}E_3. \tag{4.24}$$

And inserting eq. (4.10) and eq. (4.21) in the coupled electrical material law the eq. (4.6) can be expressed as

$$\begin{pmatrix} D_1 \\ D_2 \\ D_3 \end{pmatrix} = \begin{pmatrix} 0 & 0 & 0 & 0 & e_{15} & 0 \\ 0 & 0 & 0 & e_{15} & 0 & 0 \\ e_{31} & e_{31} & e_{33} & 0 & 0 & 0 \end{pmatrix} \begin{pmatrix} 0 \\ 0 \\ S_{33} \\ 0 \\ 0 \\ 0 \end{pmatrix} + \begin{pmatrix} \epsilon_0\epsilon_r & 0 & 0 \\ 0 & \epsilon_0\epsilon_r & 0 \\ 0 & 0 & \epsilon_0\epsilon_r \end{pmatrix} \begin{pmatrix} 0 \\ 0 \\ E_3 \end{pmatrix} \tag{4.25}$$

resulting in

$$\begin{pmatrix} D_1 \\ D_2 \\ D_3 \end{pmatrix} = \begin{pmatrix} 0 \\ 0 \\ e_{33}S_{33} + \epsilon_0\epsilon_r E_3 \end{pmatrix}. \tag{4.26}$$

Every row of eq. (4.26) is zero, except the last one in $\boldsymbol{e}_3$-direction. This is the coupled electric material law in $\boldsymbol{e_3}$-direction

$$D_3 = e_{33}S_{33} + \epsilon_0\epsilon_r E_3. \tag{4.27}$$

Die approbierte gedruckte Originalversion dieser Diplomarbeit ist an der TU Wien Bibliothek verfügbar.
The approved original version of this thesis is available in print at TU Wien Bibliothek.
TU Bibliothek WIEN Your knowledge hub

All equations for the one dimensional case are derived. The governing equations, eq. (4.15) and eq. (4.13), are automatically fulfilled for the one dimensional model, due to the boundary conditions and made assumptions. Only the material laws eq. (4.24) and eq. (4.27) have to be solved. In the following the indices of the $\boldsymbol{e_3}$-direction will not be added to the variable anymore, since from now on this thesis only considers the one dimensional case.

4.3 Nonlinear constitutive laws

The one dimensional constitutive equation eq. (4.27) and eq. (4.24) can be expanded with nonlinear terms, to include ferroelectric effects. There are many different ways to expand these equations. One way of doing so, is to split up the electric constitutive law eq. (4.27) into an reversible part D^{r} and a irreversible Part D^{i} of the dielectric displacement field,

$$D = D^{\mathrm{r}} + D^{\mathrm{i}} = \overbrace{e(P)S^{\mathrm{r}} + \epsilon_0 E}^{D^{\mathrm{r}}} + \overbrace{P}^{D^{i}} . \tag{4.28}$$

The reversible dielectric displacement field D^{r} contains the linear piezoelectric behavior, but now with an nonlinear piezoelectric modulus $e(P)$

$$e(P) = \sum_{n=0}^{N} \gamma_n \frac{P^n}{P_{\mathrm{s}}} e_{33} = f\left(P(t)\right), \tag{4.29}$$

which depends on the polarization P and on the linear piezoelectric modulus e_{33}. The irreversible dielectric displacement field D^{i} contains the ferroelectric effects, displayed in a hysteresis operator $P = \mathcal{H}[E]$. For the hysteresis operator the domain wall model (from section 3.1) is used. Similarly to the dielectric displacement field in eq. (4.28) the strain S is decomposed into a reversible part S^{r} and irreversible part S^{i}

$$S = S^{\mathrm{r}} + S^{\mathrm{i}}. \tag{4.30}$$

The reversible strain S^{r} contains the linear-elastic mechanical component of the strain, whereas $S^{\mathrm{i}} = f\left(P\right)$ models the irreversible strain caused by the polarization. To choose a more general approach a polynomial model with different parameters β_n is used [14]. The parameters have to be fitted to experimental data,

$$S^{\mathrm{i}} = \sum_{n=0}^{N} \beta_n P^n. \tag{4.31}$$

The irreversible strain seems to correspond with the quadratic function of the polarization [14] and for the considered case a quadratic function seems sufficient ($\beta_2 = 1$), leading to

Die approbierte gedruckte Originalversion dieser Diplomarbeit ist an der TU Wien Bibliothek verfügbar.
The approved original version of this thesis is available in print at TU Wien Bibliothek.
TU Bibliothek Your knowledge hub WIEN

$S^{\mathrm{i}} = \beta_2 P^2$. This definition of the irreversible strain is used in the following.

Inserting eq. (4.30) and eq. (4.29) in the mechanical material law eq. (4.24), one arrives the nonlinear mechanical-coupled constitutive law

$$\sigma = CS^{\mathrm{r}} - e(P)E. \tag{4.32}$$

The material law can also be written in compact matrix-vector denotation

$$\begin{bmatrix} \sigma \\ D \end{bmatrix} = \begin{bmatrix} C & -e(P) \\ e(P) & \epsilon_0 \end{bmatrix} \begin{bmatrix} S^{\mathrm{r}} \\ E \end{bmatrix} + \begin{bmatrix} 0 \\ P \end{bmatrix}. \tag{4.33}$$

Alternative form of the nonlinear constitutive law

A different way to write the nonlinear dielectric displacement field eq. (4.28) is to introduce a susceptibility $\chi(E)$, that allows to reformulate the polarization. Now the polarization is depended of the electric field E

$$P = \chi(E)E. \tag{4.34}$$

This leads to the following matrix-vector system

$$\begin{bmatrix} \sigma \\ D \end{bmatrix} = \begin{bmatrix} C & -e(P) \\ e(P) & \epsilon_0 + \chi(E) \end{bmatrix} \begin{bmatrix} S^{\mathrm{r}} \\ E \end{bmatrix}. \tag{4.35}$$

Due to the different structure of the matrix-vector system, this may be easier to solve.

Die approbierte gedruckte Originalversion dieser Diplomarbeit ist an der TU Wien Bibliothek verfügbar.
The approved original version of this thesis is available in print at TU Wien Bibliothek.
TU Bibliothek WIEN Your knowledge hub

Die approbierte gedruckte Originalversion dieser Diplomarbeit ist an der TU Wien Bibliothek verfügbar.
The approved original version of this thesis is available in print at TU Wien Bibliothek.

Chapter 5

Solution strategy

After deriving the equations for the one dimensional case, it is now time to think about how to solve these equations. Luckily the governing equation are fulfilled automatically for the piezoelectric model. Only the material law needs to be solved. In the first half of this chapter the main methods, the multiharmonic ansatz and harmonic balancing are introduced. In the second half several solution approaches are derived and explained.

5.1 Used methods

In this section the multiharmonic ansatz, which is a truncated Fourier series, gets explained. Some mathematical tricks for multiplying two or more Fourier series are shown and Harmonic Balancing will be introduced briefly.

5.1.1 Multiharmonic ansatz

A Fourier series of $c(t)$ is defined as

$$c(t) = \sum_{k=-\infty}^{\infty} \hat{c}_k e^{jk\omega t}. \tag{5.1}$$

with the frequency $\omega = 2\pi/T$ and j as the imaginary unit. The Fourier coefficients, the Fourier base functions and the harmonic index are denoted as $\hat{c}_k$, $e^{jk\omega t}$ and k, respectively [26]. One can imagine where the name multiharmonic ansatz comes from, because if the infinite Fourier series get truncated at N_h numbers of considered harmonics, the truncated Fourier series (or multiharmonic ansatz) is approximating the original function $c(t)$

$$c(t) = \sum_{k=-\infty}^{\infty} \hat{c}_k e^{jk\omega t} \approx c_{\text{approx}}(t) = \sum_{k=-N_\text{h}}^{N_\text{h}} \hat{c}_k e^{jk\omega t}. \tag{5.2}$$

Die approbierte gedruckte Originalversion dieser Diplomarbeit ist an der TU Wien Bibliothek verfügbar.
The approved original version of this thesis is available in print at TU Wien Bibliothek.
TU Bibliothek WIEN Your knowledge hub

The multiharmonic ansatz is a truncated Fourier series. The Fourier coefficients $\hat{c}_k$ are defined as

$$\hat{c}_k = \frac{1}{T}\int_0^T c(t)e^{jk\omega t}\mathrm{d}t \qquad k \in [-H, ...H]. \tag{5.3}$$

$c(t)$ is a real valued function, therefore it follows immedialty form eq. (5.3) that

$$\hat{c}_{-k} = \overline{\hat{c}_k} \qquad k \in [-H, ...H], \tag{5.4}$$

where $\overline{\hat{c}_k}$ is the complex conjugate of $\hat{c}_{-k}$.

Multiplying two Fourier series Let $f(t)$ and $g(t)$ be a periodic function, of same period and both can be displayed with a truncated Fourier series. Let $h(t)$ be the product of $f(t)$ and $g(t)$. For simplicity both signals consider the same number of Fourier series terms N

$$f(t) \approx \sum_{k=-N}^{N} \hat{f}_k\, e^{jk\omega t}, \tag{5.5}$$

$$g(t) \approx \sum_{l=-N}^{N} \hat{g}_l\, e^{jl\omega t} \tag{5.6}$$

and

$$h(t) = f(t)g(t) \approx \sum_{k=-N}^{N} \hat{f}_k\, e^{jk\omega t} \sum_{l=-N}^{N} \hat{g}_l\, e^{jl\omega t}. \tag{5.7}$$

Multiplying eq. (5.7) with $e^{-jn\omega t}$ and rearranging the sums results in

$$\sum_{k=-N}^{N} \hat{h}_k\, e^{j(k-n)\omega t} = \sum_{k=-N}^{N}\sum_{l=-N}^{N} \hat{f}_k\hat{g}_l\, e^{j(k+l-n)\omega t}. \tag{5.8}$$

Integrating over one period and multiplying with $\frac{\omega}{2\pi}$, exploiting the fact that

$$\int_0^{\frac{2\pi}{\omega}} e^{j(k-n)\omega t}dt = \delta_{kn} = \begin{cases} \frac{2\pi}{\omega}, \text{ if } k = n, \\ 0, \text{ if } k \neq n, \end{cases}, \tag{5.9}$$

respectively

$$\int_0^{\frac{2\pi}{\omega}} e^{j(k+l-n)\omega t}dt = \delta_{(k+l),n} = \begin{cases} \frac{2\pi}{\omega}, \text{ if } (k+l) = n, \\ 0, \text{ if } (k+l) \neq n, \end{cases}, \tag{5.10}$$

Die approbierte gedruckte Originalversion dieser Diplomarbeit ist an der TU Wien Bibliothek verfügbar.
The approved original version of this thesis is available in print at TU Wien Bibliothek.
TU Bibliothek WIEN Your knowledge hub

Equation (5.8) can be rewritten as a matrix vector system for N_h considered harmonics

$$\underbrace{\begin{pmatrix} \hat{h}_{-N_h} \\ \vdots \\ \hat{h}_{-1} \\ \hat{h}_0 \\ \hat{h}_1 \\ \vdots \\ \hat{h}_{N_h} \end{pmatrix}}_{\hat{\boldsymbol{h}}} = \underbrace{\begin{pmatrix} \hat{f}_0 & \hat{f}_{-1} & \cdots & \hat{f}_{-N_h} & & \\ \hat{f}_1 & \hat{f}_0 & \hat{f}_{-1} & & \ddots & \\ \vdots & & \hat{f}_0 & & & \hat{f}_{-N_h} \\ \hat{f}_{N_h} & & \ddots & & & \vdots \\ & \ddots & & & \hat{f}_0 & \hat{f}_{-1} \\ & & \hat{f}_{N_h} & \cdots & \hat{f}_1 & \hat{f}_0 \end{pmatrix}}_{\hat{\underset{\sim}{\boldsymbol{f}}}} \underbrace{\begin{pmatrix} \hat{g}_{-N_h} \\ \vdots \\ \hat{g}_{-1} \\ \hat{g}_0 \\ \hat{g}_1 \\ \vdots \\ \hat{g}_{N_h} \end{pmatrix}}_{\hat{\boldsymbol{g}}}. \tag{5.11}$$

Equation (5.11) can also written in compact form as

$$\hat{\boldsymbol{h}} = \hat{\underset{\sim}{\boldsymbol{f}}}\hat{\boldsymbol{g}}, \tag{5.12}$$

where $\hat{\underset{\sim}{\boldsymbol{f}}}$ is now a matrix

$$\hat{\underset{\sim}{\boldsymbol{f}}} = \begin{pmatrix} \hat{f}_0 & \hat{f}_{-1} & \cdots & \hat{f}_{-N_h} & & \\ \hat{f}_1 & \hat{f}_0 & \hat{f}_{-1} & & \ddots & \\ \vdots & & \hat{f}_0 & & & \hat{f}_{-N_h} \\ \hat{f}_{N_h} & & \ddots & & & \vdots \\ & \ddots & & & \hat{f}_0 & \hat{f}_{-1} \\ & & \hat{f}_{N_h} & \cdots & \hat{f}_1 & \hat{f}_0 \end{pmatrix}. \tag{5.13}$$

And $h(t)$ can now be approximated and rewritten as follows

$$h(t) \approx h_{N_h}(t) = \mathcal{F}^{-1}(\hat{\boldsymbol{h}}) = \mathcal{F}^{-1}(\hat{\underset{\sim}{\boldsymbol{f}}}\hat{\boldsymbol{g}}). \tag{5.14}$$

$\mathcal{F}^{-1}$ denotes the inverse Fourier transformation.

Multiplying three Fourier series The idea is to use the associative property of multiplication for functions. The product of multiple time dependent functions can be approximated by a truncated Fourier series

$$k(t) = f(t)h(t)g(t), \tag{5.15}$$

$$\hat{\boldsymbol{k}} = \mathcal{F}\left\{k(t)\right\}. \tag{5.16}$$

The time dependent functions can be independently approximated with a truncated Fourier series.

$$\hat{\underset{\sim}{\boldsymbol{g}}}\hat{\boldsymbol{h}} = \mathcal{F}\left\{g(t)h(t)\right\}, \tag{5.17}$$

Die approbierte gedruckte Originalversion dieser Diplomarbeit ist an der TU Wien Bibliothek verfügbar.
The approved original version of this thesis is available in print at TU Wien Bibliothek.
TU Bibliothek Your knowledge hub WIEN

$$\hat{\boldsymbol{f}} = \mathcal{F}\left\{f(t)\right\}, \tag{5.18}$$

The product of these Fourier coefficients should be similar to the Fourier coefficients of the first product regardless of the permutation of the multiplication

$$\hat{\boldsymbol{k}} \approx \hat{\underset{\sim}{\boldsymbol{f}}}(\hat{\underset{\sim}{\boldsymbol{g}}}\hat{\boldsymbol{h}}) \approx \hat{\underset{\sim}{\boldsymbol{h}}}(\hat{\underset{\sim}{\boldsymbol{f}}}\hat{\boldsymbol{g}}) \approx \dots . \tag{5.19}$$

This was only tested numerically and the results are converging to the exact value for increasing numbers of considered harmonics.

5.1.2 Harmonic balancing

Another essential method beside the multiharmonic ansatz in this thesis, is the so called harmonic balancing (HB).

It is widely used in electric engineering [27], but is used for mechanical problems as well [26]. The underlying principle idea behind HB is, to solve as much as possible in the frequency domain, in order to reduce computational effort. Only the non-linearities which can't be evaluated in the frequency domain are evaluated in the time domain, and then approximated as a truncated Fourier series. But the system is solved in the frequency domain as shown schematically in Fig. 5.1.

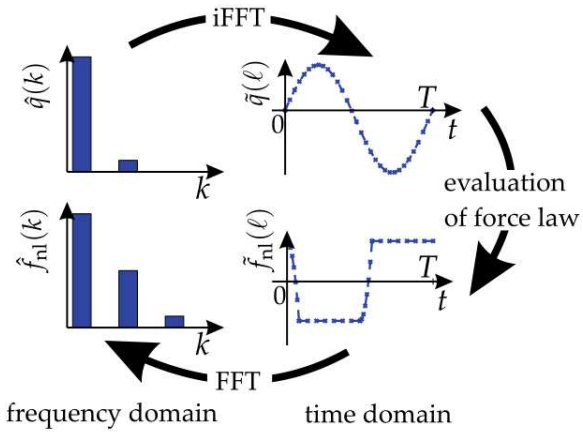

Figure 5.1: Schematic work flow of harmonic balancing: the evaluation of the (nonlinear) force law takes place in the time domain, is then transferred into the frequency domain, where the harmonics are balanced, then transferred back to the time domain, and the circle starts again, until the approximation error is small enough. Figure from [26].

This method can only be used for periodic or quasi-periodic steady state solutions [28], since the variables are represented with Fourier series. Variables with a fast time variation can be challenging to represent in a sinusoidal base, therefore the application of harmonic balancing is limited to relatively mild nonlinear regimes [28]. In practice the Fourier series

Die approbierte gedruckte Originalversion dieser Diplomarbeit ist an der TU Wien Bibliothek verfügbar.
The approved original version of this thesis is available in print at TU Wien Bibliothek.
TU Bibliothek WIEN Your knowledge hub

must be truncated to a finite numbers of harmonics N_h in order to be computationally affordable. A truncated Fourier series might not be convenient for some periodic signals with low rise and fall times [28]. If small numbers of considered harmonics are used an artificial ringing can occur, which can be related to the Gibbs phenomenon [29].

Harmonic balance equations [26] One wants to find an approximated T-periodic solution $\boldsymbol{q}_{N_h}(t, \hat{\boldsymbol{q}}) \approx \boldsymbol{q}(t)$ in the form of a multiharmonic ansatz,

$$\boldsymbol{q}_{N_h}(t, \hat{\boldsymbol{q}}) = \sum_{k=-N_h}^{N_h} \hat{q}_k \, e^{jk\omega t}. \tag{5.20}$$

Lets introduce a new variable $\boldsymbol{r}$

$$\boldsymbol{r}(\boldsymbol{q}, \dot{\boldsymbol{q}}, \ddot{\boldsymbol{q}}, t) = \boldsymbol{f}_{\text{lin}}(\boldsymbol{q}, \dot{\boldsymbol{q}}, \ddot{\boldsymbol{q}}, t) + \boldsymbol{f}_{\text{nl}}(\boldsymbol{q}, \dot{\boldsymbol{q}}, \ddot{\boldsymbol{q}}, t) - \boldsymbol{f}_{\text{ex}}(t), \tag{5.21}$$

called the residuum of the system. $\boldsymbol{f}_{\text{lin}}$, $\boldsymbol{f}_{\text{nl}}$ and $\boldsymbol{f}_{\text{ext}}$ are the linear, nonlinear and external terms of the system, respectively. After applying the multiharmonic ansatz to each term in eq. (5.21) the coefficients of the truncated residuum can be written as

$$\hat{\boldsymbol{r}}_{N_h} = \hat{\boldsymbol{f}}_{\text{lin},N_h} + \hat{\boldsymbol{f}}_{\text{nl},N_h} - \hat{\boldsymbol{f}}_{\text{ex},N_h}. \tag{5.22}$$

Harmonic Balancing requires that the Fourier coefficients of the residuum $\boldsymbol{r}$ vanishes

$$\boldsymbol{r} \approx \hat{\boldsymbol{r}}_{N_h} = \sum_{k=-N_h}^{N_h} \hat{r}_k \, e^{jk\omega t} = \begin{pmatrix} \hat{r}_{-N_h} \\ \vdots \\ \hat{r}_{-1} \\ \hat{r}_0 \\ \hat{r}_1 \\ \vdots \\ \hat{r}_{N_h} \end{pmatrix} = \boldsymbol{0}. \tag{5.23}$$

It is possible for some iterative schemes that the requirement of HB, stated in eq. (5.23), is too strict. Therefore to save computational effort the requirements are relaxed. For the residuum approach, explained in section 5.2, the L_2-Norm of the residuum coefficients $\|\hat{\boldsymbol{r}}\|$ have to be lower than a certain threshold $\epsilon \geq 0$

$$\|\hat{\boldsymbol{r}}\| < \epsilon. \tag{5.24}$$

Die approbierte gedruckte Originalversion dieser Diplomarbeit ist an der TU Wien Bibliothek verfügbar.
The approved original version of this thesis is available in print at TU Wien Bibliothek.
TU Bibliothek Your knowledge hub WIEN

5.1.3 Notation explanation

In the following a few different notations will be used. For clarification and as a short overview all different notations of variables used will be explained briefly.

Scalar: A scalar is a value at a certain time or just a constant parameter and is denoted as

$$a = a_{t_i}. \tag{5.25}$$

Time-Vector: A time vector contains for each time step a scalar value and is noted as

$$\boldsymbol{a} = a(t) = \begin{pmatrix} {}^{t_0}a \\ {}^{t_1}a \\ {}^{t_2}a \\ \vdots \\ {}^{t_{n-2}}a \\ {}^{t_{n-1}}a \\ {}^{t_n}a \end{pmatrix}. \tag{5.26}$$

Diagonal matrix: A diagonal matrix with only real values is denoted as

$$\underset{\sim}{a} = a\underset{\sim}{\boldsymbol{I}} = \begin{pmatrix} a & 0 & 0 & \cdots & 0 \\ & a & 0 & \ddots & \vdots \\ & & \ddots & \ddots & 0 \\ & & & a & 0 \\ & & & & a \end{pmatrix}, \tag{5.27}$$

with $\underset{\sim}{\boldsymbol{I}}$ as identity matrix. If a scalar is multiplied with a time vector in the time domain, the scalar becomes a diagonal matrix in the frequency domain for a correct multiplication,

$$\mathcal{F}\left\{af(t)\right\} = \mathcal{F}\left\{a\boldsymbol{f}\right\} = \underset{\sim}{a}\hat{\boldsymbol{f}}. \tag{5.28}$$

Fourier coefficient vector: A periodic time vector can be displayed in the frequency domain as Fourier coefficient vector. The hat indicates that it contains complex valued

Die approbierte gedruckte Originalversion dieser Diplomarbeit ist an der TU Wien Bibliothek verfügbar.
The approved original version of this thesis is available in print at TU Wien Bibliothek.
TU Bibliothek Your knowledge hub WIEN

components. Its denoted as

$$\mathcal{F}\{\boldsymbol{a}\} = \hat{\boldsymbol{a}} = \begin{pmatrix} \hat{a}_{-N_h} \\ \vdots \\ \hat{a}_{-1} \\ \hat{a}_0 \\ \hat{a}_1 \\ \vdots \\ \hat{a}_{N_h} \end{pmatrix}. \tag{5.29}$$

Fourier coefficient matrix: If two Fourier series get multiplied in the frequency domain, one Fourier coefficient vector must be transformed into a Fourier coefficient matrix, which is denoted as follows

$$\underset{\sim}{\hat{\boldsymbol{a}}} = \begin{pmatrix} \hat{a}_0 & \hat{a}_{-1} & \cdots & \hat{a}_{-N_h} & & \\ \hat{a}_1 & \hat{a}_0 & \hat{a}_{-1} & & \ddots & \\ \vdots & & \hat{a}_0 & & & \hat{a}_{-N_h} \\ \hat{a}_{N_h} & & \ddots & & & \vdots \\ & \ddots & & & \hat{a}_0 & \hat{a}_{-1} \\ & & \hat{a}_{N_h} & \cdots & \hat{a}_1 & \hat{a}_0 \end{pmatrix}. \tag{5.30}$$

5.2 r-Approach (algorithm 1)

Now, prepared with the multiharmonic ansatz and harmonic balancing, it is possible to construct a solution algorithm for a quasi-periodic steady state solution of the piezoelectric-mechanical coupled system for ferroelectric materials.

Reducing the system

The coupled constitutive law in e-form can be written as vector-matrix system

$$\begin{bmatrix} \sigma \\ D \end{bmatrix} = \begin{bmatrix} C & -e(P) \\ e(P) & \epsilon_0 \end{bmatrix} \begin{bmatrix} S^{\mathrm{r}} \\ E \end{bmatrix} + \begin{bmatrix} 0 \\ P(E) \end{bmatrix}. \tag{5.31}$$

Note that each scalar in these equations is representing one value of a time vector. It contains two coupled equations with two unknowns, the reversible strain S^{r} and electric field E. Since this model is controlled by mechanical force and electric charges the variables $\sigma = \mathrm{f}/A$ and $D = Q/A$ are known. The polarization P and the variable piezoelectric couple-tensor $e(P)$ are a function of E. The variable piezoelectric coupling-tensor

Die approbierte gedruckte Originalversion dieser Diplomarbeit ist an der TU Wien Bibliothek verfügbar.
The approved original version of this thesis is available in print at TU Wien Bibliothek.
TU Bibliothek WIEN Your knowledge hub

is defined for this approach as follows

$$e(t) = \frac{P(t)}{P_{\mathrm{s}}} e_{33}. \tag{5.32}$$

Because only two unknown variables are in eq. (5.1) and it contains two equations,

$$\sigma = CS^{\mathrm{r}} - e(P)E, \tag{5.33}$$

and

$$D = e(P)S^{\mathrm{r}} + \epsilon_0 E + P(E), \tag{5.34}$$

it can be reduced to one equation. Therefore S^{r} from eq. (5.33) can be expressed as

$$S^{\mathrm{r}} = \frac{1}{C}\left(\sigma + e(P)E\right) \tag{5.35}$$

and inserted in eq. (5.34) to obtain this equation

$$D = e(P)\overbrace{\left[\frac{1}{C}\left(\sigma + e(P)E\right)\right]}^{eq.\ (5.35)} + \epsilon_0 E + P(E). \tag{5.36}$$

which is now only dependent on the electric field E.

Multiharmonic approach and harmonic balancing

Equation (5.36) is multiplied out

$$D = e(P)\frac{1}{C}\sigma + \frac{1}{C}e(P)e(P)E + \epsilon_0 E + P(E), \tag{5.37}$$

and the multiharmonic ansatz for N_h harmonics is applied for every time dependent variable (D, E, $e(P)$, $P(E)$) and is resulting in

$$\hat{\boldsymbol{D}} = \frac{1}{C}\hat{\underset{\sim}{\boldsymbol{e}}}\hat{\boldsymbol{\sigma}} + \frac{1}{C}\hat{\underset{\sim}{\boldsymbol{e}}}\hat{\underset{\sim}{\boldsymbol{e}}}\hat{\boldsymbol{E}} + \epsilon_0\hat{\boldsymbol{E}} + \hat{\boldsymbol{P}}. \tag{5.38}$$

Equation (5.38) is the equation which needs to be solved.

Residuum based fix point iteration

Now lets define the residuum as

$$\hat{\boldsymbol{r}} = \frac{1}{C}\hat{\underset{\sim}{\boldsymbol{e}}}\hat{\boldsymbol{\sigma}} + \frac{1}{C}\hat{\underset{\sim}{\boldsymbol{e}}}\hat{\underset{\sim}{\boldsymbol{e}}}\hat{\boldsymbol{E}} + \epsilon_0\hat{\boldsymbol{E}} + \hat{\boldsymbol{P}} - \hat{\boldsymbol{D}}. \tag{5.39}$$

Die approbierte gedruckte Originalversion dieser Diplomarbeit ist an der TU Wien Bibliothek verfügbar.
The approved original version of this thesis is available in print at TU Wien Bibliothek.
TU Bibliothek Your knowledge hub WIEN

The residuum is used for the fix-point iteration in the frequency domain and the new Fourier coefficients of the electric field are calculated as followed, where the index k denotes the iteration step

$$^{k+1}\hat{\boldsymbol{E}} = f(^{k}\hat{\boldsymbol{E}}) = {}^{k}\hat{\boldsymbol{E}} + \eta\, {}^{k}\hat{\boldsymbol{r}}. \tag{5.40}$$

To update the Fourier coefficients of the electric field a relaxation parameter η is introduced.

Short overview of the iteration scheme

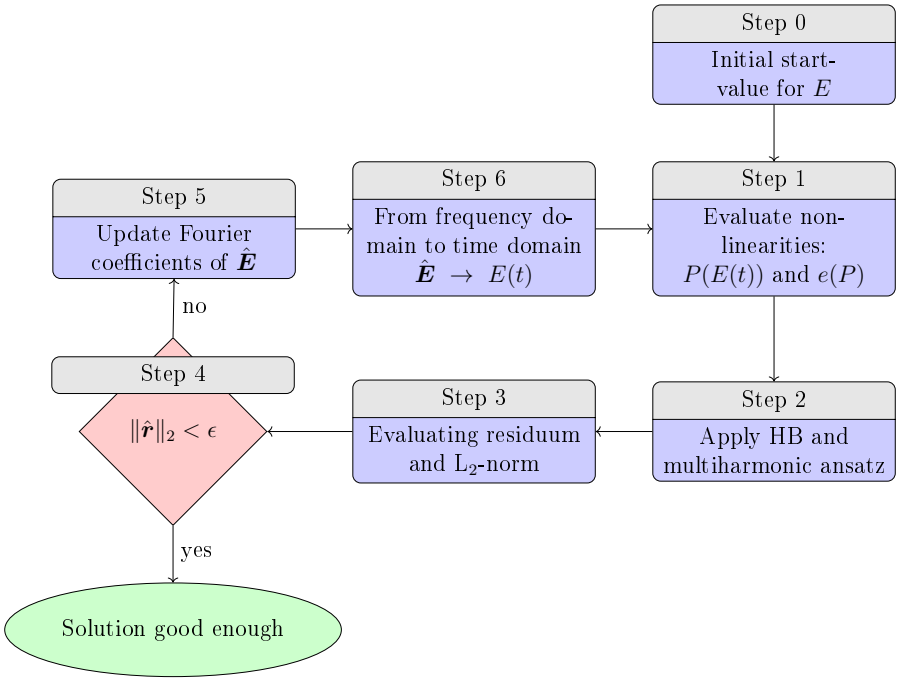

Figure 5.2: Flow chart of the r-approach.

The flowchart of the used solution algorithm is displayed in Figure 5.2. It can be roughly divided into seven steps, which are explained briefly.

- **Initial step** As a initial step a start value of the electric field is needed. This start value can be obtained for example from solving the linear system.
- **Evaluating nonlinear terms** The next step is to evaluate the polarization and the variable piezoelectric modulus in the time domain.
- **Multiharmonic ansatz and harmonic balancing** Now the system is transferred into the frequency domain via fast Fourier transformation (FFT), using the multiharmonic ansatz and harmonic balancing. The Fourier series gets truncated to N_h terms, which is equivalent to $2N_h + 1$ Fourier coefficients.

Die approbierte gedruckte Originalversion dieser Diplomarbeit ist an der TU Wien Bibliothek verfügbar.
The approved original version of this thesis is available in print at TU Wien Bibliothek.
TU Bibliothek Your knowledge hub WIEN

- **Evaluating the residuum** In this step the Fourier coefficients of residuum and the L_2-Norm of the Fourier coefficients of the residuum are calculated.
- **Checking stop criteria** If the L_2-norm is smaller than a certain threshold, the iteration is stopped and the solution is accurate enough.
- **Updating $\hat{\boldsymbol{E}}$** Now the Fourier coefficient of the electric field are updated according to the described fix-point iteration.
- **Transformation in time domain** All necessary variables are transformed back into the time domain in order to evaluate the non linearities again.
- $\cdots$ start the iteration from the beginning until stop criteria is met.

5.3 E-S-Approach (algorithm 2)

Instead of reducing the coupled material law eq. (5.31) the linear system is solved to obtain the unknowns

$$\begin{bmatrix} S^{\mathrm{r}} \\ E \end{bmatrix} = \begin{bmatrix} C & -e(P) \\ e(P) & \epsilon_0 \end{bmatrix}^{-1} \begin{bmatrix} \sigma \\ D - P \end{bmatrix}, \tag{5.41}$$

in order to get the electric field E and reversible strain S^{r}. The piezoelectric modulus is defined different as in eq. (5.32)

$$e(P) = \frac{1}{8}\frac{P}{P_{\mathrm{s}}}e_{33} + \frac{7}{8}e_{33}. \tag{5.42}$$

Because if the modulus $e(P)$ is strongly nonlinear, this approach diverges. Since only periodic variables are considered, the multiharmonic ansatz and harmonic balancing can be applied to eq. (5.41) as shown in section 5.1 and are leading to a fix point iteration in the frequency domain.

Applying multiharmonic ansatz and harmonic balancing

In eq. (5.41) the material law is written in the time domain for one time step with the reversible strain S^{r}, the electric field E, the dielectric displacement field D, the mechanical stress σ, the polarization P and the variable piezo modulus e as time dependent variable (the variable piezeo modulus could also be a constant, in this case it would be not dependent on time). For all time dependent periodic variable the multiharmonic ansatz is applied with N_h harmonics and Harmonic Balancing is done. This results in a fix point scheme for the frequency domain

$$\begin{bmatrix} {}^{k+1}\hat{\boldsymbol{S}}^{\mathrm{r}} \\ {}^{k+1}\hat{\boldsymbol{E}} \end{bmatrix} = \begin{bmatrix} \underset{\sim}{C} & -{}^{k}\hat{\underset{\sim}{\boldsymbol{e}}} \\ {}^{k}\hat{\underset{\sim}{\boldsymbol{e}}} & \underset{\sim}{\epsilon}_0 \end{bmatrix}^{-1} \begin{bmatrix} {}^{k+1}\hat{\boldsymbol{\sigma}} \\ {}^{k+1}\hat{\boldsymbol{D}} - {}^{k}\hat{\boldsymbol{P}} \end{bmatrix} = f\left(\begin{bmatrix} {}^{k}\hat{\boldsymbol{S}}^{\mathrm{r}} \\ {}^{k}\hat{\boldsymbol{E}} \end{bmatrix}\right). \tag{5.43}$$

Die approbierte gedruckte Originalversion dieser Diplomarbeit ist an der TU Wien Bibliothek verfügbar.
The approved original version of this thesis is available in print at TU Wien Bibliothek.
TU Bibliothek Your knowledge hub WIEN

The scalar stiffness tensor C and the scalar permittivity tensor ϵ_0 are now written as a diagonal matrix with the shape of $N_h \times N_h$ in order to multiply each Fourier coefficient with the scalar value.

$$\underset{\sim}{C} = C\underset{\sim}{\boldsymbol{I}} \begin{pmatrix} C & 0 & 0 & \cdots & 0 \\ & C & 0 & \ddots & \vdots \\ & & \ddots & \ddots & 0 \\ & & & C & 0 \\ & & & & C \end{pmatrix}, \tag{5.44}$$

$$\underset{\sim}{\epsilon}_0 = \epsilon_0 \underset{\sim}{\boldsymbol{I}} = \begin{pmatrix} \epsilon_0 & 0 & 0 & \cdots & 0 \\ & \epsilon_0 & 0 & \ddots & \vdots \\ & & \ddots & \ddots & 0 \\ & & & \epsilon_0 & 0 \\ & & & & \epsilon_0 \end{pmatrix}, \tag{5.45}$$

The variable piezo moduli is now a $N_h \times N_h$-matrix, to allow correct Fourier coefficient multiplication

$$\underset{\sim}{\hat{\boldsymbol{e}}} = \begin{pmatrix} \hat{e}_0 & \hat{e}_{-1} & \cdots & \hat{e}_{-N_h} & & \\ \hat{e}_1 & \hat{e}_0 & \hat{f}_{-1} & & \ddots & \\ \vdots & & \hat{e}_0 & & & \hat{e}_{-N_h} \\ \hat{e}_{N_h} & & & \ddots & & \vdots \\ & \ddots & & & \hat{e}_0 & \hat{e}_{-1} \\ & & \hat{e}_{N_h} & \cdots & \hat{e}_1 & \hat{e}_0 \end{pmatrix}, \tag{5.46}$$

and the Fourier coefficient vectors ${}^{k+1}\hat{\boldsymbol{S}}^{\mathrm{r}}$, ${}^{k+1}\hat{\boldsymbol{E}}$, ${}^{k+1}\hat{\boldsymbol{\sigma}}$, ${}^{k+1}\hat{\boldsymbol{D}}$ and ${}^{k}\hat{\boldsymbol{P}}$ are a vector of N_h rows, in form of

$$\hat{\boldsymbol{h}} = \begin{pmatrix} \hat{h}_{-N_h} \\ \vdots \\ \hat{h}_{-1} \\ \hat{h}_0 \\ \hat{h}_1 \\ \vdots \\ \hat{h}_{N_h} \end{pmatrix}. \tag{5.47}$$

Variable piezoelectric modulus versus constant piezoelectric modulus

If variable piezoelectric modulus e is chosen, two Fourier series are multiplied in eq. (5.43). If a constant piezoelectric modulus is assumed, this approach does not multiply two or more Fourier series, because the scalar constant piezoelectric modulus would get a $N_h \times N_h$

Die approbierte gedruckte Originalversion dieser Diplomarbeit ist an der TU Wien Bibliothek verfügbar.
The approved original version of this thesis is available in print at TU Wien Bibliothek.
TU Bibliothek Your knowledge hub WIEN

diagonal matrix

$$\underset{\sim}{e} = \begin{pmatrix} e & 0 & 0 & \cdots & 0 \\ & e & 0 & \ddots & \vdots \\ & & \ddots & \ddots & 0 \\ & & & e & 0 \\ & & & & e \end{pmatrix}, \tag{5.48}$$

resulting in this system

$$\begin{bmatrix} {}^{k+1}\hat{\boldsymbol{S}}^{\mathrm{r}} \\ {}^{k+1}\hat{\boldsymbol{E}} \end{bmatrix} = \underbrace{\begin{bmatrix} \underset{\sim}{C} & -\underset{\sim}{e} \\ \underset{\sim}{e} & \underset{\sim}{\epsilon}_0 \end{bmatrix}}_{\underset{\sim}{M}}^{-1} \begin{bmatrix} {}^{k+1}\hat{\boldsymbol{\sigma}} \\ {}^{k+1}\hat{\boldsymbol{D}} - {}^{k}\hat{\boldsymbol{P}} \end{bmatrix}, \tag{5.49}$$

where the system matrix $\underset{\sim}{M}$ is only composed out of constant diagonal matrices.

Short overview of the iteration scheme

The flow chart of the second solution algorithm is displayed in Fig. 5.3. There are mainly five steps:

- **Initial step** Starting with a initial estimation
- **Multiharmonic ansatz and harmonic balancing** Applying the mutliharmonic ansatz to every time dependent variable and harmonic balancing to the system.
- **Solve the system** Solve the system (eq. (5.43)) for the next strain and electric field.
- **Stop criteria** See if stop criteria is met. If yes, solution is good enough. If not go to the next step.
- **Update nonlinear terms** Evaluate the nonlinear term with the new solution in the time domain.

5.4 χ-Approach (algorithm 3)

In this section a different approach, regarding the polarization is used. Instead of writing the coupled material law as previously in eq. (5.31), the coupled material law is reformulated

$$\begin{bmatrix} \sigma \\ D \end{bmatrix} = \begin{bmatrix} C & -e(P) \\ e(P) & \epsilon_0 + \chi(E) \end{bmatrix} \begin{bmatrix} S^{\mathrm{r}} \\ E \end{bmatrix}. \tag{5.50}$$

Die approbierte gedruckte Originalversion dieser Diplomarbeit ist an der TU Wien Bibliothek verfügbar.
The approved original version of this thesis is available in print at TU Wien Bibliothek.
TU Bibliothek WIEN Your knowledge hub

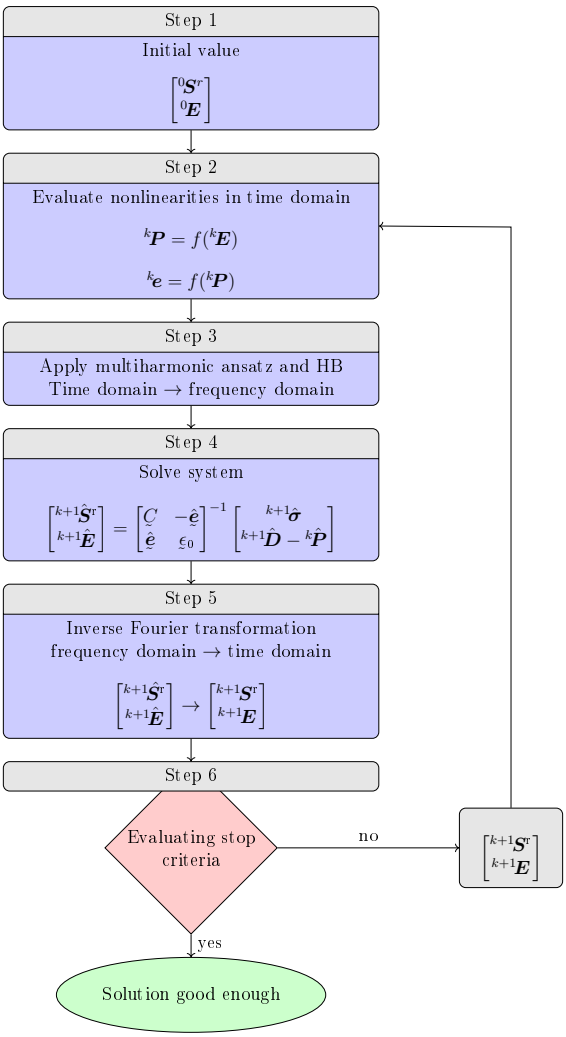

Figure 5.3: Flow chart of the E-S-approach.

In eq. (5.50) the susceptibility χ is introduced. It is defined as

$$P = \chi E \tag{5.51}$$

To calculate χ one has to divide the polarization by the the electric field

$$\chi(E) = \frac{P(E)}{E}. \tag{5.52}$$

This can result in a division by zero, because the electric field can be positive or negative, including zero. To avoid this division by zero, lets do a variable transformation of the electric field by introducing E^*, which can not be zero anymore and is defined as

$$E^* = E + \underbrace{\kappa|E_{\max} - E_{\min}|}_{E_{\text{off}}} \text{ and } \kappa > 1. \tag{5.53}$$

Die approbierte gedruckte Originalversion dieser Diplomarbeit ist an der TU Wien Bibliothek verfügbar.
The approved original version of this thesis is available in print at TU Wien Bibliothek.
TU Bibliothek Your knowledge hub WIEN

With this new electric field E^*, which is the electric field E with an offset

$$E_{\text{off}} = \kappa |E_{\max} - E_{\min}| = \text{const.}\,, \tag{5.54}$$

one can calculate χ^*

$$\chi^*(E, E^*) = \frac{P(E)}{E^*} = f(E, E^*). \tag{5.55}$$

Please note that χ^* is now a function of the original electric field E and the transformed electric field E^*. The polarization is still evaluated with the original electric field E,

$$P = f(E) = f(E^* - E_{\text{off}}), \tag{5.56}$$

because the polarization is described by the hysteresis operator $\mathcal{H}[E]$ and a different electric field would result in a different polarization. The piezoelectric modulus is defined as in eq. (5.42), because if the piezoelectric modulus $e(P)$ is strongly nonlinear this approach diverges. Lets now write the material law eq. (5.50) with the new χ^* from eq. (5.55) and the new electric field from eq. (5.53) resulting in

$$\begin{bmatrix} \sigma \\ D \end{bmatrix} = \begin{bmatrix} C & -e(P) \\ e(P) & \epsilon_0 + \chi^*(E, E^*) \end{bmatrix} \begin{bmatrix} S^{\text{r}} \\ E^* \end{bmatrix}. \tag{5.57}$$

Equation (5.57) and Equation (5.50) are not equal. To be equal on must add one term to eq. (5.57) resulting in

$$\begin{bmatrix} \sigma \\ D \end{bmatrix} = \begin{bmatrix} C & -e(P) \\ e(P) & \epsilon_0 + \chi^*(E, E^*) \end{bmatrix} \begin{bmatrix} S^{\text{r}} \\ E^* \end{bmatrix} + \begin{bmatrix} e(P)E_{\text{off}} \\ -\epsilon_0 E_{\text{off}} \end{bmatrix}. \tag{5.58}$$

For a better understanding eq. (5.57) and eq. (5.58) are multiplied out and set equal

$$\sigma = CS^{\text{r}} - e(P)E = CS^{\text{r}} \overbrace{-e(P)E^* + e(P)E_{\text{off}}}^{-e(P)E}\,, \tag{5.59}$$

$$D = e(P)S^{\text{r}} + \epsilon_0 E + \underbrace{\chi(E)E}_{P(E)} = e(P)S^{\text{r}} + \underbrace{\epsilon_0 E^*}_{\epsilon_0 E + \epsilon_0 E_{\text{off}}} + \underbrace{\chi^*(E)E^*}_{P(E)} - \epsilon_0 E_{\text{off}} \tag{5.60}$$

Reformulating eq. (5.58) results in this vector matrix system

$$\begin{bmatrix} \sigma - e(P)E_{\text{off}} \\ D + \epsilon_0 E_{\text{off}} \end{bmatrix} = \begin{bmatrix} C & -e(P) \\ e(P) & \epsilon_0 + \chi^*(E, E^*) \end{bmatrix} \begin{bmatrix} S^{\text{r}} \\ E^* \end{bmatrix}. \tag{5.61}$$

Die approbierte gedruckte Originalversion dieser Diplomarbeit ist an der TU Wien Bibliothek verfügbar.
The approved original version of this thesis is available in print at TU Wien Bibliothek.
TU Bibliothek Your knowledge hub WIEN

Now solve the linear system eq. (5.61) to obtain the unknown quantities

$$\begin{bmatrix} S^{\mathrm{r}} \\ E^{*} \end{bmatrix} = \begin{bmatrix} C & -e(P) \\ e(P) & \epsilon_0 + \chi^{*}(E,E^{*}) \end{bmatrix}^{-1} \begin{bmatrix} \sigma - e(P)E_{\mathrm{off}} \\ D + \epsilon_0 E_{\mathrm{off}} \end{bmatrix}. \tag{5.62}$$

Applying multiharmonic ansatz and harmonic balancing

After deriving a solution in eq. (5.62) for scalar values, lets change the scalars with periodic time functions and apply the multiharmonic ansatz and haromonic balancing on it. This results in this fix point iteration, where the index k denotes the iteration step

$$\begin{bmatrix} {}^{k+1}\hat{\boldsymbol{S}}^{\mathrm{r}} \\ {}^{k+1}\hat{\boldsymbol{E}}^{*} \end{bmatrix} = \begin{bmatrix} \underset{\sim}{C} & -{}^{k}\hat{\underset{\sim}{e}} \\ {}^{k}\hat{\underset{\sim}{e}} & \underset{\sim}{\epsilon}_0 + {}^{k}\hat{\underset{\sim}{\chi}}^{*} \end{bmatrix}^{-1} \begin{bmatrix} {}^{k+1}\hat{\boldsymbol{\sigma}} - {}^{k}\hat{\underset{\sim}{e}}\,{}^{k}\hat{\boldsymbol{E}}_{\mathrm{off}} \\ {}^{k+1}\hat{\boldsymbol{D}} + \underset{\sim}{\epsilon}_0\,{}^{k}\hat{\boldsymbol{E}}_{\mathrm{off}} \end{bmatrix}. \tag{5.63}$$

Short overview of the iteration scheme

The scheme is graphically displayed in Fig. 5.4.

- **Initial starting guess** Starting which initial values for strain and electric field.
- **Evaluate polarization** Calculate the polarization out of the electric field.
- **Variable transformation** Transform the electric field $\boldsymbol{E}$ to $\boldsymbol{E}^{*}$.
- **Evaluate χ^{*}** Evalute χ^{*} out of the polarization and the transformed electric field.
- **Apply multiharmonic ansatz and HB** Apply multiharmonic ansatz and harmonic balance for the transformed system.
- **Solve transformed system** Solve the transformed system in the frequency domain.
- **Inverse Fourier transformation** Getting the transformed electric field for the time domain.
- **Inverse variable transformation** Transform back to the initial electric field.
- **Check stop criteria** Check if stop criteria is fulfilled, if not go back to the second step and continue.

Die approbierte gedruckte Originalversion dieser Diplomarbeit ist an der TU Wien Bibliothek verfügbar.
The approved original version of this thesis is available in print at TU Wien Bibliothek.
TU Bibliothek Your knowledge hub WIEN

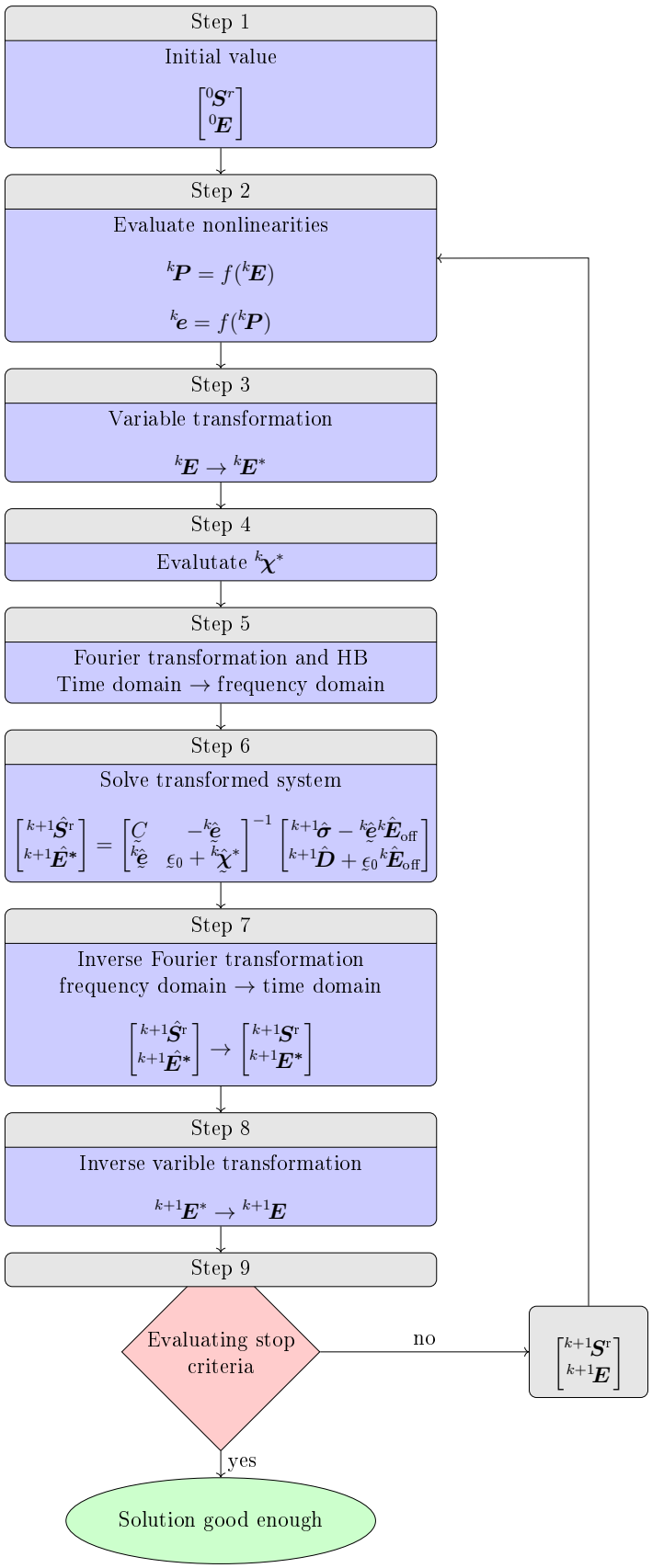

Figure 5.4: Flow chart of the χ-approach.

Die approbierte gedruckte Originalversion dieser Diplomarbeit ist an der TU Wien Bibliothek verfügbar.
The approved original version of this thesis is available in print at TU Wien Bibliothek.
TU Bibliothek Your knowledge hub WIEN

Chapter 6

Results and discussion

The following chapter will present the results of the different approaches and includes the discussion. The results of the algorithms are purely qualitative, since no experimental data is used for parameter fitting. All parameters used for this simulation are shown in the Appendix A in table A.1 and table A.2.

In the beginning the results of the domain wall model for ferroelectric behavior are shown. Afterwards the ferroelastic hysteresis is briefly shown. In the next section the general behavior of the nonlinear piezoelectric coupled system is presented and discussed. For visualizing the general physical behavior the first algorithm is used (r-approach). This algorithm is the only approach which can handle bipolar loading cycles and a fully nonlinear coupling tensor. However in the following section the results of all the approaches (r-approach, E-S-approach and χ-approach) are compared. In the end of this chapter the performance of the different approaches are analyzed and interpreted.

6.1 Ferroelectric hysteresis

This section will display the behavior and results of the hysteresis model from section 3.1. As previously mentioned, the polarization model is based on the domain wall theory for ferroelectric materials [25], which was first established by Jiles and Artherton [11]. The hysteretic behavior is described by a differential equation, which is solved with a finite difference method in the time domain.

6.1.1 Bipolar voltage excitation

This model is voltage driven, therefore it gets excited with a sinusoidal electric field

$$E = 2 \cdot 10^7 \sin(2\pi f t) \text{ V/m}, \tag{6.1}$$

Die approbierte gedruckte Originalversion dieser Diplomarbeit ist an der TU Wien Bibliothek verfügbar.
The approved original version of this thesis is available in print at TU Wien Bibliothek.
TU Bibliothek Your knowledge hub WIEN

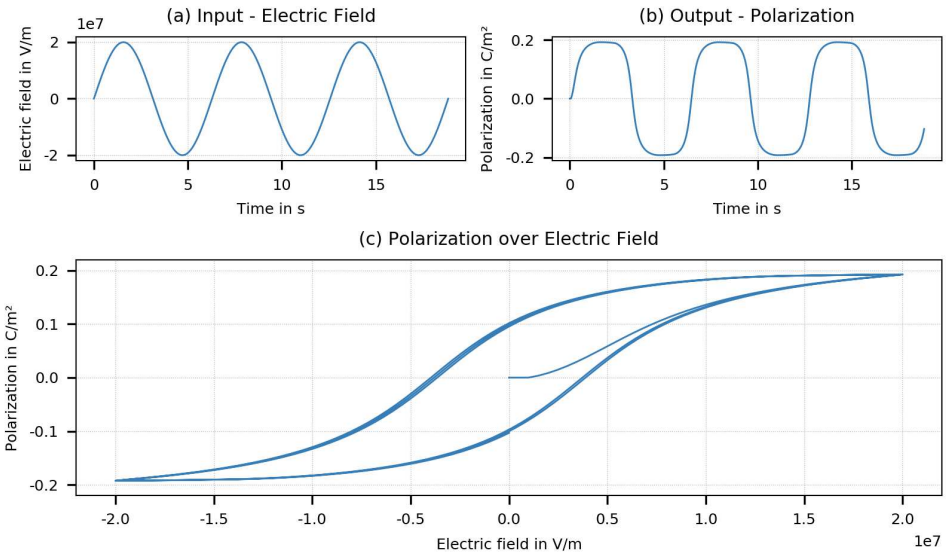

Figure 6.1: Full hysteresis for $E = 2 \cdot 10^7 \sin(2\pi f t)$. In (a) the electric field in V/m as input quantity. In (b) the outcome, the polarization in C/m^2 is plotted over the time. In (c) the polarization over the electric field is displayed, forming a full hysteresis loop.

which is displayed in Fig. 6.1(a). The outcome of the applied electric field is a polarization, which is displayed in Fig. 6.1(b). The electric field can increase or decrease the polarization.

As shown in Fig. 6.1(c) the polarization hysteresis starts at a non-polarized state, with a overall net polarization of zero. When applying an electric field for the first time an initial polarization curve appears. The polarization reaches its peak when the applied electric field attains its maximum. The initial curve is only passed in the beginning, every other period is only visible as outer hysteresis loop.

6.1.2 Bipolar increasing voltage excitation

Additionally the model is also able to handle increasing and decreasing electric fields as shown in Fig. 6.2. For the first two periods the amplitude of the sinusoidal electric field is increased to a peak of $E_{\max} = 8 \cdot 10^7$ V/m. In the third period the amplitude decreases and after the third period the amplitude remains consistent at a level of $E_{\mathrm{A}} = 2 \cdot 10^7$ V/m. By increasing the electric field amplitude, the polarization hysteresis gets bigger and the polarization saturates. Decreasing the electric field to the values of the previous case results in the same limit cycle. Such a behavior is illustrated in Fig. 6.2. One can see that the same limit cycle in the E-P plane is obtained for the same harmonic forcing, independent of the previous loading history. The dashed black lines in Fig. 6.2(b) and (c) are the polarization and polarization hysteresis of the previous case (shown in Fig. 6.1).

Die approbierte gedruckte Originalversion dieser Diplomarbeit ist an der TU Wien Bibliothek verfügbar.
The approved original version of this thesis is available in print at TU Wien Bibliothek.
TU Bibliothek WIEN Your knowledge hub

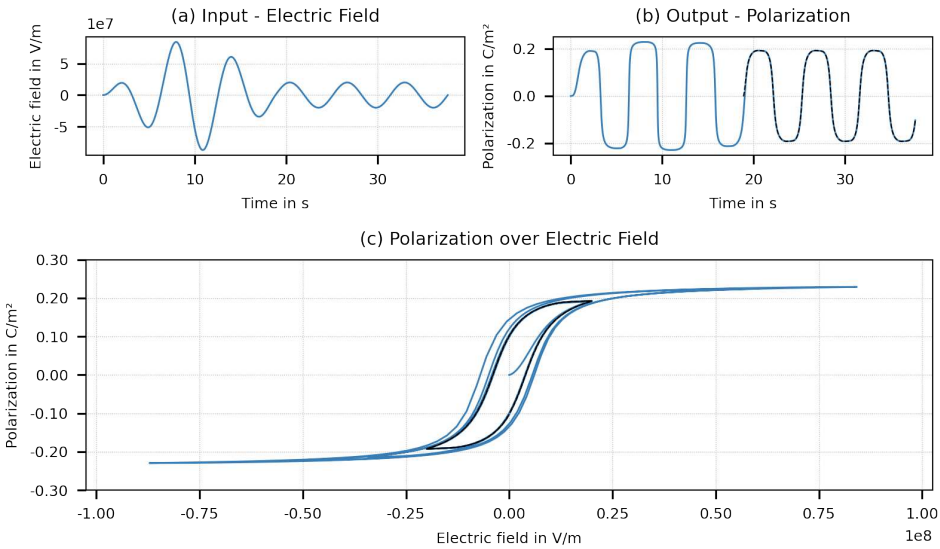

Figure 6.2: Full hysteresis with a increasing electric field. In (a) the electric field in V/m as input quantity. In (b) the outcome, the polarization in C/m^2 is plotted over the time. In (c) the polarization over the electric field is visualized, forming a full hysteresis loop with inner loops. The polarization over time and the polarization hysteresis from Fig. 6.1 are plotted with dashed lines as reference in (b).

6.1.3 Unipolar increasing voltage excitation

Unipolar loading cycles can be modeled as well. This is an important case because a piezoelectric actuator usually operates in such unipolar cycles, which are displayed in Fig. 6.3. The domain wall model gets excited with an electric field in the form of

$$E = -\frac{E_\mathrm{A}(t)}{2}\cos(t) + \frac{E_\mathrm{A}(t)}{2}. \tag{6.2}$$

The variable E_A increases linearly (from 0 to $1 \cdot 10^7$ V/m) over the first three periods resulting in a maximum applied electric field of $2 \cdot 10^7$ V/m.

The hysteresis loop for this excitation is shown in Fig. 6.3(c). The hysteresis loop is open, while the variable E_A is still raising. After the first three periods the variable E_A is constant. Now the model has a closed inner hysteresis loops, which are also called minor hystereses. As a reference value the full hysteresis loop from Fig. 6.1(c) is plotted in Fig. 6.3(c) with a dashed curve.

Discussion

The used hysteresis model can describe all previously presented cases. The real behavior of ferroelectric materials are explained with the used domain wall model and matches the presented theory in chapter 2. A remnant polarization occurs after the initial polarization curve, if the electric field vanishes. Additionally the polarization saturates if the electric field raises. Furthermore major and minor loops can be modeled. The limit cycle for a

Die approbierte gedruckte Originalversion dieser Diplomarbeit ist an der TU Wien Bibliothek verfügbar.
The approved original version of this thesis is available in print at TU Wien Bibliothek.
TU Bibliothek WIEN Your knowledge hub

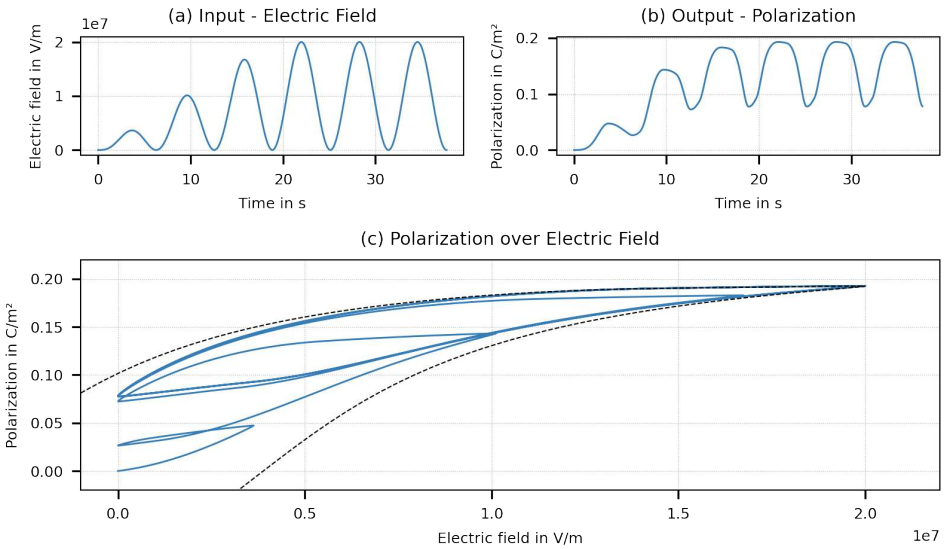

Figure 6.3: Unipolar hysteresis with a maximal electric field of $E_{\max} = 2 \cdot 10^7$ V/m. The amplitude of the electric field increases linearly for the first 3 periods. In (a) the electric field in V/m as input quantity. In (b) the outcome, the polarization in C/m^2 is plotted over the time. And in (c) the polarization over the electric field is displayed, forming a unipolar hysteresis loop. The dashed line shows the full hysteresis from Fig. 6.1(c).

constant periodic excitation only depends on the excitation signal and not on the previous loading history. As long as the last periods are equal, the same limit cycles result. This is important, because without the same limit cycles no unique steady state solution of the piezoelectric system can be obtained.

6.2 Ferroelastic hysteresis

Ferroelastic effects are not included in the nonlinear piezeoelectric system used in this thesis. For the sake of completeness the results of the ferroelastic hysteresis model from section 3.2 are presented briefly.

Ferroelastic behavior describes the interaction between the stress and the strain, due to the polarization properties of the material. The remnant polarization causes a irreversible strain. Mechanical stress can depolarize the material, and neutralize the irreversible strain.

The relation between the stress and strain is visualized in Fig. 6.4. Figure 6.4(a) displays the input signals σ_1 and σ_2 with and amplitude $\sigma_a = 10^7 \mathrm{N/m}^2$,

$$\sigma_1 = 2\sigma_\mathrm{a} \sin(t), \tag{6.3}$$

$$\sigma_2 = |\sigma_\mathrm{a} \sin(t)|. \tag{6.4}$$

Figure 6.4(b) shows the calculated strain. In Fig. 6.4(c)-(f) the stress-strain hysteresis

Die approbierte gedruckte Originalversion dieser Diplomarbeit ist an der TU Wien Bibliothek verfügbar.
The approved original version of this thesis is available in print at TU Wien Bibliothek.
TU Bibliothek Your knowledge hub WIEN

are illustrated.

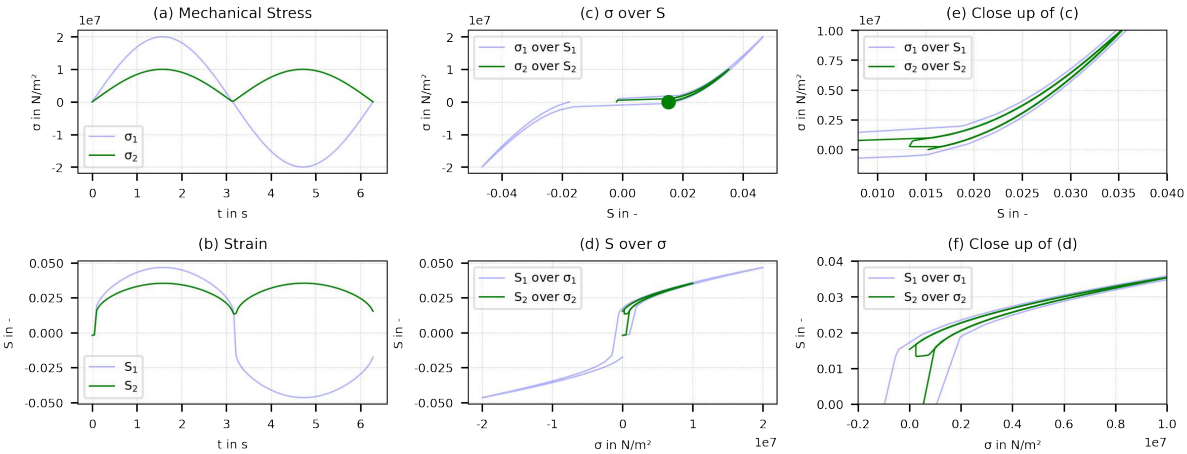

Figure 6.4: Mechanical hysteresis: In blue the bipolar loading cycle is visualized and in green a unipolar loading cycle is plotted.

Discussion

Figure 6.4 qualitatively matches the experimental data shown in Fig. 2.14 from section 2.3.2. However this model focuses only on the relation between the stress and strain for a polarized material. For example the stress can not affect the polarization in this model. In Fig. 6.4(c) the hysteresis is shown. There are areas where the strain changes with small increments of the mechanical stress. This occurs when the mechanical stress is near zero. This represents the switching of the polarization direction and the accompanied volume change, due to the mechanical stress as shown in section 2.2. For σ_2 in Fig. 6.4(f) one can see a remnant strain after the first initial mechanical loading cycle, which is in line with the experimental data shown in section 2.3.2. Note that the ferroelastic behavior is not implemented in the coupled model.

6.3 Physical behavior of the coupled system

To illustrate the physical behavior of the nonlinear coupled system, different loading scenarios are presented. The coupled system gets excited with a mechanical force f and electric current $I = \mathrm{d}Q/\mathrm{d}t$ (current excitation is equal to charge excitation). This leads to the two input quantities of this system, the mechanical stress $\sigma = \mathrm{f}/A$ and the dielectric displacement field $D = Q/A$. The used system extends the linear coupled piezoelectric system with the nonlinear polarization behavior.

These showcases are solved with the r-approach, which is quite a robust algorithm and the only one which converges for a full nonlinear piezoelectric modulus (seen at

Die approbierte gedruckte Originalversion dieser Diplomarbeit ist an der TU Wien Bibliothek verfügbar.
The approved original version of this thesis is available in print at TU Wien Bibliothek.
TU Bibliothek Your knowledge hub WIEN

eq. (5.32) versus eq. (5.42)). In the appendices A.2.1 to A.2.3 additional showcases from the other approaches are presented. Here are the four selected showcases (solved with the r-approach and a full nonlinear piezoelectric modulus eq. (5.32)):

- **General behavior:** The model gets excited with various dielectric displacement fields (corresponding to charge excitation) under different mechanical stress levels, but with the same electric field as outcome.
- **Bipolar charge excitation:** In this case one charge excitation under different mechanical stress levels are applied on the model.
- **Unipolar charge excitation:** A unipolar charge excitation is used to excite the model under different mechanical stress levels in a way that only positive polarization occurs.
- **Constant charge excitation:** Harmonic mechanical excitation under constant charges at the boundaries are used to excite the model.

6.3.1 General behavior

This case is presented first because it shows the impact of the mechanical stress and the resulting relationships well. Various dielectric displacement fields and mechanical stress combinations are used to excite the system. In Fig. 6.5(a) and (b) the input quantities are plotted. The input is chosen in a way that the solution of the system is the same electric field

$$E_{\text{solution}} = 10^7 \sin(t) \text{ V/m.} \approx E_{0\text{-}4} \tag{6.5}$$

as shown in Fig. 6.5(c). To get these specific dielectric displacement fields, the system

$$\begin{bmatrix} \sigma \\ D \end{bmatrix} = \begin{bmatrix} C & -e(P) \\ e(P) & \epsilon_0 \end{bmatrix} \begin{bmatrix} S^{\text{r}} \\ E \end{bmatrix} + \begin{bmatrix} 0 \\ P \end{bmatrix}. \tag{6.6}$$

is first solved with a electric field and mechanical stress in the time domain. This is a trivial task, because the system can be directly solved for the dielectric displacement field

$$D = e(P)S^{\text{r}} + \epsilon_0 E + P, \tag{6.7}$$

and strain

$$\sigma = CS^{\text{r}} - e(P)E \rightarrow S^{\text{r}}. \tag{6.8}$$

This is done for each applied mechanical stress ($\sigma_{0\text{-}4}$) and the dielectric displacement fields $D_{0\text{-}4}$ are obtained. The calculated dielectric displacement fields serves in the following as a input quantity along with the mechanical stress and is shown in Fig. 6.5(a). In

Die approbierte gedruckte Originalversion dieser Diplomarbeit ist an der TU Wien Bibliothek verfügbar.
The approved original version of this thesis is available in print at TU Wien Bibliothek.
TU Bibliothek Your knowledge hub WIEN

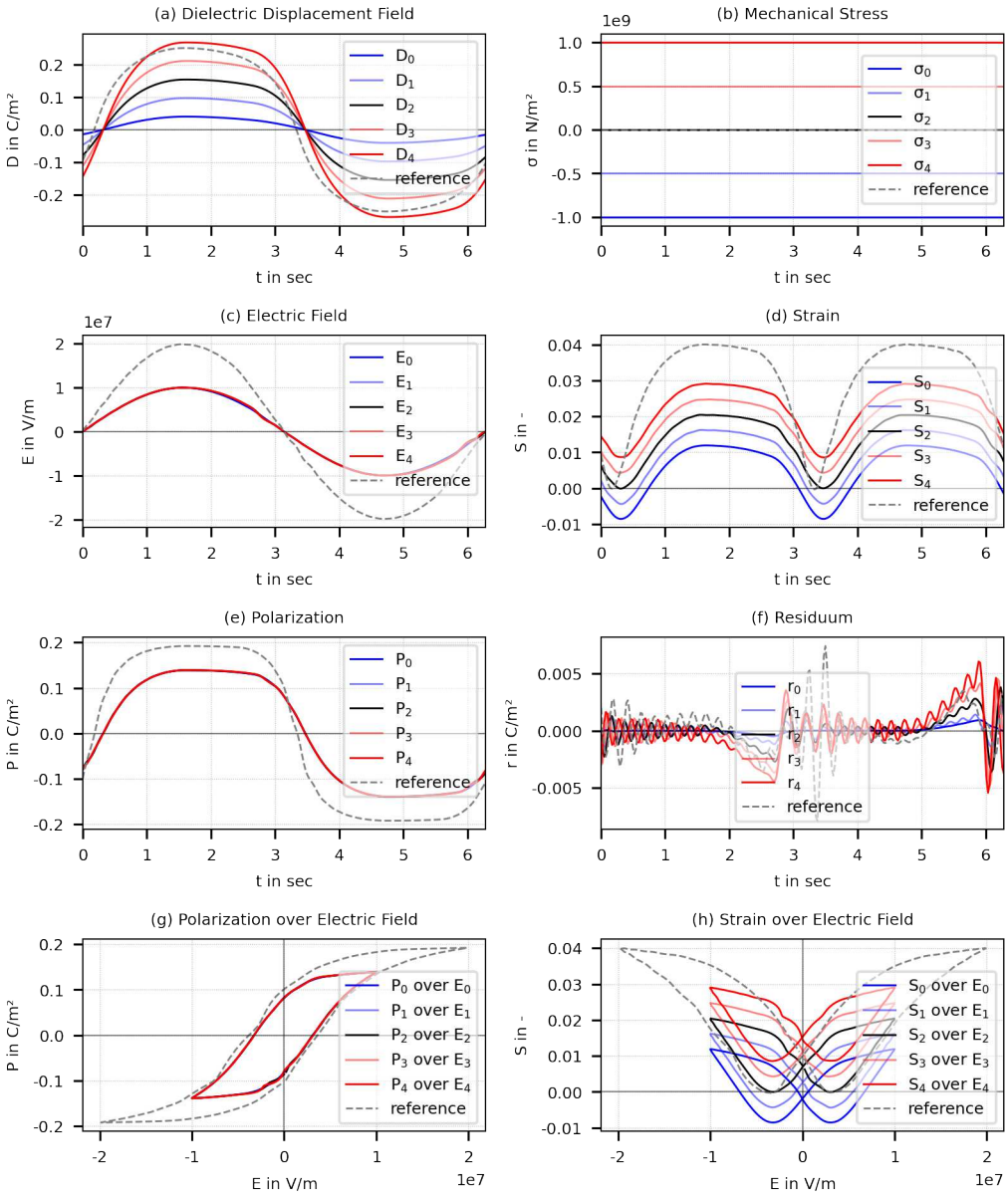

Figure 6.5: A general case where the resulting electric field is the same for various dielectric displacement field - mechanical stress combinations. The influence of the mechanical stress on the strain is clearly visible.

Fig. 6.5(b) the mechanical stress is displayed. The electric field and strain are visualized in Fig. 6.5(c) and (d), respectively. The polarization is shown in Fig. 6.5(e) and the residuum in Fig. 6.5(f). In Fig. 6.5(g) and (h) the polarization hystereses and butterfly loops are sketched. Additionally in Fig. 6.5 a reference case is plotted in dashed lines. This case is plotted as reference in the upcoming figures.

Discussion

In Fig. 6.5(a) and (b) the excitation quantities are shown. While the same electric field serves as outcome, the dielectric displacement field has to be bigger when a positive me-

Die approbierte gedruckte Originalversion dieser Diplomarbeit ist an der TU Wien Bibliothek verfügbar.
The approved original version of this thesis is available in print at TU Wien Bibliothek.
TU Bibliothek Your knowledge hub WIEN

chanical stress is applied. For a negative stress this is reversed, the dielectric displacement field decreases.

The dielectric displacement D can be seen as the "overall" polarization while the polarization P is only the internal polarization of the material. The dielectric displacement field (eq. (6.7)) is the sum of the polarization, the electric field term and the coupled term. A high mechanical stress increases the coupled term. If a high positive stress (tension) is applied in direction of the polarization, the dielectric displacement field raises because of the increased couple term, due to the mechanical stress. For a negative stress (compression) the dielectric displacement field decreases.

It is important to remember that the polarization is only able to expand the material. The sign of the polarization does not matter, only the absolute value of the polarization is responsible for the expansion of the material. The strain is composed of the reversible strain and the irreversible strain. Reversible strain is caused by the mechanical stress and vanishes if no stress is applied. Any possible negative strain in this system occurs due to the mechanical stress. Irreversible strain depends on the internal polarization and only disappears if the polarization is zero. Figure 6.5(h) shows the butterfly loop. The polarization for all excitation combinations is equal, because the same electric field results as outcome. Therefore the irreversible strain is the same and the shift on the strain-axis of the butterfly loops in Fig. 6.5(h) is only caused by the reversible strain. In Figure 6.5(h) the limitations of the system can be seen. No ferroelastic effects are considered, therefore the shape of the butterfly loop is the same. If ferroelastic effects would be considered, the butterfly loop would change the size and form depending of the applied mechanical stress. The mechanical stress would modify the polarization hysteresis too. The residuum is displayed in Fig. 6.5(f) and is bigger under positive mechanical stress.

6.3.2 Bipolar charge excitation

For this showcase, one charge excitation and five different mechanical forces are applied (results in $\sigma_{0\text{-}4}$). The charge excitation results in a occurring dielectric displacement field D. The input quantities dielectric displacement field and mechanical stress are displayed in Fig. 6.6(a) and (b), respectively. The polarization hystereses and butterfly loops are visualized in Fig. 6.6(c) and (d).

Discussion

For this setup the mechanical stress modifies the amplitude of the electric field. One dielectric displacement field is forced as input on the system under different stress levels. As mentioned previously, the dielectric displacement field can be seen as "overall" polarization and by applying different stress levels while the "overall polarization" must be the same, the electric field increases for negative stress and decreases for positive stress. A

Die approbierte gedruckte Originalversion dieser Diplomarbeit ist an der TU Wien Bibliothek verfügbar.
The approved original version of this thesis is available in print at TU Wien Bibliothek.
TU Bibliothek Your knowledge hub WIEN

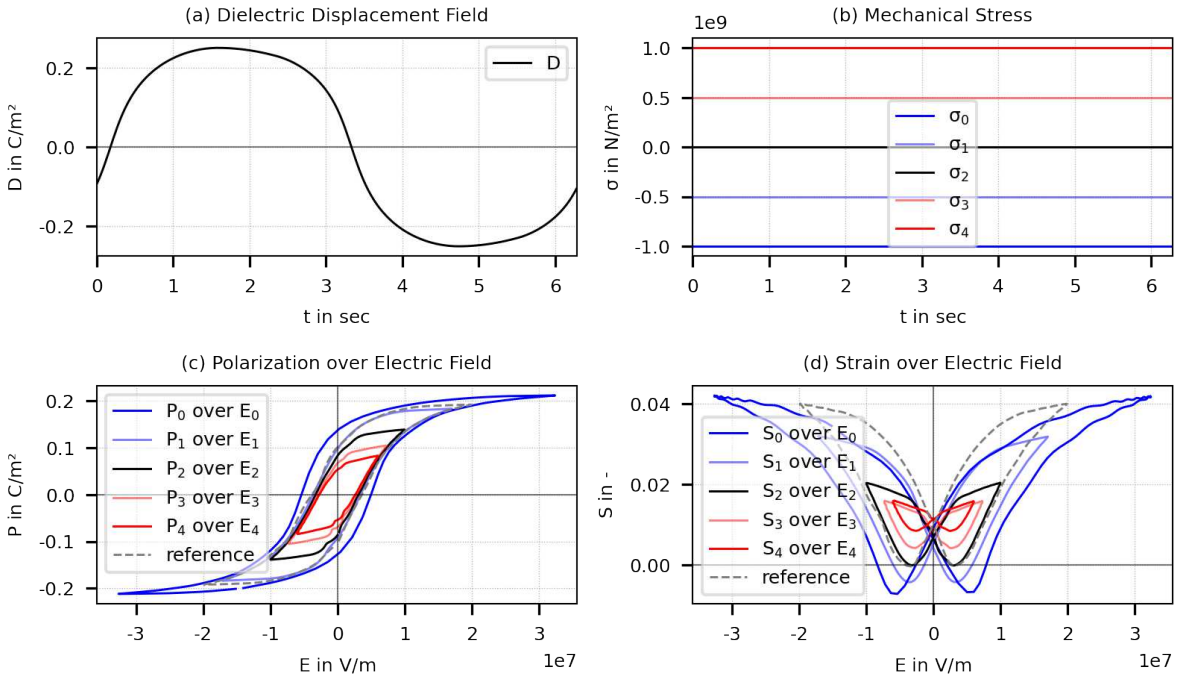

Figure 6.6: Bipolar Dielectric Displacement Field (a) with different constant mechanical stresses (b) and the resulting polarization hystereses (c) and butterfly loops (d). The extended output quantities of the algorithm are shown in Fig. A.1. The reference case is the same as shown in Fig. 6.5.

different electric field produces a different polarization. In general the polarization raises if the electric field is increasing, until the polarization is saturated. As shown in Fig. 6.6(c) the hystereses get smaller for a higher positive applied stress. This is reversed if negative stress is applied, increasing the maximal polarization.

Now one dielectric displacement field is given, due to the charge excitation. Different constant mechanical stress alters the output (electric field and strain). First lets look into the electric field. A positive mechanical stress reduces the amplitude of the electric field, whereas a negative mechanical stress increases the amplitude. This can be seen indirectly due to the smaller hysteresis in Fig. 6.6(c) or in the appendix. If we look at the strain one can notice a smaller amplitude but higher offset with higher positive applied stress, visible in Fig. 6.6(d). With a higher negative applied stress the effects reverse, resulting in a higher amplitude and a smaller remnant strain. The strain is composed of the reversible and irreversible strain. The irreversible strain is dependent on the polarization, and the reversible strain depends on the mechanical stress. For a negative applied stress, the reversible strain gets negative due to the compression. However the electric field amplitude and remnant polarization increases for this loading case. This results in a higher irreversible strain, which is caused by the overall higher polarization of the material. The irreversible strain is the reason why the dark blue butterfly loop in Fig. 6.6(c) has a higher remnant strain then the light blue butterfly loop. The remnant

Die approbierte gedruckte Originalversion dieser Diplomarbeit ist an der TU Wien Bibliothek verfügbar.
The approved original version of this thesis is available in print at TU Wien Bibliothek.
TU Bibliothek Your knowledge hub WIEN

strain is best visible in the butterfly loop, Fig. 6.6(d), where the electric field becomes zero. The remnant polarization can be seen in Fig. 6.6(c), where the polarization crosses the y-axis.

Overall the positive mechanical stress decreases the achieved polarization in this case, resulting in a smaller strain amplitude but in a higher static strain (offset). The negative stress increases the polarization and the strain amplitude, leading to a bigger polarization hysteresis and bigger butterfly loop.

6.3.3 Unipolar charge excitation

This case is similar to the previous case, except a unipolar charge excitation is used as excitation. This excitation results in a unipolar dielectric displacement field D. The maximal dielectric displacement field is equal to the previous dielectric displacement field, but the shape is different. The applied mechanical stress levels are equal to the bipolar case. The input quantities, the dielectric displacement field D and different mechanical stresses $\sigma_{0,4}$ are displayed in Fig. 6.7(a) and (b), respectively. In Fig. 6.7(c) and (d) the resulting polarization hystereses and the butterfly loops visualized, respectively.

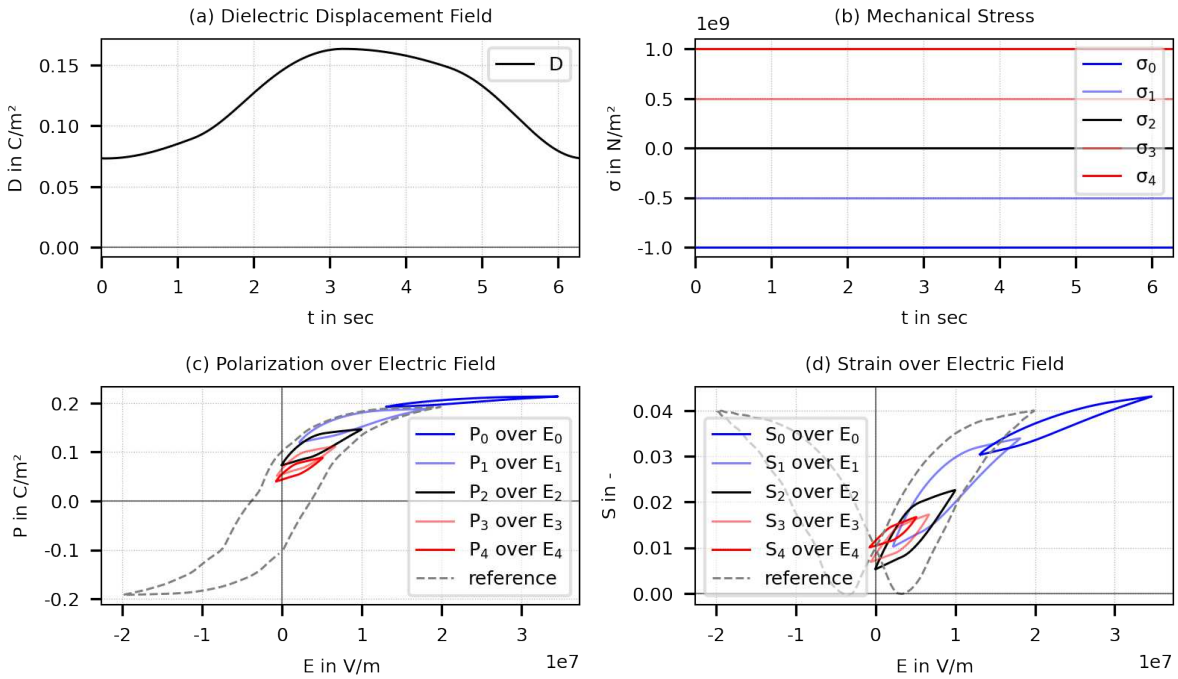

Figure 6.7: Unipolar Dielectric Displacement Field (a) with different constant mechanical stresses (b) and the resulting polarization hystereses (c) and butterfly loops (d). The reference case from section 6.3.1 is displayed in (c) and (d) with dashed lines. Additional output quantities of this case are displayed in Fig. A.2.

Die approbierte gedruckte Originalversion dieser Diplomarbeit ist an der TU Wien Bibliothek verfügbar.
The approved original version of this thesis is available in print at TU Wien Bibliothek.
TU Bibliothek Your knowledge hub WIEN

Discussion

This case shows similar results as the previous one. The system acts the same for positive and negative stress as in the bipolar charge excitation. In Fig. 6.8 the results are compared and the similarities are visible. Since the system got excited with unipolar loading cycles "only one side" of the previous results are displayed. The resulting minor polarization- and butterfly-loops corresponds well to the according bipolar polarization- and butterfly-loops. For the butterlfy loops only one "wing" occurs.

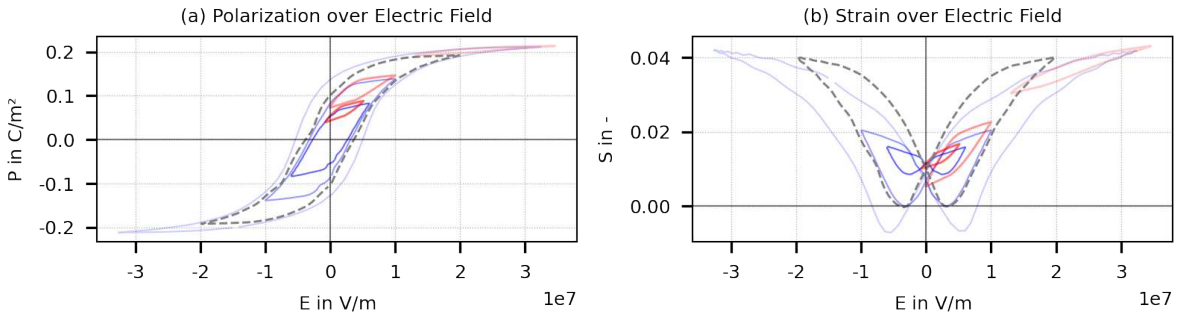

Figure 6.8: Comparison of bipolar (blue) and unipolar (red) dielectric displacement excitation under different constant stress levels: (a) Polarization hystereses; (b) butterfly loops. The reference case from section 6.3.1 is displayed with dashed lines.

Since the input quantities are not exactly equal, the unipolar results do not fit the bipolar results perfectly. The unipolar results achieves a slightly higher polarization, even though the maximal dielectric displacement field is the same. The difference is obtained because of the explicit evaluation of the polarization. Due to the higher polarization in the unipolar case, the irreversible strain raises and therefore the unipolar butterfly loops do not fit perfectly too. The comparison of these two cases is of qualitative nature, to get a better feeling and understanding of the results.

6.3.4 Constant charge excitation

Instead of exciting the system with various variable charge excitations under constant mechanical stress levels, the system gets excited with a constant charge excitation under one sinusoidal mechanical stress. The three different resulting constant dielectric fields are ranging from $D_0 = -0.15$ C/m^2 to $D_2 = 0.0$ C/m^2 to $D_3 = 0.1$ C/m^2. The dielectric displacement fields and mechanical stresses are displayed in Fig. 6.9(a), respectively (b). The resulting polarization hystereses and butterfly loops are shown in Fig. 6.9(c) respectively (d).

Die approbierte gedruckte Originalversion dieser Diplomarbeit ist an der TU Wien Bibliothek verfügbar.
The approved original version of this thesis is available in print at TU Wien Bibliothek.
TU Bibliothek Your knowledge hub WIEN

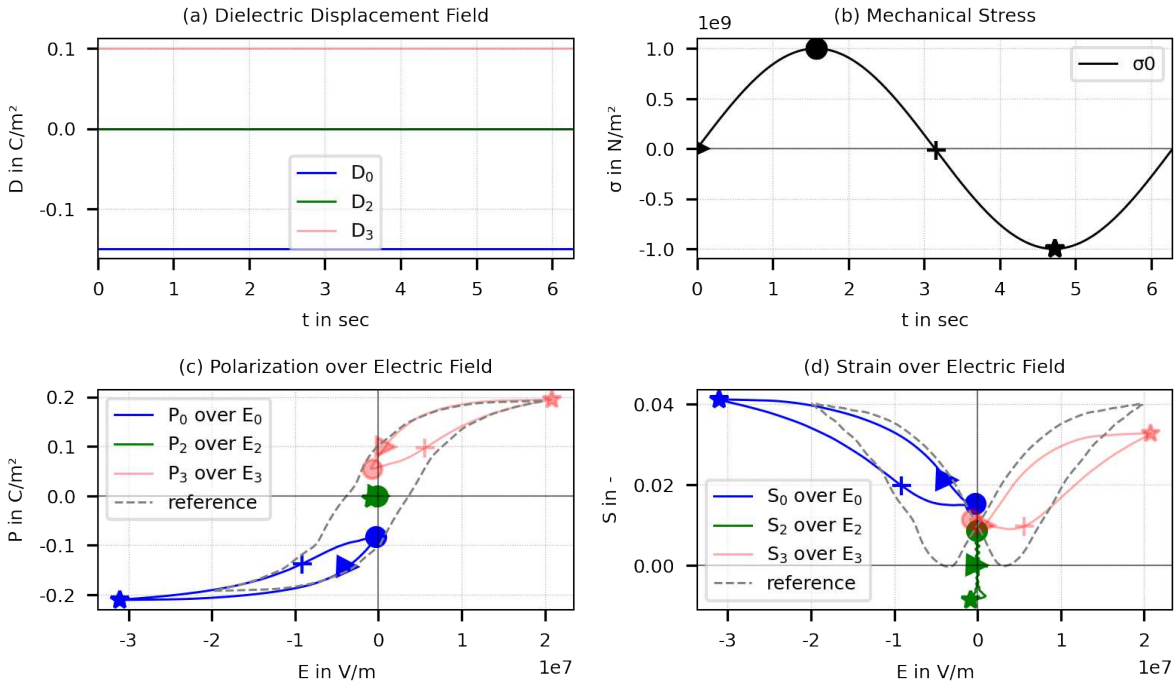

Figure 6.9: The inputs of the model are shown in (a) and (b) as the dielectric displacement field and mechanical stress, respectively. In (c) and (d) the resulting polarization hysteresis and butterfly loops are visualized. The triangle marks the start of the hysteresis. The circle and star are indicating the maximum or minimum of the mechanical stress, respectively. The plus represent the zero crossing of the mechanical stress. All the input and output quantities are displayed in Fig. A.3.

Discussion

First we discuss the results of an excitation with equal charges at every boundary. This results in a dielectric displacement field of zero, which is displayed in Fig. 6.9 with green color. No dielectric displacement is allowed, which can be seen as overall polarization. In Fig. 6.9(b) the mechanical stress is shown and four points of interest are marked. The triangle marks the start of the period, the circle and star are indicating the maximum and minimum of the mechanical stress, respectively. The plus marks the zero crossing at half period time. As visible in Fig. 6.9(c) no polarization and electric field occurs leading to no polarization hysteresis. The butterfly curve is a "straight" line along the strain axis, because the strain in this case is only dependent on the mechanical stress and no coupling occurs. The highest stretch occurs while the maximal tensile stress is applied and the minimum of the strain appears at maximal compression stress.

Secondly we discuss the blue excitation case from Fig. 6.9 (D_0). The applied dielectric displacement field is constant at -0.15 C/m^2 over the whole period. Polarization occurs in the material, due to the applied mechanical stress which produces an electric field. Tensile stress reduces the electric field, while compression stress induces an electric field, as visible in the appendix under Fig. A.3(c). The polarization decreases for tensile stress

Die approbierte gedruckte Originalversion dieser Diplomarbeit ist an der TU Wien Bibliothek verfügbar.
The approved original version of this thesis is available in print at TU Wien Bibliothek.
TU Bibliothek Your knowledge hub WIEN

and increases for compression stress, because of the electric field. The strain shown in Fig. A.3(d) (in the appendix) decreases if tensile stress is applied and raises if compression stress is applied. This is a counter intuitive behavior, but since the polarization is modeled out of the electric field and the strain is modeled as

$$S = S^{\mathrm{r}} + S^{\mathrm{irr}}, \tag{6.9}$$

the model acts as intended. The irreversible strain is a polynomial based model on the polarization. This indicates that the polynomial approach for the irreversible strain is only valid for certain loading scenarios.

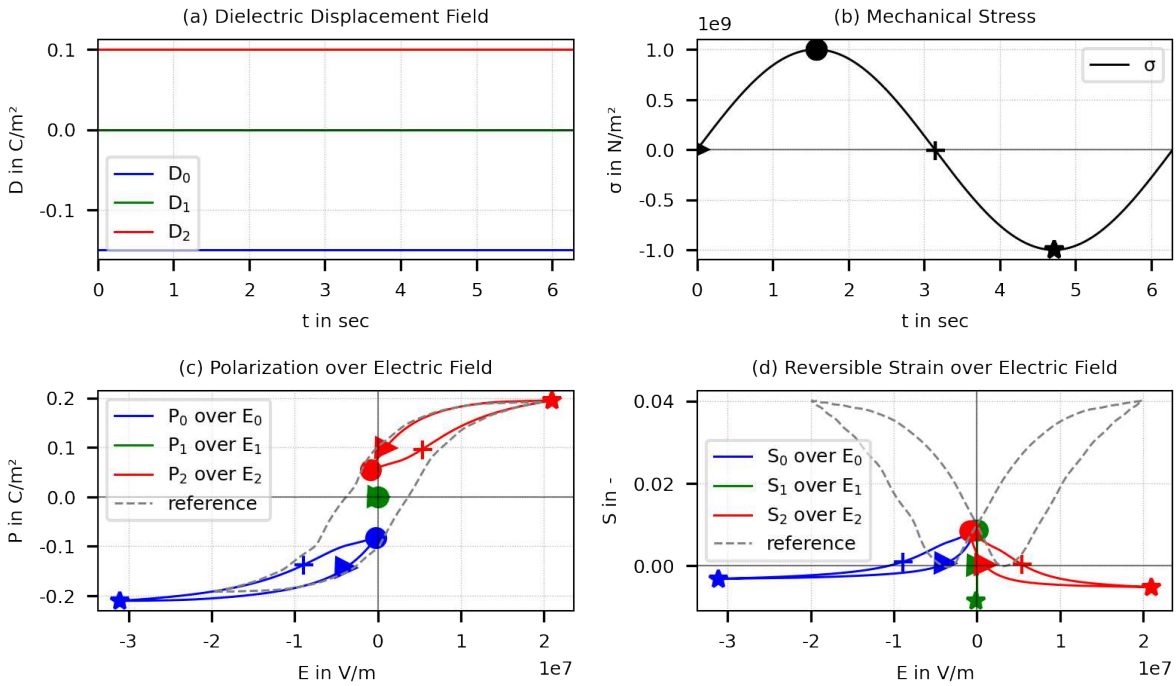

Figure 6.10: Constant charge excitation: (a) to (c) is the same as in Fig. 6.9. (d) shows the reversible strain over the electric field.

In Fig. 6.10(d) the butterfly curve for the reversible strain is displayed. Now the model has the biggest strain if tensile stress is applied and the smallest strain if compression strain is occurs, which is another indicator that the irreversible strain might need a different approach to model the polarization-dependent strain more accurately. However the reversible part of the strain, as shown in Fig. 6.10, acts as expected. This displays the real behavior of piezoelectric ceramics materials more accurately, speaking in a qualitative meaning.

The same results occur for a constant applied dielectric displacement field of D_3 which is displayed in red, expect the results are mirrored on the polarization and strain axis. This is caused by the different sign of the dielectric displacement field.

Die approbierte gedruckte Originalversion dieser Diplomarbeit ist an der TU Wien Bibliothek verfügbar.
The approved original version of this thesis is available in print at TU Wien Bibliothek.
TU Bibliothek Your knowledge hub WIEN

A interesting point worth mentioning is the behavior of the polarization and the strain at zero stress. The mechanical stress becomes zero at the beginning and in the middle of the period, which is indicated with the triangle and plus throughout the plots, respectively. The strain and polarization is the same for both points (at triangle and plus mark), but the occurring electric field is different.

6.3.5 Showcases of the E-S-approach and χ-approach

In appendices A.2.1 to A.2.3 additional showcases for the E-S-approach and χ-approach are provided. Three showcases are displayed which are orientated on the unipolar cases presented earlier:

- **Case 1: General behavior (unipolar loading):** The system gets excited with various charges under different stress levels. The dielectric displacement field and mechanical stresses are chosen in a manner that the resulting electric field is the same for each combination.
- **Case 2: Unipolar charge excitation:** One unipolar charge excitation under different constant mechanical stress levels is applied.
- **Case 3: Constant charge excitation:** The system gets excited under a constant charge excitation and two different mechanical stresses.

However, there are some differences between theses showcases and the previous ones. The showcases in sections 6.3.1 to 6.3.4 are solved with the r-approach, which can handle bipolar loading cycles. To solve the system for bipolar loading cycles the algorithm needs to handle a piezoelectric modulus, which changes sign according to the polarization. With a constant modulus only unipolar solutions can be displayed correctly. This is best visualized for the butterfly loops in Fig. 6.11. With the constant piezoelectric modulus and mild nonlinear piezoelectric modulus only one half of the butterfly loop is approximated accurately. For the other side the piezoelectric modulus would have to flip sign, according to the polarization. Since the E-S-approach and χ-approach can only handle a mildly nonlinear variable piezoelectric modulus, the used cases are restricted to unipolar solutions and the coupling tensor is defined different as

$$e(P) = \frac{1}{8} e_{33} \frac{P(t)}{P_{\mathrm{s}}} + \frac{7}{8} e_{33}. \tag{6.10}$$

The restriction for unipolar solutions is not a big problem since in most applications use unipolar loading cycles. In Fig. 6.11(b) the difference between the strong linear coupling tensor and mild linear coupling tensor is visible, but it is a magnitude under the total strain, which is displayed in Fig. 6.11(d), therefore this difference is less problematic.

Die approbierte gedruckte Originalversion dieser Diplomarbeit ist an der TU Wien Bibliothek verfügbar.
The approved original version of this thesis is available in print at TU Wien Bibliothek.
TU Bibliothek WIEN Your knowledge hub

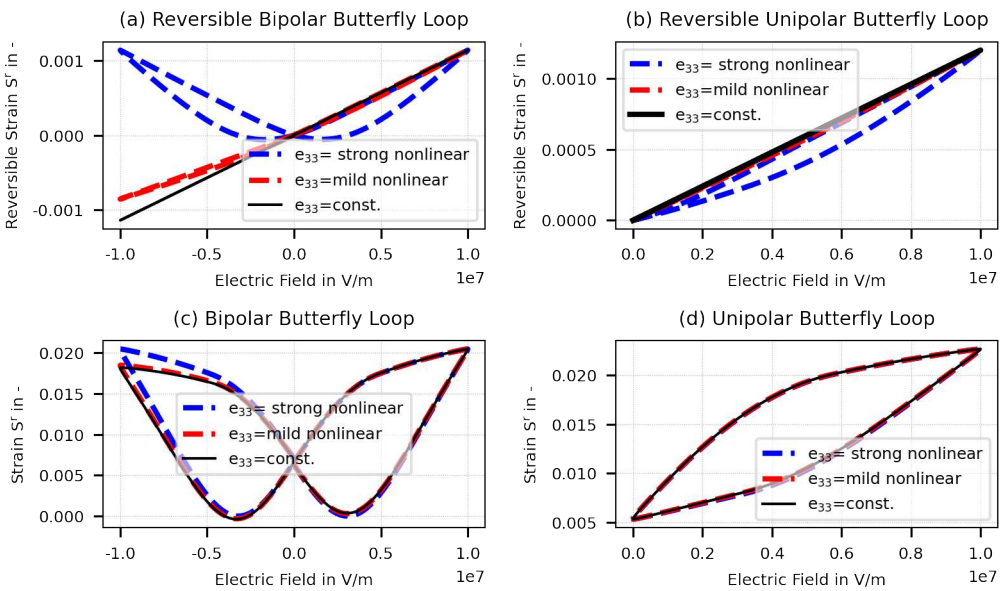

Figure 6.11: Comparison of the different piezoelectric modulus. In (a) the bipolar butterfly loops of the reversible strain are shown and in (c) the bipolar butterfly loop of the total strain. In (b) and (d) the unipolar butterfly loops of the reversible strain and unipolar butterfly loops of the total strain are visualized, respectively. The mild nonlinear piezoelectric modulus is defined in eq. (6.10) and the strong nonlinear piezoelectric modulus in eq. (5.32).

6.4 Comparison of the physical behavior of all three approaches

In the following two specific showcases are presented and the results of the three different approaches are compared. Only unipolar loading cycles are allowed and the piezoelectric couple modulus is only mild nonlinear (eq. (6.10)). To compare the results one has to solve the system independently in order to quantify if the results of the approaches are correct. Therefore all the input quantities are calculated with a reference solution directly in the time domain. With these calculated input quantities and the according solution, the results of the approaches can be compared.

6.4.1 Used Showcase

One unipolar dielectric displacement field and a constant mechanical stress is used for excitation. The piezoelectric couple modulus is defined as previous mentioned. If the modulus would be more nonlinear, the E-S-approach and χ-approach would not converge and a comparision would not be possible.

Die approbierte gedruckte Originalversion dieser Diplomarbeit ist an der TU Wien Bibliothek verfügbar.
The approved original version of this thesis is available in print at TU Wien Bibliothek.
TU Bibliothek Your knowledge hub WIEN

Reference Solution

First the coupled system eq. (5.31) is solved for the reversible strain and dielectric displacement field. An electric field

$$E_{\text{solution}} = 10^7 - 10^7 \cos(t) \text{ V/m} , \tag{6.11}$$

and a constant stress

$$\sigma_{\text{in}} = 10^8 \text{ N/m}^2, \tag{6.12}$$

are used to calculate the dielectric displacement field D_{in} and the reversible strain $S^{\text{r}}_{\text{solution}}$. Now all quantities of the system eq. (5.31) are known. The mechanical stress σ_{in} and the calculated dielectric displacement field D_{in} serve as input in the following, where as E_{solution} and $S^{\text{r}}_{\text{solution}}$ are now the reference solution. All quantities for the reference case are shown explicitly in Fig. A.11, but are also plotted in Fig. 6.12. For the second case in Fig. 6.13 the same procedure is used to validate the outcome

6.4.2 Comparision

In Fig. 6.12 the results of all three approaches are displayed. No visible deviation occurs after 25 iteration steps. Each approach converges to the same result. However some approaches converge faster than others. Another case is compared in Fig. 6.13. There the E-S-approach does not converge and minor deviations of the χ-approach are visible. In appendix A.4 more showcases are compared and displayed in figures. In this section only two case are presented, to keep the section rather compact.

Discussion

Not all showcases from section 6.3 can be compared, due to the fact that the E-S-approach and χ-approach are only valid for unipolar cases. Therefore only unipolar loading cycles are compared. For the unipolar case 0 which is plotted in Fig. 6.12, all approaches converge to the exact solution.

However for some excitation cases the E-S-approach does not converge as shown in Fig. 6.13. This disqualifies the E-S-algorithm in its current state for the implementation in a FE-software. Maybe with under- or over-relaxation a better convergence behavior can be achieved.

In the context of describing bipolar loading cycles the r-approach is superior, but most applications for piezoelectric actuators are driven in unipolar loading cycles, therefore the χ-approach can be used for most application simulations as well. In the next section the performance regarding the resulting error per iteration step is presented and discussed.

Die approbierte gedruckte Originalversion dieser Diplomarbeit ist an der TU Wien Bibliothek verfügbar.
The approved original version of this thesis is available in print at TU Wien Bibliothek.
TU Bibliothek WIEN Your knowledge hub

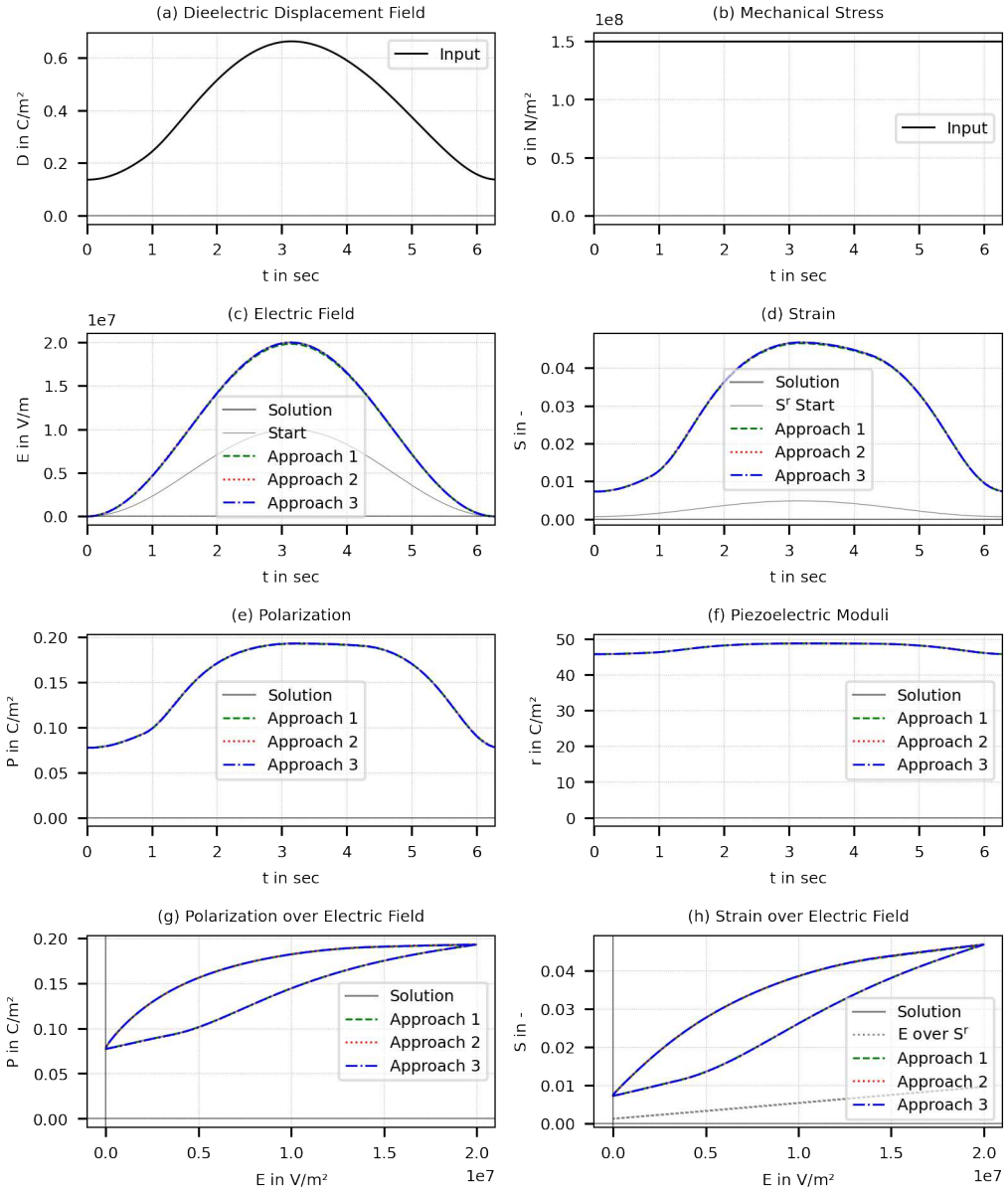

Figure 6.12: Case 0: Comparison of all three approaches after 25 iterations. All approaches converging to the same result and no deviations are visible. The starting values of the algorithm are displayed with a thin grey line in (c) and (d). In (h) the reversible strain over the electric field is displayed with dotted grey line.

Die approbierte gedruckte Originalversion dieser Diplomarbeit ist an der TU Wien Bibliothek verfügbar.
The approved original version of this thesis is available in print at TU Wien Bibliothek.

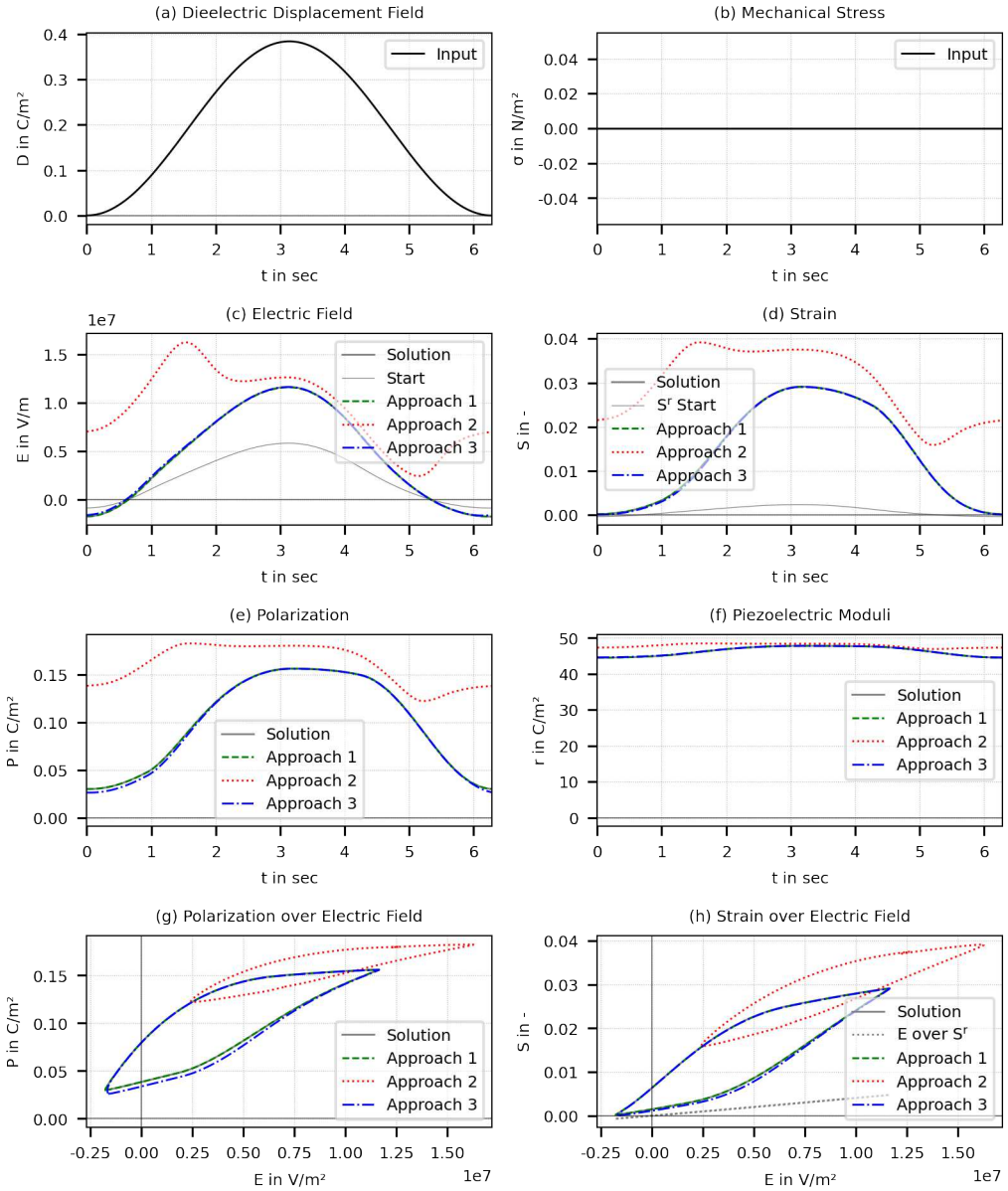

Figure 6.13: Case 5: Comparison of the results of all three approaches after 25 iteration. The starting values of the algorithm are displayed with a thin grey line in (c) and (d). The E-S-approach does not converge to the exact solution and minor deviations of the χ-approach are visible.

Die approbierte gedruckte Originalversion dieser Diplomarbeit ist an der TU Wien Bibliothek verfügbar.
The approved original version of this thesis is available in print at TU Wien Bibliothek.

6.5 Performance of the approaches

After looking if all approaches converge to the exact solution, the performance differences are investigated. All approaches use 15 considered harmonics in this section. The influence of the numbers of the considered harmonics regarding the performance will presented and discussed in the next section.

A relative error $\text{Error}_{\text{rel}}$ is defined in the time domain as

$$\text{Error}_{\text{rel}} = \frac{\|E_{\text{approach}}(t) - E_{\text{solution}}(t)\|_2}{\|E_{\text{solution}}(t)\|_2}. \tag{6.13}$$

The error over the iteration steps for various cases is displayed in figs. 6.14 to 6.17. All of the approaches starting with the same initial value

$$S^{\text{r}}_{\text{start}} = 0.5 S^{\text{r}}_{\text{solution}}, \text{ and} \tag{6.14}$$

$$E_{\text{start}} = 0.5 E_{\text{solution}}. \tag{6.15}$$

This can be seen throughout the plots as each error starts at the same value. The input- and output-quantities of the compared cases are shown in appendix A.4 and only the error over the iterations are displayed in this section.

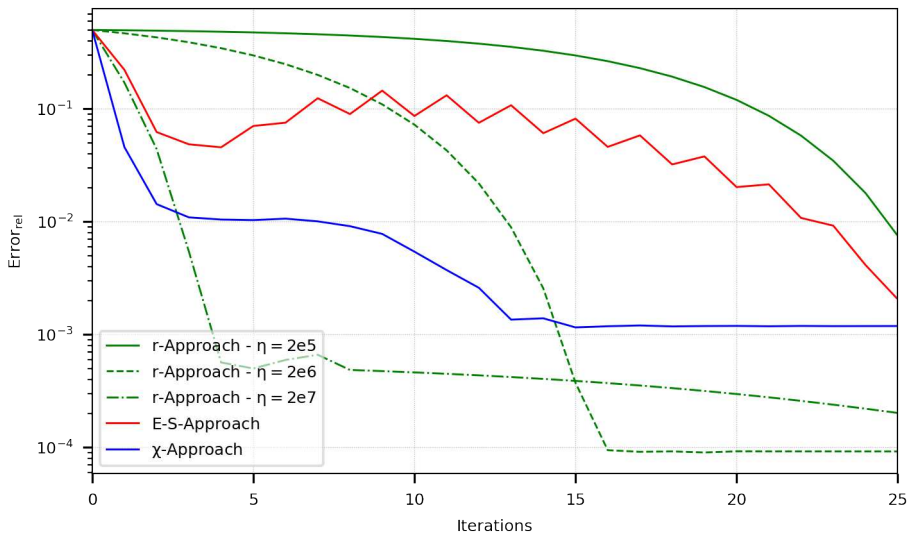

Figure 6.14: Relative errors for each approach for the case 0 displayed in Fig. 6.12.

Discussion

r-Approach

The performance of r-approach depends strongly on the relaxation parameter η. In figs. 6.14 to 6.16 the error is plotted with a green color for three different η parame-

Die approbierte gedruckte Originalversion dieser Diplomarbeit ist an der TU Wien Bibliothek verfügbar.
The approved original version of this thesis is available in print at TU Wien Bibliothek.
TU Bibliothek WIEN Your knowledge hub

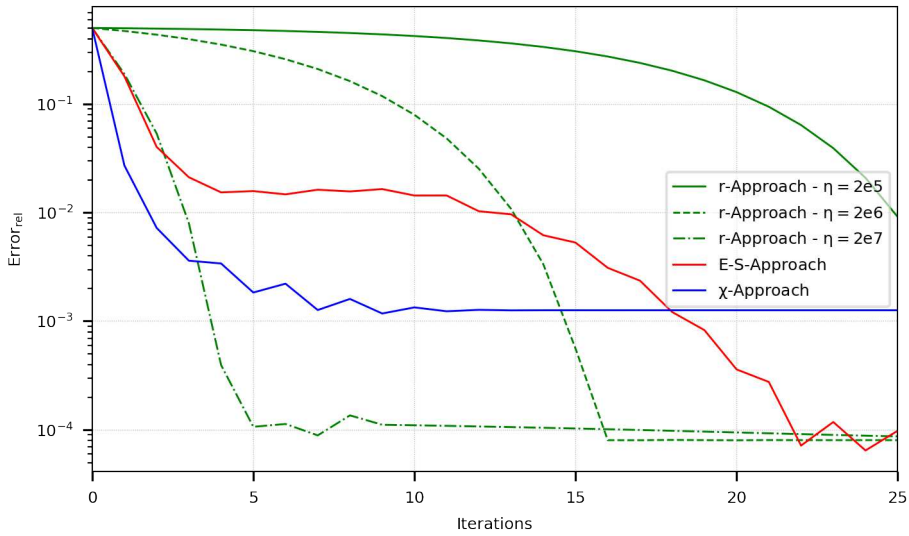

Figure 6.15: Relative errors for each approach for the case 1 displayed in Fig. A.12.

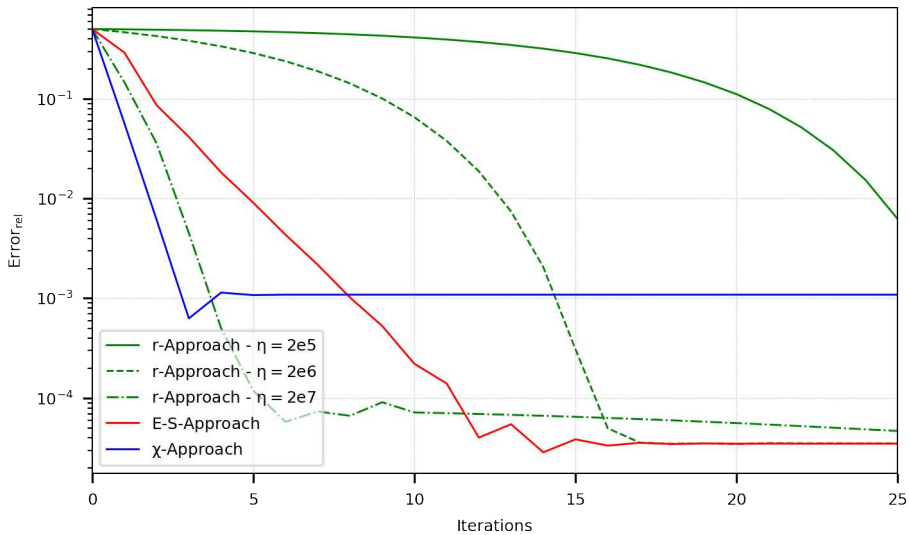

Figure 6.16: Relative errors for each approach for the case 2 displayed in Fig. A.13.

ters. If η is not chosen optimal, the approach converges slowly, but with a suitable η the r-approach can perform very well. It outperforms the other approaches after the third step. For this approach an additional line search for the best η parameter would be useful to improve the performance of this algorithm further.

E-S-Approach

This approach (plotted in red) does not always converge as in shown Fig. 6.17. Additionally for some cases this approaches does not show monotone convergence as in Fig. 6.14 visible. Even if the approach converges, the convergence is slower compared to the other approaches. However, since this approach does not converge for all excitation signals, it is not practical to use this approach in its current state at all.

Die approbierte gedruckte Originalversion dieser Diplomarbeit ist an der TU Wien Bibliothek verfügbar.
The approved original version of this thesis is available in print at TU Wien Bibliothek.
TU Bibliothek Your knowledge hub WIEN

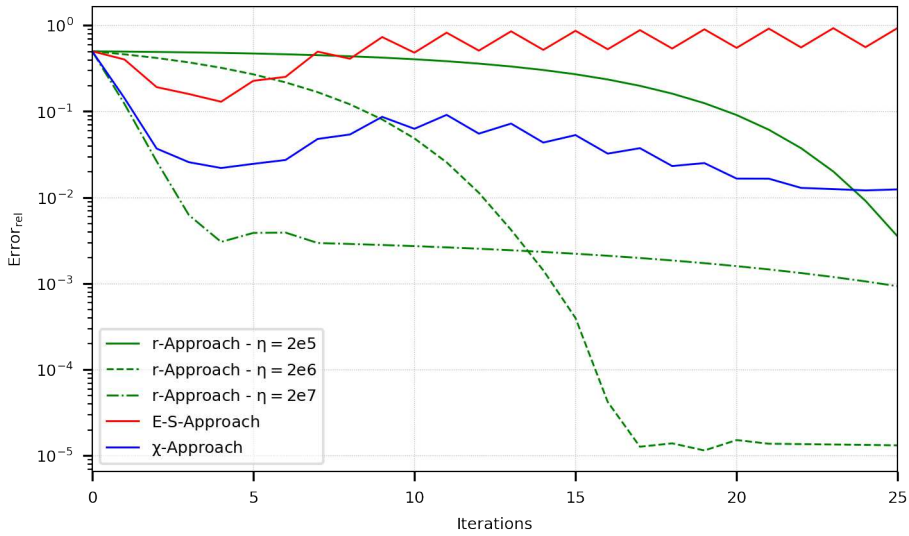

Figure 6.17: Error of case 5: The E-S approach do not converge.

χ-Approach

In the initial iteration steps this approach (plotted in blue) is very fast. However after the first three iterations the convergence rate decreases significantly. In Fig. 6.14 it reaches a plateau, before the error decreases again. Similar behavior occurs in Fig. 6.17, where the error even increases again. This can be problematic, because without further investigation its not clear if the approach diverges or converges again. The accuracy of this algorithm is not as good as the accuracy from the r-approaches. The magnitude of the relative error never goes below 10^{-3} and in Fig. 6.17 the relative error even never gets below 1%. Somehow, maybe because of the variable transformation, this approach looses accuracy.

6.6 Influence of considered harmonics

In the previous section the performance was only investigated with 15 considered harmonics. The number of considered harmonics does have influence on the results, accuracy and performance. This is investigated in this section. In Fig. 6.18 the polarization from case 0 (Fig. 6.12) is displayed for different numbers of considered harmonics. The polarization is calculated with 25 iteration steps for all three approaches. Different numbers of considered harmonics N_h are used. The considered harmonics are ranging from 1 to 31 . The error for the different excitation cases and different N_h are visualized in Fig. 6.19. The according input- and output-quantities are displayed in Fig. 6.12 and in the appendix A.4.

Die approbierte gedruckte Originalversion dieser Diplomarbeit ist an der TU Wien Bibliothek verfügbar.
The approved original version of this thesis is available in print at TU Wien Bibliothek.
TU Bibliothek Your knowledge hub WIEN

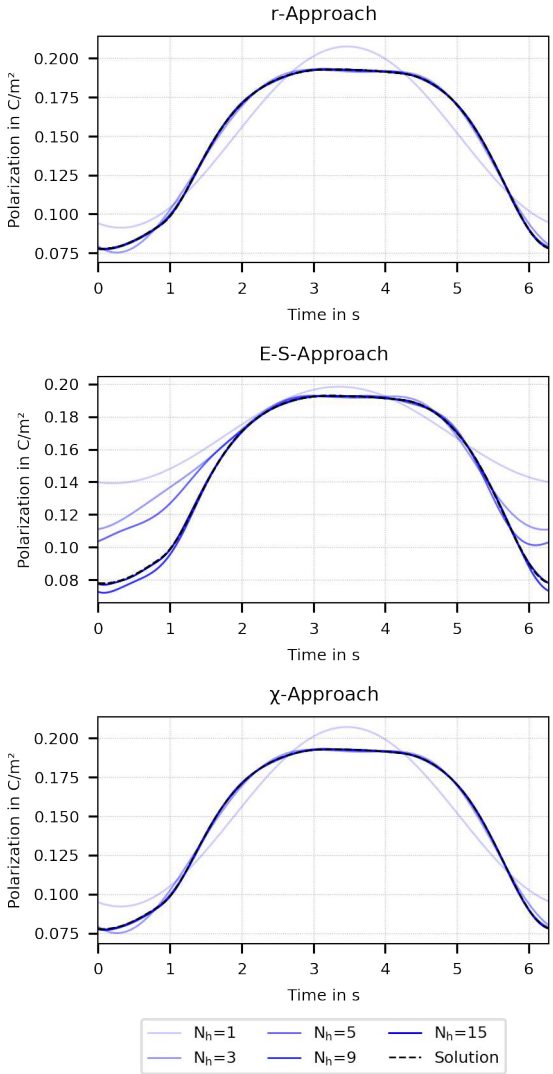

Figure 6.18: The polarization is displayed for different numbers of considered harmonics for Case 0 after 25 iterations. The polarization is from the case 0 shown in Fig. 6.12. The relative error for this case for various harmonics is displayed in Fig. 6.19 among other cases.

Discussion

The polarization is used to visualize the effect of different numbers of considered harmonics, because there the effects are distinguishable best. As one can see in Fig. 6.18 the more harmonics are used the better the result can be approximated. The *E-S* approach does not converge for every case as in previous sections mentioned. This can be seen in Fig. 6.19 too and the convergence/divergence is not dependent on the numbers of considered harmonics.

In Fig. 6.19 the influence of the different number of harmonics are visualized with respect to the performance and accuracy. More harmonics do increase the accuracy of the used approach in general. The relative error after 25 iterations is lower with a higher number of considered harmonics. This is expected, as Fourier series with more terms can

Die approbierte gedruckte Originalversion dieser Diplomarbeit ist an der TU Wien Bibliothek verfügbar.
The approved original version of this thesis is available in print at TU Wien Bibliothek.
TU Bibliothek WIEN Your knowledge hub

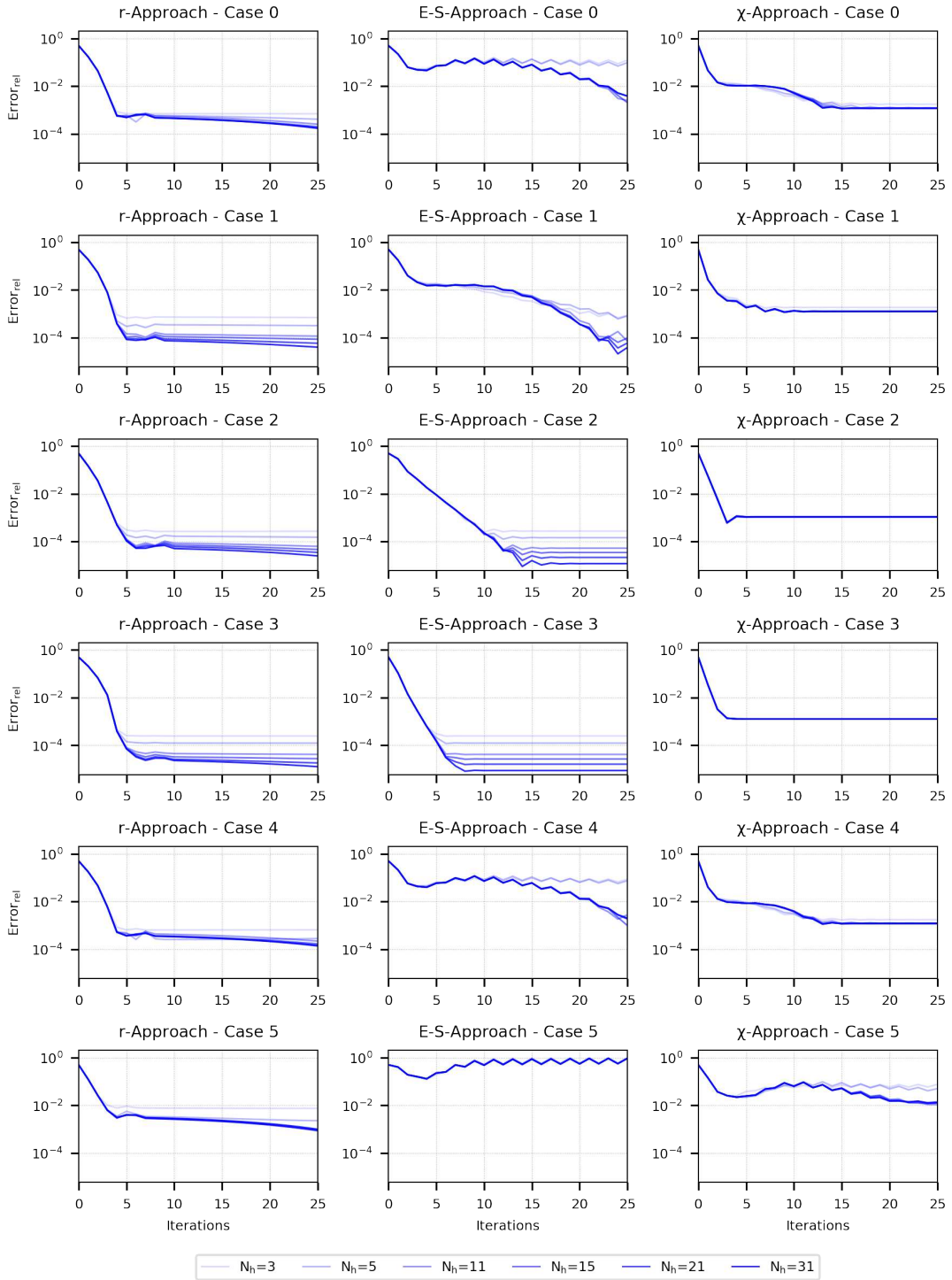

Figure 6.19: This figure shows the influence of the considered harmonics on the performance of the approaches. All three approaches are compared for five different cases. In the columns the results of r-approach, E-S-approach and the χ-approach are shown, respectively. In the rows the results of the different cases are displayed. All input- and output-quantities of these cases are displayed in Fig. 6.12 and appendix A.4.

Die approbierte gedruckte Originalversion dieser Diplomarbeit ist an der TU Wien Bibliothek verfügbar.
The approved original version of this thesis is available in print at TU Wien Bibliothek.
TU Bibliothek Your knowledge hub WIEN

approximate signals more accurately.

Another interesting point is that for the initial iteration steps the considered numbers of harmonics do not have a visible influence for the convergence of the approaches. The first significant deviations between the approaches occur around the fourth iteration step. This is important to know for implementing the approaches in a FE-software, because it allows to save computational effort. However the E-S approach and the χ-approach are easier to implement in a FE-software. The r-approach is the most accurate and stable approach, if all cases are taken into account.

Die approbierte gedruckte Originalversion dieser Diplomarbeit ist an der TU Wien Bibliothek verfügbar.
The approved original version of this thesis is available in print at TU Wien Bibliothek.
TU WIEN Bibliothek Your knowledge hub

Chapter 7

Summary

The goal of this thesis is to derive a one dimensional system of the nonlinear piezoelectric-mechanical coupled system, in order to provide a solution for the steady state. First, a short overview was given and the basics of piezoelectric ceramics were explained. Afterwards the used hysteresis models were presented. Furthermore the one dimensional system was derived from the linear three dimensional piezoelectric-mechanical system. To arrive at the nonlinear system, the linear system was extended with ferroelectric effects. The hysteresis model was solved in the time domain using a forward finite difference scheme. For solving the piezoelectric coupled system, three solution algorithms were presented (r-approach, E-S-approach and χ-approach).

All of the solution approaches were fix point iteration schemes, which evaluate the nonlinear parts in the time domain. The variables were then transformed into the frequency domain using the multiharmonic ansatz and with harmonic balancing the fix point schemes were derived. The fix point iteration was done in the frequency domain.

The physical behavior of the nonlinear system was presented and discussed on different loading cases. The solutions of the approaches were compared to each other. The E-S-approach did not converge in every case. In order to compare the convergence over the iteration steps the approaches were benchmarked. The r-approach converged very fast with the optimal chosen parameter but for finding this parameter a additional line search is needed. The E-S-approach had some difficulties for specific loading cases where the approach did not converge. In the initial steps the χ-approach converges faster, however after some iteration steps the r-approach overtakes. The r-approach was the most accurate and stable algorithm. The influence of the harmonics regarding the convergence was investigated. For the first iteration steps the numbers of considered harmonics did not have an impact. This is important because it allows to start the iteration with few harmonics. The numbers of considered harmonics only needs to be increased if better accuracy is required.

Die approbierte gedruckte Originalversion dieser Diplomarbeit ist an der TU Wien Bibliothek verfügbar.
The approved original version of this thesis is available in print at TU Wien Bibliothek.
TU WIEN Bibliothek Your knowledge hub

Bibliography

[1] USound GmbH. Mems speakers for a superior audio expericence. https://www.usound.com/, 2020. Online; accessed 2020-09-28.

[2] Stefan Johann Rupitsch. *Piezoelectric Sensors and Actuators*. Springer, 2019.

[3] Jan Tichý, Jiří Erhart, Erwin Kittinger, and Jana Přívratská. *Fundamentals of Piezoelectric Sensorics*. Springer, 2010.

[4] Vahid Hassani, Tegoeh Tjahjowidodo, and Thanh Nho Do. A survey on hysteresis modeling, identification and control. *Mechanical Systems and Signal Processing*, 49:209–233, 2014.

[5] Phuang-Bac Nguyen, Seung-Bok Choi, and Byung-Keun Song. A new approach to hysteresis modelling for a piezoelectric actuator using preisach model and recursive method with an application to open-loop position tracking control. *Sensors and Actuators A: Physical*, 270:136–152, 2018.

[6] E. Preisach. Über die magnetische nachwirkung. *Zeitschrift für Physik*, 1935.

[7] Frederik Stefanski, Bartosz Minorowics, Johan Persson, Andrew Plummer, and Chris Bowen. Non-linear control of a hydraulic piezo-valve using a generalised prandtl–ishlinskii hysteresis model. *Mechanical Systems and Signal Processing*, 82:412–431, 2017.

[8] J.P. Lien, Alexander York, Tiegang Fang, and Gregory D. Bruckner. Modeling piezoelectric actuators with hysteretic recurrent neural networks. *Sensors and Actuators A: Physical*, 163/2:516–525, 2010.

[9] F. Liorzou, D. Phelps, and D. L. Atherton. Macroscopic models of magnetization. *IEEE TRANSACTIONS ON MAGNETICS*, 36/2:418–428, 2000.

[10] Ralph C. Smith and Zoubeida Ounaies. A domain wall model for hysteresis in piezoelectric materials. *ICASE Report No.99-52*, 1999.

[11] D.C. Jiles and D.L. Atherton. Theory of ferromagnetic hysteresis. *Journal of Magnetism and Magnetic Materials*, 61(1):48 – 60, 1986.

Die approbierte gedruckte Originalversion dieser Diplomarbeit ist an der TU Wien Bibliothek verfügbar.
The approved original version of this thesis is available in print at TU Wien Bibliothek.
TU WIEN Bibliothek Your knowledge hub

[12] Ralph C. Smith, Andrew G. Hatch, Binu Makuherjee, and Shifang Liu. A homogenized energy model for hysteresis in ferroelectric materials: General density formulation. *Journal of Intelligen Material Systems and Structures*, 16:713–732, 2005.

[13] Cfs++ website. https://cfs-doc.mdmt.tuwien.ac.at/, 2020. Online; accessed 2020-09-28.

[14] Manfred Kaltenbacher. *Numerical Simulation of Mechatronic Sensors and Actuators*. Springer, 2015.

[15] M. Kamlah. Ferroelectric and ferrelastic piezoceramics - modeling of electromechanical hysteresis phenomena. *Continuum Mech. Thermodyn.*, 13, 2001.

[16] Michel W. Barsoum. *Fundamentals of Ceramics*. CRC Press, 2020.

[17] C. Lynch et Al. Crack growth in ferroelectric ceramics driven by cyclic polarization switching. *Journal of Intelligent Material Systems and Structures*, 1995.

[18] Methee Promsawat, Marco Deluca, Sirirat Kampoosiri, Boonruang Marungsri, and Soodkhet Pojprapai. Electrical fatigue behavior of lead zirconate titanate ceramic underelevated temperatures. *Journal of the European Ceramic Society*, 37:2047–2055, 2016.

[19] Alexander York. Experimental investigation of rate-dependent inner hysteresis loops in pzt. Master's thesis, North Carolina State University, 2005.

[20] Yao Yu, Xu-Sheng Wand, Yan-Xia Li, , and Xi Yao. Fatigue behaviors in pzt ceramics induced by mechanical cyclic load. *Ferroelectrics Letters Section*, 41:4-6:123–128, 2014.

[21] Jose M. Calderon-Morenoa and Monica Popa. Stress dependence of reversible and irreversible domain switching in pzt during cyclic loading. *Materials Science and Engineering*, 336:1-2:124–128, 2002.

[22] Mitsuhiro Okayasu, Eriko Sugiyama, and Mamoru Mizuno. In situ measurement of material properties of lead zirconate titanate piezoelectric ceramics during cyclic mechanical loading. *Journal of the European Ceramic Society*, 30:1445–1452, 2009.

[23] S. C. Hwang, C. S. Lynch, and R.M. McMeeking. Ferroelectric/feroelastic interations and a polarization switching model. *Acta metall. mater*, 43/5:2073–2084, 1994.

[24] C.S. Lynch. The effect of uniaxial stress on the electro-mechanical responst of 8/65/35 plzt. *Acta mater*, 44/10:4137–4148, 1996.

Die approbierte gedruckte Originalversion dieser Diplomarbeit ist an der TU Wien Bibliothek verfügbar.
The approved original version of this thesis is available in print at TU Wien Bibliothek.
TU Bibliothek Your knowledge hub WIEN

[25] Ralph C. Smith and Jordan E. Massad. Ferroelectric, ferromagnetic and ferroelastic materials, 2001.

[26] Malte Krack and Johann Gross. *Harmonic Balance for Nonlinear Vibration Problems.* Springer, 2019.

[27] Junwei Lu, Ciaojun Zhao, and Sotoshi Yamada. *Harmonic Balance Finite Element Method.* Wiley, 2016.

[28] Suáres Almudena. *Analysis and design of autonomous microwave circuits.* Wiley, 2015.

[29] A. Bruce Carlson and Paul B. Crilly. *Communication Systems: An Introduction to Signals and Noise in electrical Communication.* McGraw Hill, 2010.

Die approbierte gedruckte Originalversion dieser Diplomarbeit ist an der TU Wien Bibliothek verfügbar.
The approved original version of this thesis is available in print at TU Wien Bibliothek.
TU Bibliothek Your knowledge hub WIEN

Die approbierte gedruckte Originalversion dieser Diplomarbeit ist an der TU Wien Bibliothek verfügbar.
The approved original version of this thesis is available in print at TU Wien Bibliothek.

List of Figures

2.1 Spontaneous polarization 4
2.2 Electronic polarization 5
2.3 Ionic polarization 6
2.4 Probability of dipolar polarization 6
2.5 Dipolar polarization 7
2.6 Polarization direction of a unit cell 8
2.7 Unit cell under mechanical stress 8
2.8 Electric loading cycles: First experiment 9
2.9 Electric loading cycle: Schematic hysteresis 10
2.10 Electric loading cycle: Schematic butterfly loop 11
2.11 Minor loops 12
2.12 Mechanic loading cycle: Schematic hysteresis 12
2.13 Mechanical loading cycle: Polarized material 1 13
2.14 Mechanic loading cycle: Polarized material 2 13
2.15 Mixed loading cycles: Polarization hysteresis 14
2.16 Mixed loading cycles: Butterfly loop 15

4.1 Applied boundary conditions for one dimensional case 25

5.1 Harmonic balance 34
5.2 Flowchart of algorithm 1 39
5.3 Flowchart of algorithm 2 43
5.4 Flowchart of algorithm 3 46

6.1 Bipolar polarization hysteresis 48
6.2 Increasing bipolar polarization hysteresis 49
6.3 Increasing unipolar polarization hysteresis 50
6.4 Mechanical hysteresis: In blue the bipolar loading cycle is visualized and in green a unipolar loading cycle is plotted. 51
6.5 Approach 1: General case 53
6.6 Approach 1: Bipolar case 55
6.7 Approach 1: Unipolar case 56

Die approbierte gedruckte Originalversion dieser Diplomarbeit ist an der TU Wien Bibliothek verfügbar.
The approved original version of this thesis is available in print at TU Wien Bibliothek.
TU WIEN Bibliothek Your knowledge hub

6.8 Comparison of bipolar and unipolar loading cycles 57
6.9 Approach 1: Constant charge excitation 58
6.10 Approach 1: Constant charge excitation - reversible strain 59
6.11 Butterfly loop for different piezoelectric modulus 61
6.12 Comparison: Unipolar general case 63
6.13 Comparison of case 5 64
6.14 Error of unipolar case with positive stress 65
6.15 Error of unipolar case with negative stress 66
6.16 Error of unipolar case with negative stress and dielectric displacement field offset 66
6.17 Error of case 5: The E-S approach do not converge. 67
6.18 Polarization displayed with different numbers of harmonics 68
6.19 Influence of harmonics on performance 69

A.1 Approach 1: Bipolar case - all output quantities XIII
A.2 Approach 1: Unipolar case - all output quantities XIV
A.3 Approach 1: Constant charge excitation - all output quantities XV
A.4 Approach 1: Different numbers of considered harmonics XVI
A.5 Approach 2: Unipolar general case XVII
A.6 Approach 2: Unipolar case XVIII
A.7 Approach 2: Constant charge excitation XIX
A.8 Approach 3: Unipolar general case XX
A.9 Approach 3: Unipolar case XXI
A.10 Approach 3: Constant charge excitation XXII
A.11 Comparison- reference case XXIII
A.12 Comparison - unipolar with negative stress XXIV
A.13 Comparison - unipolar with positive stress XXV
A.14 Comparison - unipolar with positive stress (higher dielectric displacement field) XXVI
A.15 Comparison - unipolar with variable negativ stress XXVII

Die approbierte gedruckte Originalversion dieser Diplomarbeit ist an der TU Wien Bibliothek verfügbar.
The approved original version of this thesis is available in print at TU Wien Bibliothek.
TU Bibliothek WIEN Your knowledge hub

Appendix A

Appendix

A.1 Parameters for simulation

Die approbierte gedruckte Originalversion dieser Diplomarbeit ist an der TU Wien Bibliothek verfügbar.
The approved original version of this thesis is available in print at TU Wien Bibliothek.

Ferroelectric and mixed case		
Parameter	**Value**	**Descripiton**
α in Vm/C	$2e^7$	
a in C/m^2	$3.9e^6$	
k in C/m^2	$4.1e^6$	Parameters for JA-Model
c	0.25	
P_s in C/m^2	0.24	
β_1	0	
β_2	1	Parameters for irreversible Strain
β_3	0	
β_4	0	
η	$1e^7$	Update control for E
N_t	2^{10}	Number of time steps per period
N_p	3	Number of periods
N_h	15*	Number of considered harmonics
ϵ_0 in As/Vm	1500	Permittivity of vacuum
ϵ_r	$8.854e^{-12}$	Relative permittivity for material
e_{33} in C/m^2	23	constant piezomoduli in 33-direction
Definition of coupled piezeelectric modulus		
$e(P) = \frac{P(t)}{P_s} e_{33}$		for section 6.3
$e(P) = \frac{P(t)}{8P_s} e_{33} + \frac{7}{8} e_{33}$		for section 6.4

Table A.1: Parameters for the ferroelectric and mixed model.

Ferroelastic case		
Parameter	**Value**	**Description**
α' in N/m^2	$-2.5414e^3$	
α_1 in N/Km^2	$2.0810e^4$	
α_2 in N/m^2	$9.5445e^6$	
α_3 in N/m^2	$1.8630e^9$	Parameters for ferroelastic hysteresis
k'	-2.8356	
c'	0.1	

Table A.2: Parameters for the ferroelastic hysteresis.

Die approbierte gedruckte Originalversion dieser Diplomarbeit ist an der TU Wien Bibliothek verfügbar.
The approved original version of this thesis is available in print at TU Wien Bibliothek.
TU Bibliothek Your knowledge hub WIEN

A.2 Addition physical behavior plots

A.2.1 Physical behavior of the r-approach

Bipolar charge excitation

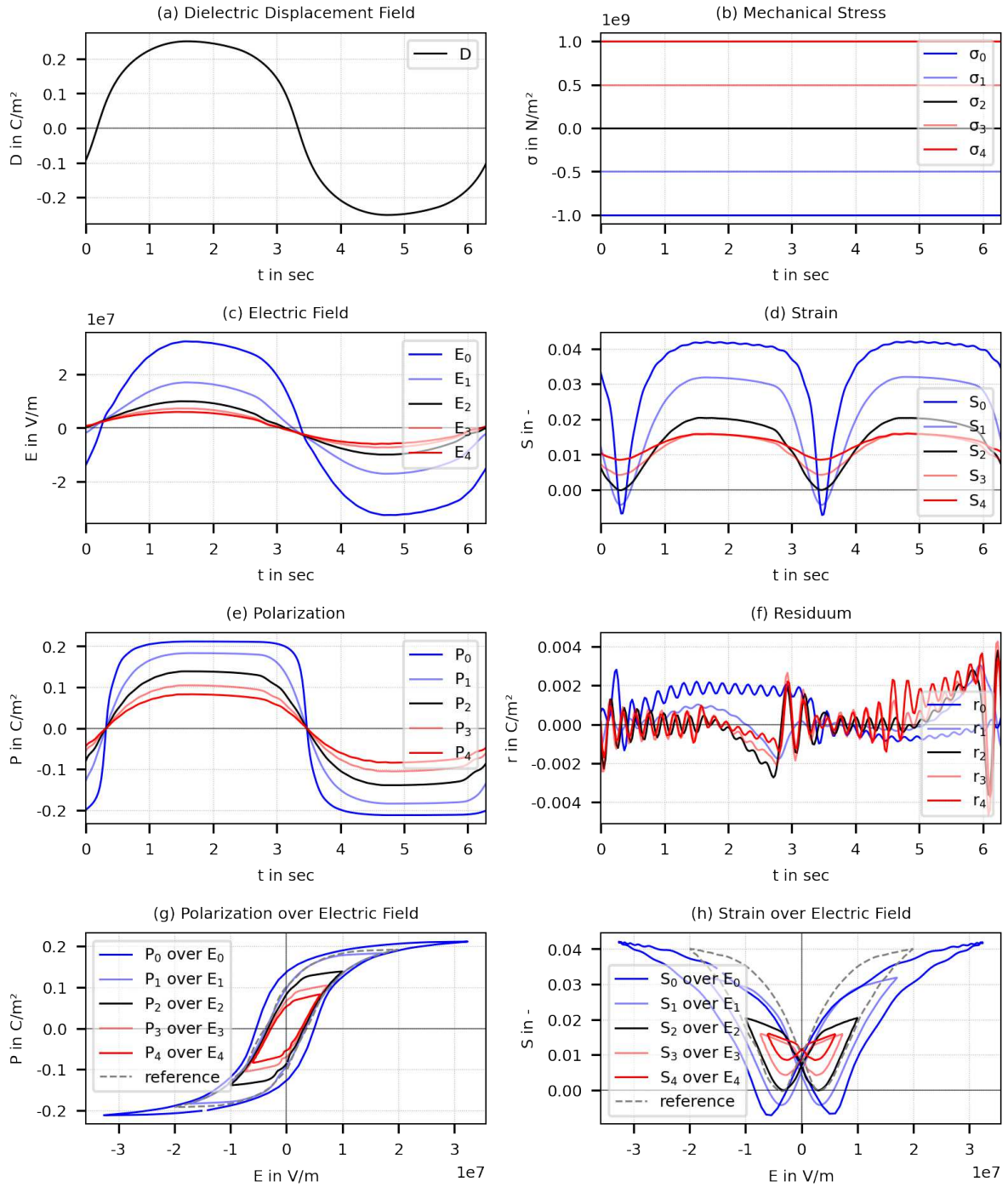

Figure A.1: Bipolar charge excitation with different constant mechanic stresses: All input and output quantities

Die approbierte gedruckte Originalversion dieser Diplomarbeit ist an der TU Wien Bibliothek verfügbar.
The approved original version of this thesis is available in print at TU Wien Bibliothek.

Unipolar charge excitation

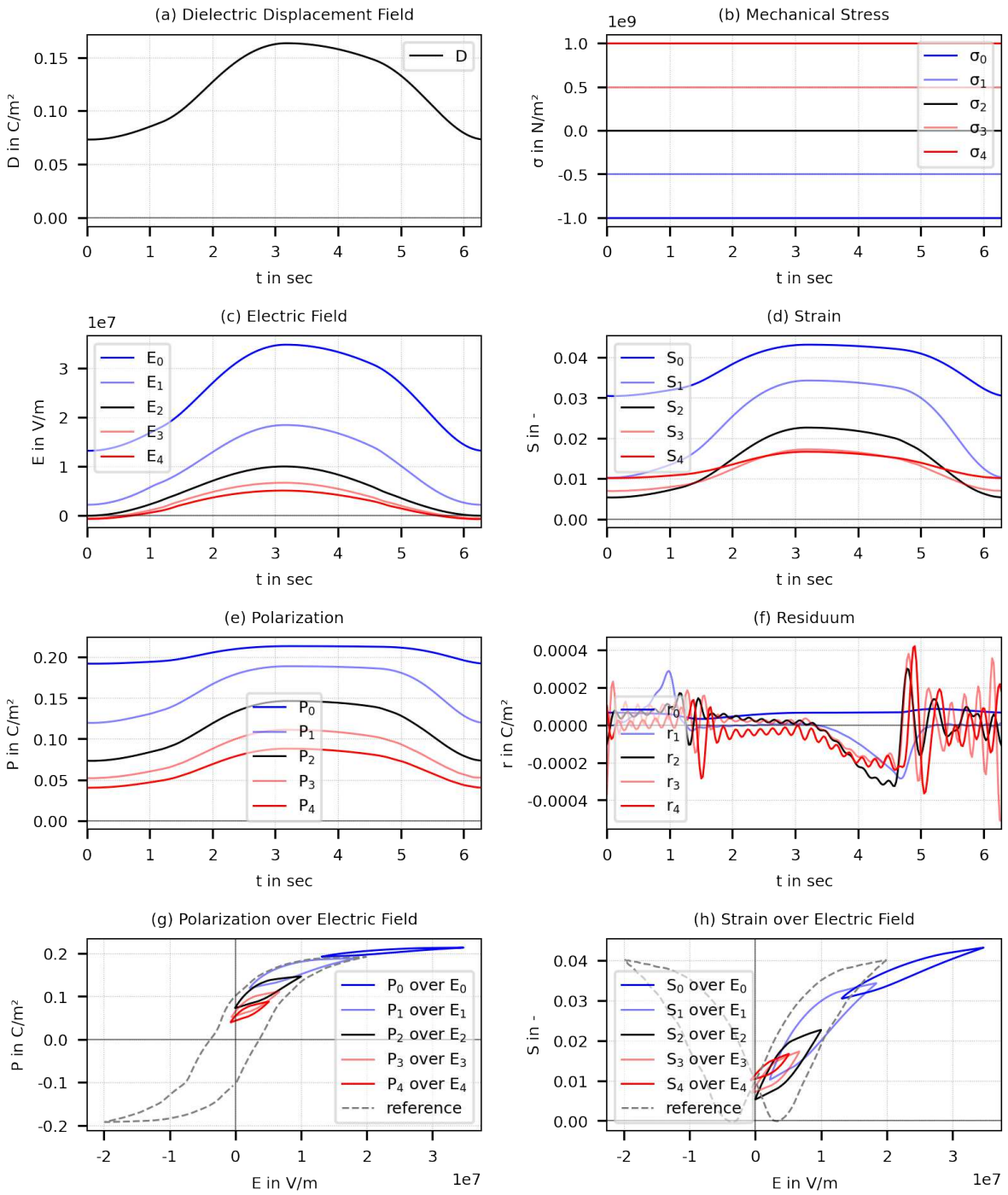

Figure A.2: Unipolar charge excitation with different constant mechanic stresses: All input and output quantities

Die approbierte gedruckte Originalversion dieser Diplomarbeit ist an der TU Wien Bibliothek verfügbar.
The approved original version of this thesis is available in print at TU Wien Bibliothek.
TU Bibliothek Your knowledge hub WIEN

Constant charge excitation

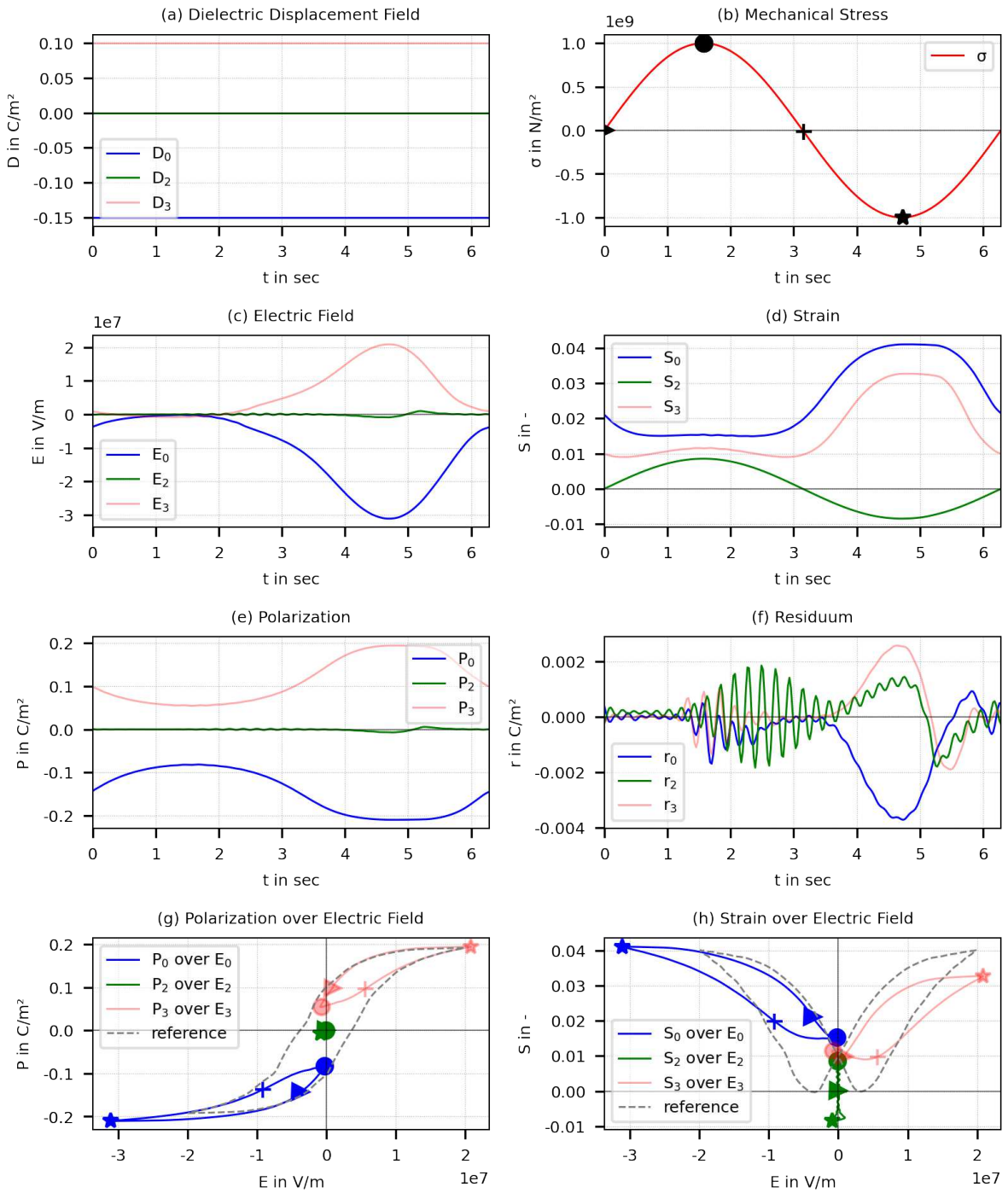

Figure A.3: All input and output quantities for various constant charge excitation under sinus-like mechanic stress excitation. Triangle marks the start of the hysteresis. The circle and star indicating the maxim or minimum of the mechanic stress respectively. The plus marks the zero crossing of the mechanic stress.

Die approbierte gedruckte Originalversion dieser Diplomarbeit ist an der TU Wien Bibliothek verfügbar.
The approved original version of this thesis is available in print at TU Wien Bibliothek.

Multiharmonic ansatz

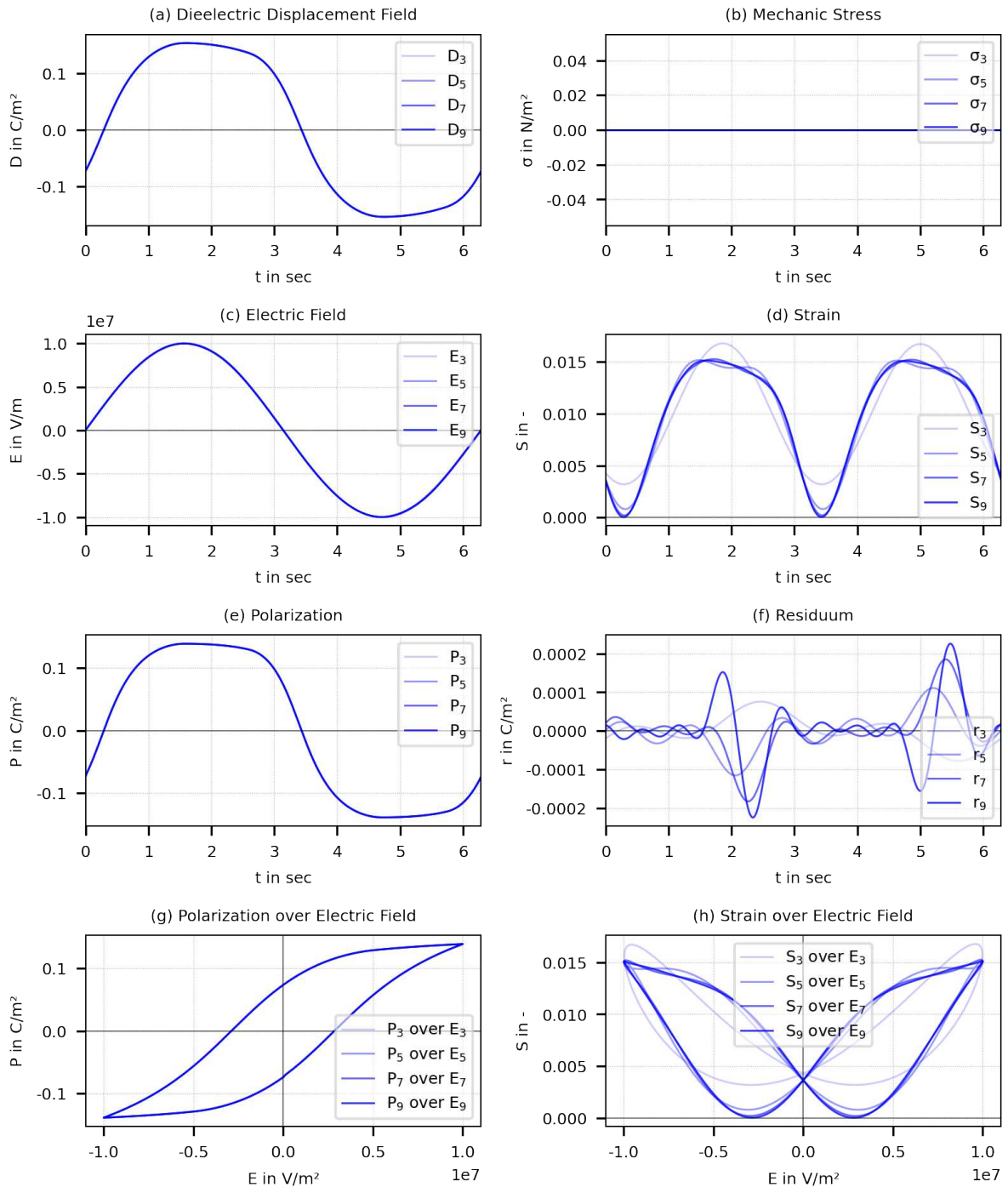

Figure A.4: System solved with different harmonics

Die approbierte gedruckte Originalversion dieser Diplomarbeit ist an der TU Wien Bibliothek verfügbar.
The approved original version of this thesis is available in print at TU Wien Bibliothek.

A.2.2 Physical behavior of the E-S-approach

Unipolar general behavior

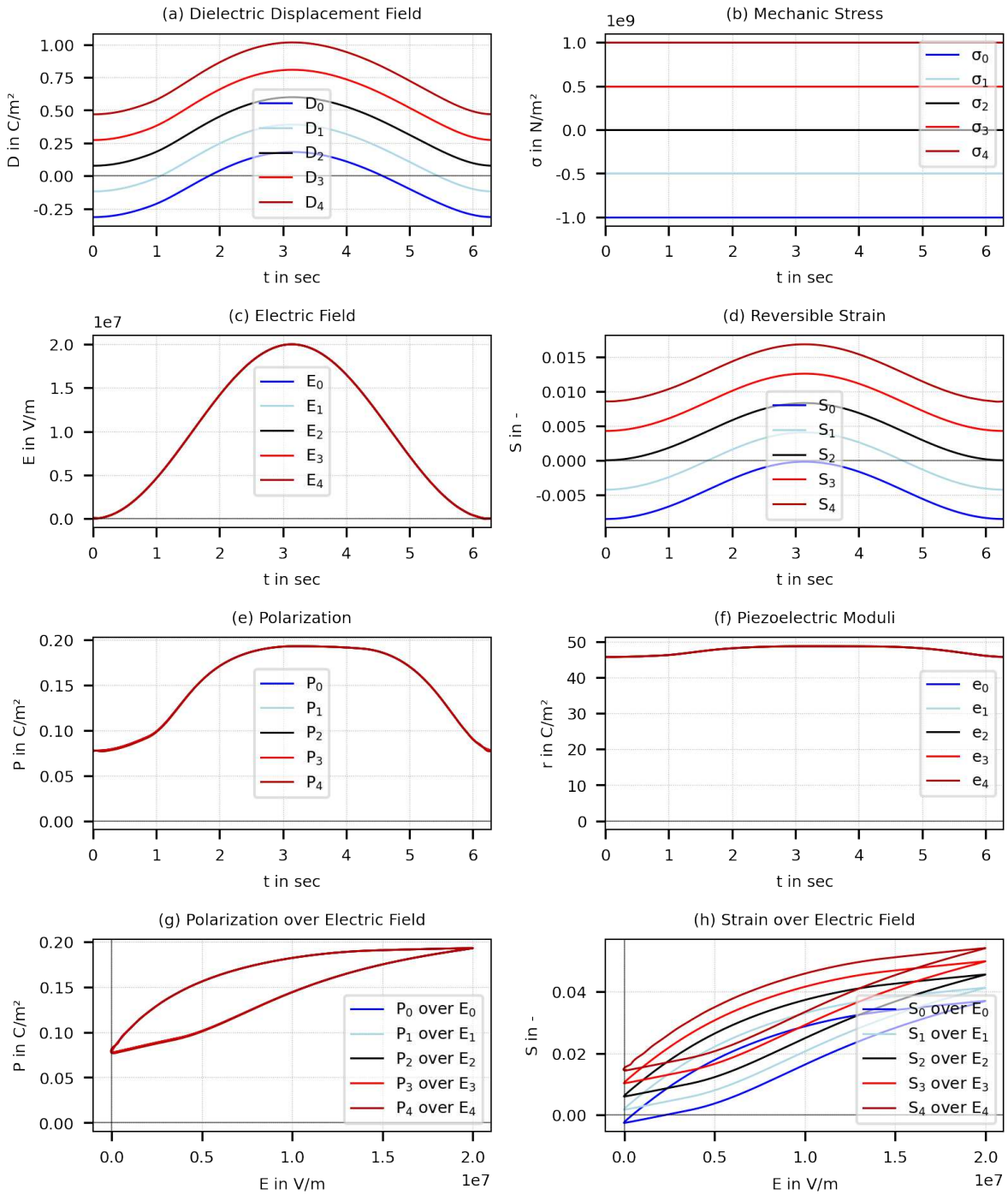

Figure A.5: All input and output quantities for the unipolar general case of the second model.

Die approbierte gedruckte Originalversion dieser Diplomarbeit ist an der TU Wien Bibliothek verfügbar.
The approved original version of this thesis is available in print at TU Wien Bibliothek.

Unipolar charge excitation

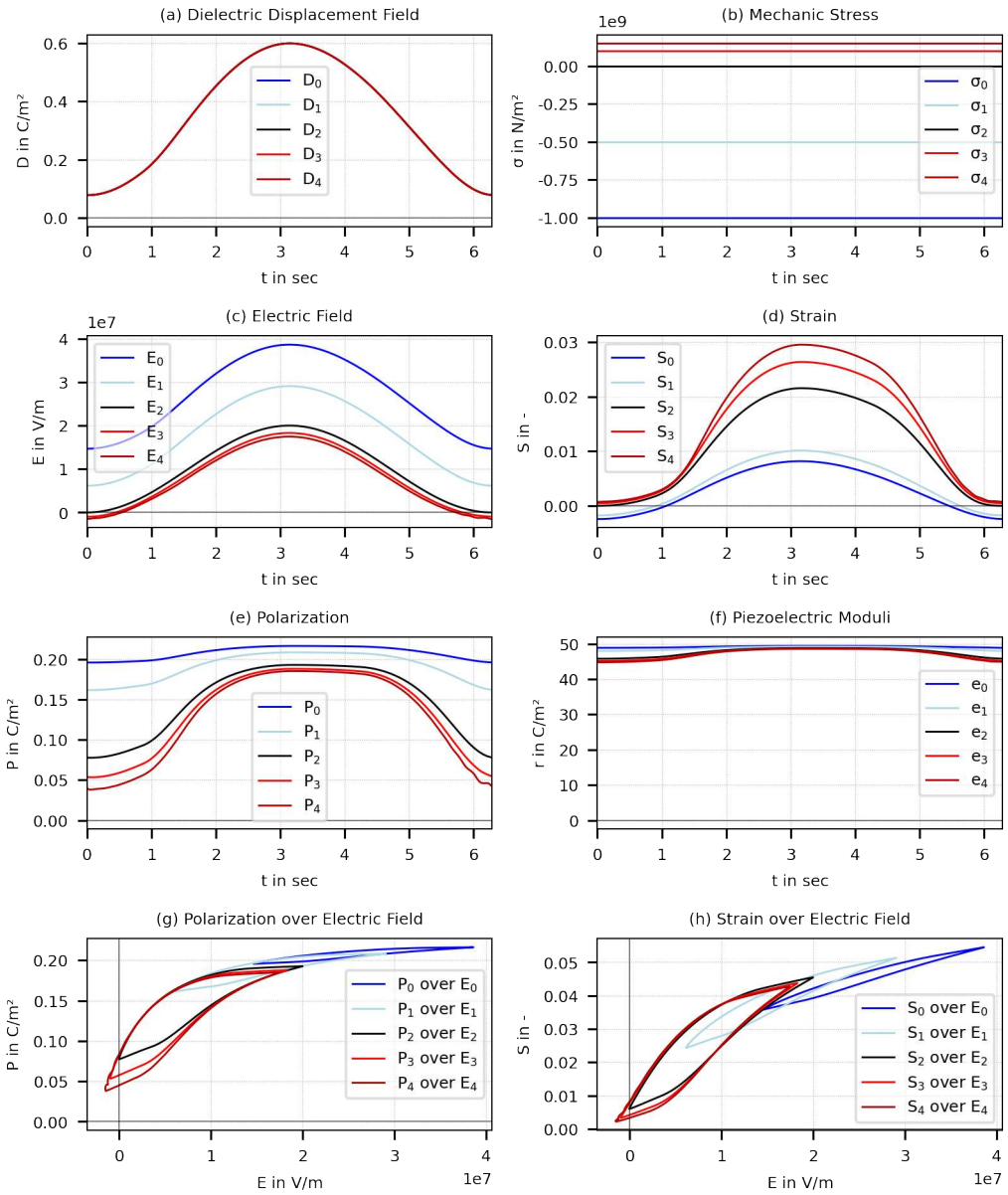

Figure A.6: All input and output quantities for the unipolar charge excitation of the second model.

Die approbierte gedruckte Originalversion dieser Diplomarbeit ist an der TU Wien Bibliothek verfügbar.
The approved original version of this thesis is available in print at TU Wien Bibliothek.
TU Bibliothek Your knowledge hub WIEN

Constant charge excitation

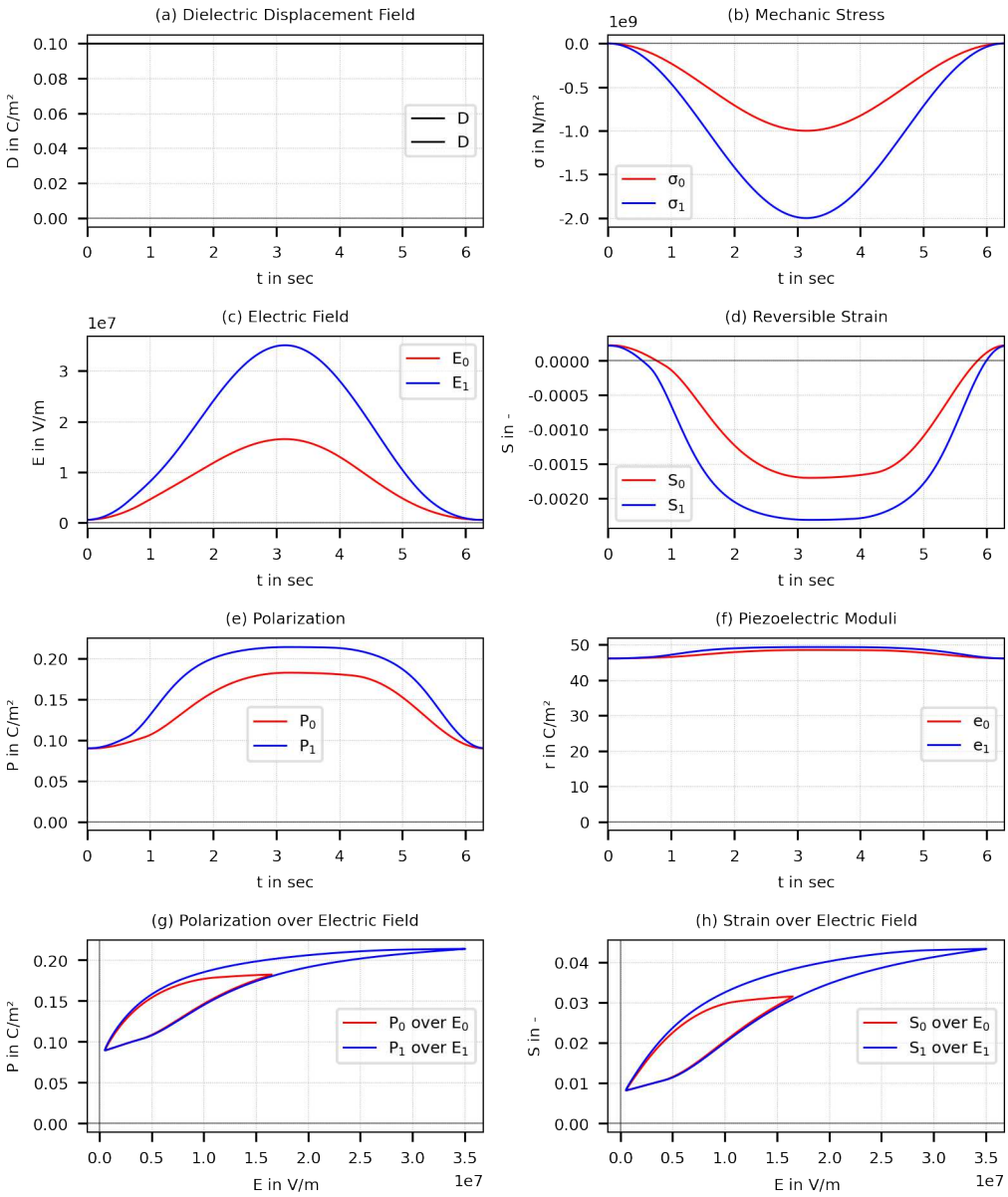

Figure A.7: All input and output quantities for the constant charge excitation of the second model.

Die approbierte gedruckte Originalversion dieser Diplomarbeit ist an der TU Wien Bibliothek verfügbar.
The approved original version of this thesis is available in print at TU Wien Bibliothek.

A.2.3 Physical behavior of the χ-approach

Unipolar general behavior

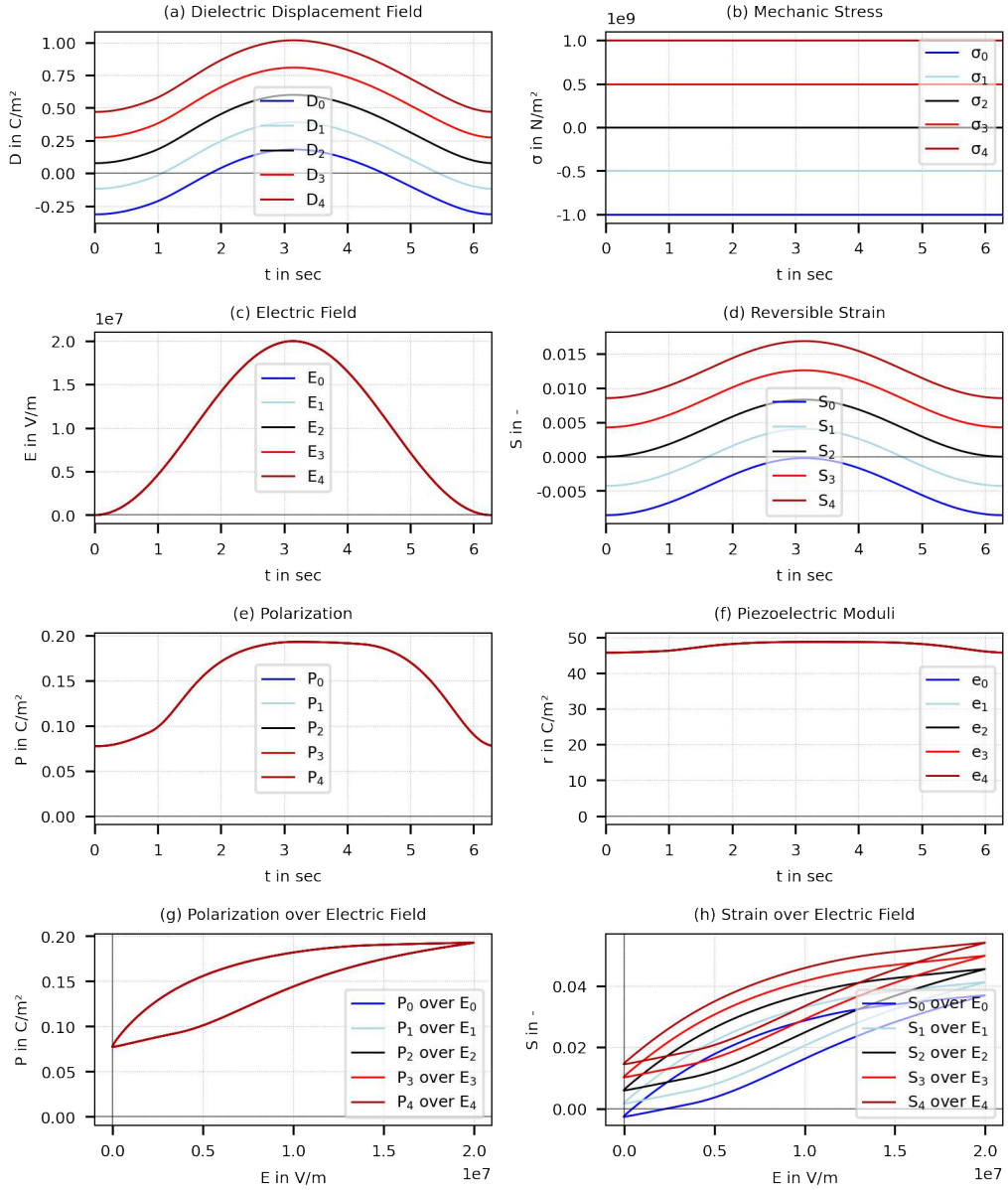

Figure A.8: All input and output quantities for the unipolar general case of the third model.

Die approbierte gedruckte Originalversion dieser Diplomarbeit ist an der TU Wien Bibliothek verfügbar.
The approved original version of this thesis is available in print at TU Wien Bibliothek.
TU Bibliothek Your knowledge hub WIEN

Unipolar charge excitation

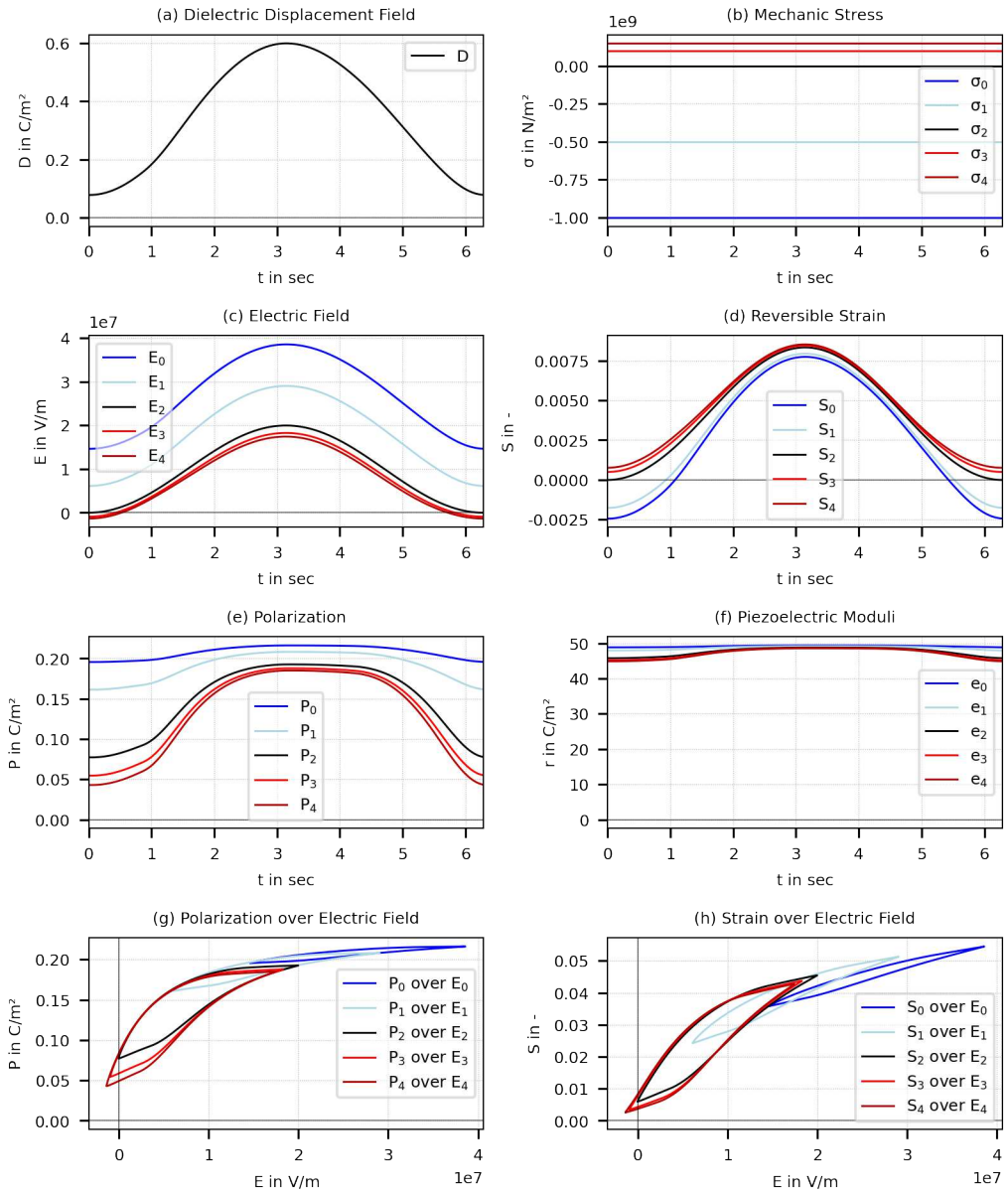

Figure A.9: All input and output quantities for the unipolar charge excitation of the third model.

Die approbierte gedruckte Originalversion dieser Diplomarbeit ist an der TU Wien Bibliothek verfügbar.
The approved original version of this thesis is available in print at TU Wien Bibliothek.
TU Bibliothek WIEN Your knowledge hub

Constant charge excitation

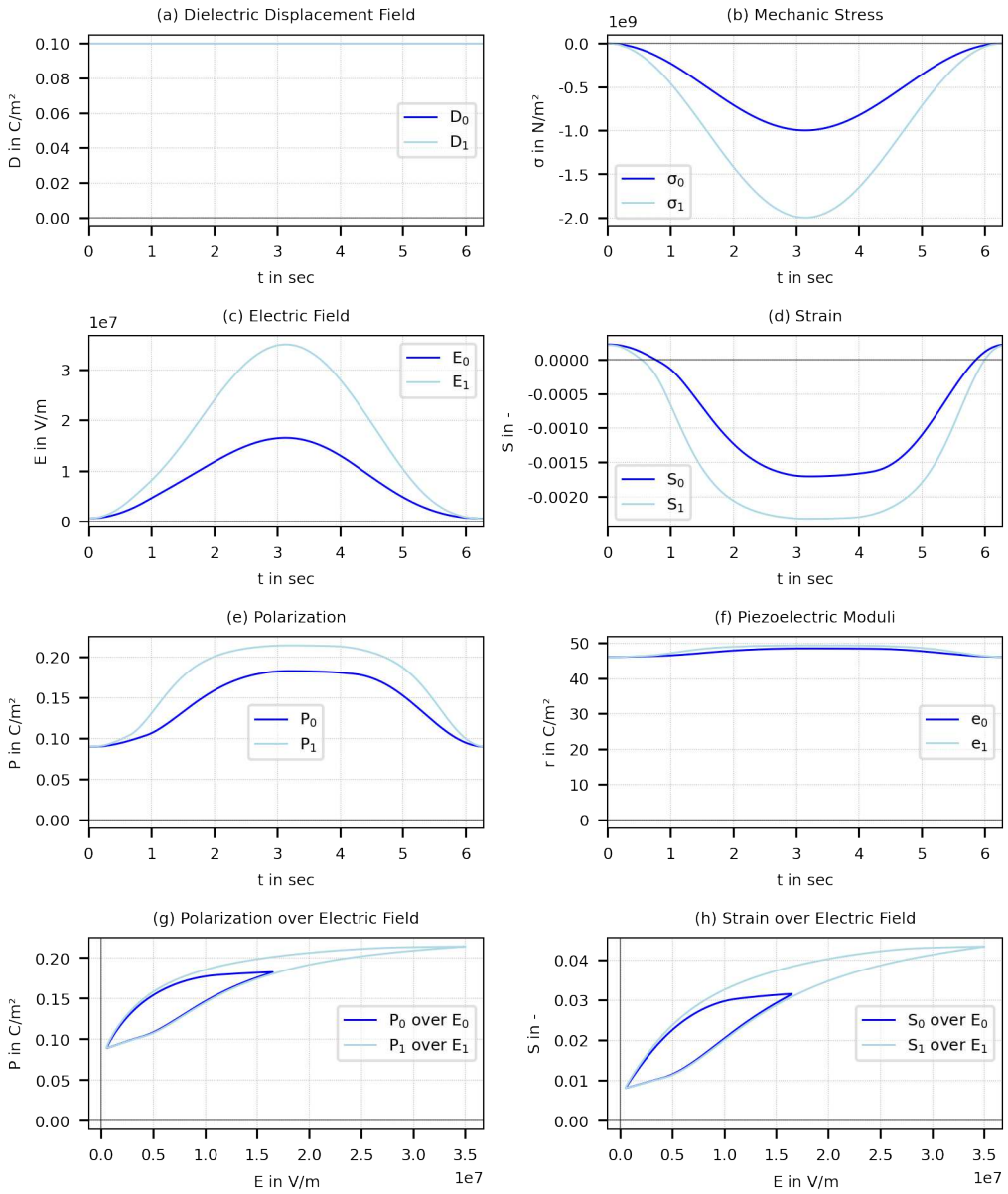

Figure A.10: All input and output quantities for the constant charge excitation of the third model.

Die approbierte gedruckte Originalversion dieser Diplomarbeit ist an der TU Wien Bibliothek verfügbar.
The approved original version of this thesis is available in print at TU Wien Bibliothek.

A.3 Reference case

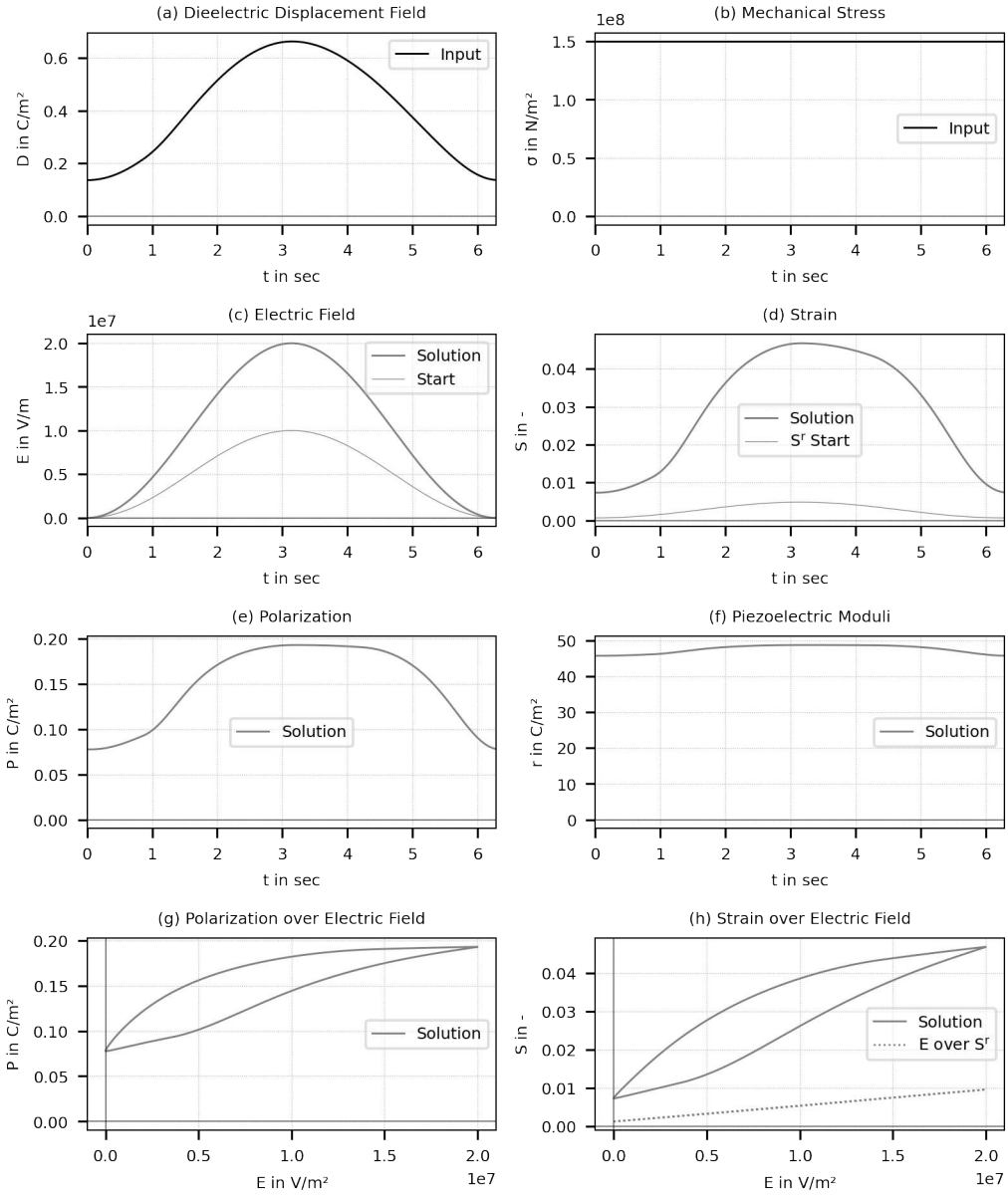

Figure A.11: Reference case evaluated in the time domain. In (c) and (d) the initial starting values are displayed in thin lines. The butterfly loop is displayed for the strain in (h) where the reversible butterfly loop is visualized with dashed line.

Die approbierte gedruckte Originalversion dieser Diplomarbeit ist an der TU Wien Bibliothek verfügbar.
The approved original version of this thesis is available in print at TU Wien Bibliothek.

A.4 Comparison for various cases

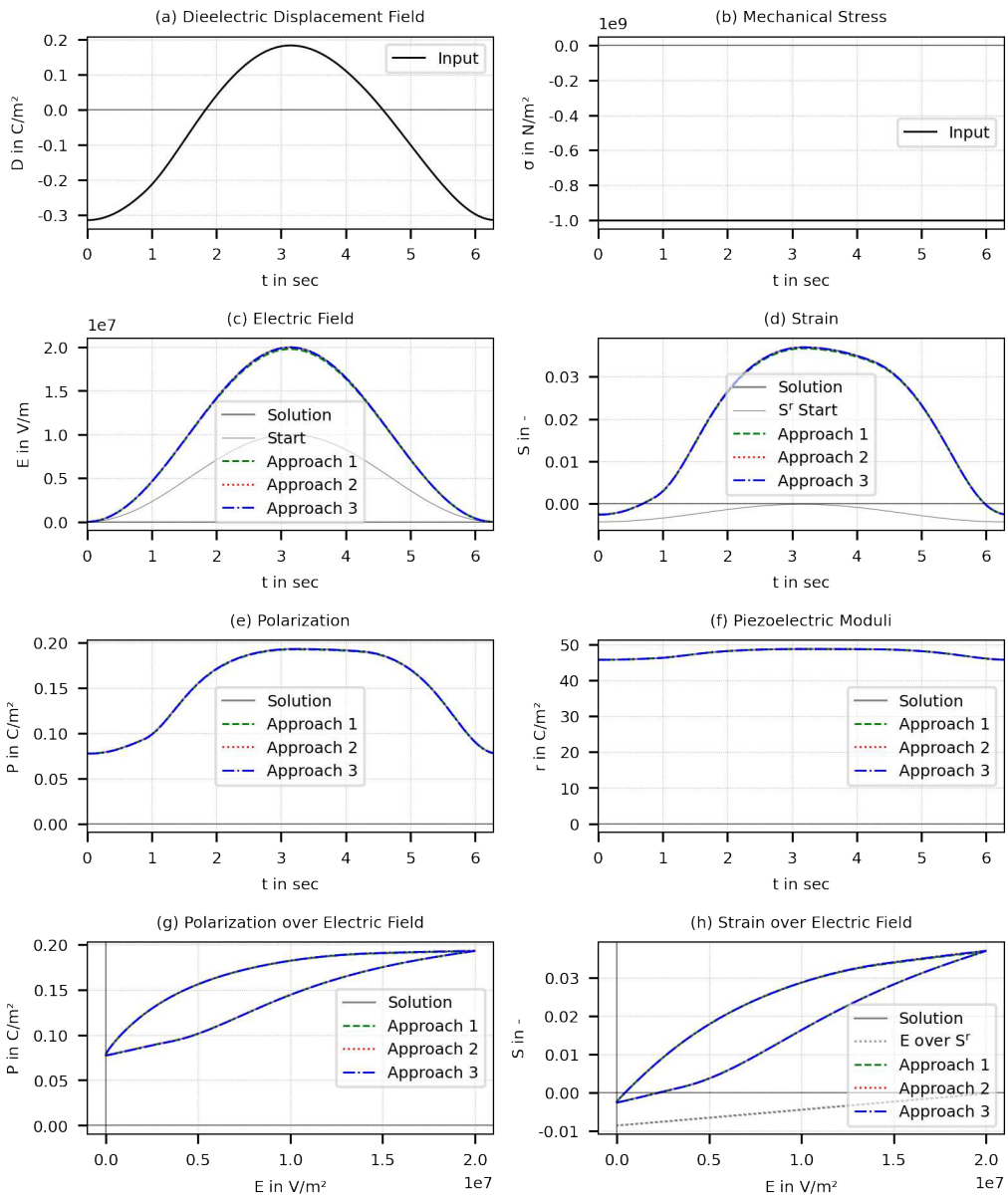

Figure A.12: Case 1: Comparison of all three approaches after 25 iterations. All three approaches converging to the same result and only minor deviations are visible.

Die approbierte gedruckte Originalversion dieser Diplomarbeit ist an der TU Wien Bibliothek verfügbar.
The approved original version of this thesis is available in print at TU Wien Bibliothek.
TU Bibliothek Your knowledge hub WIEN

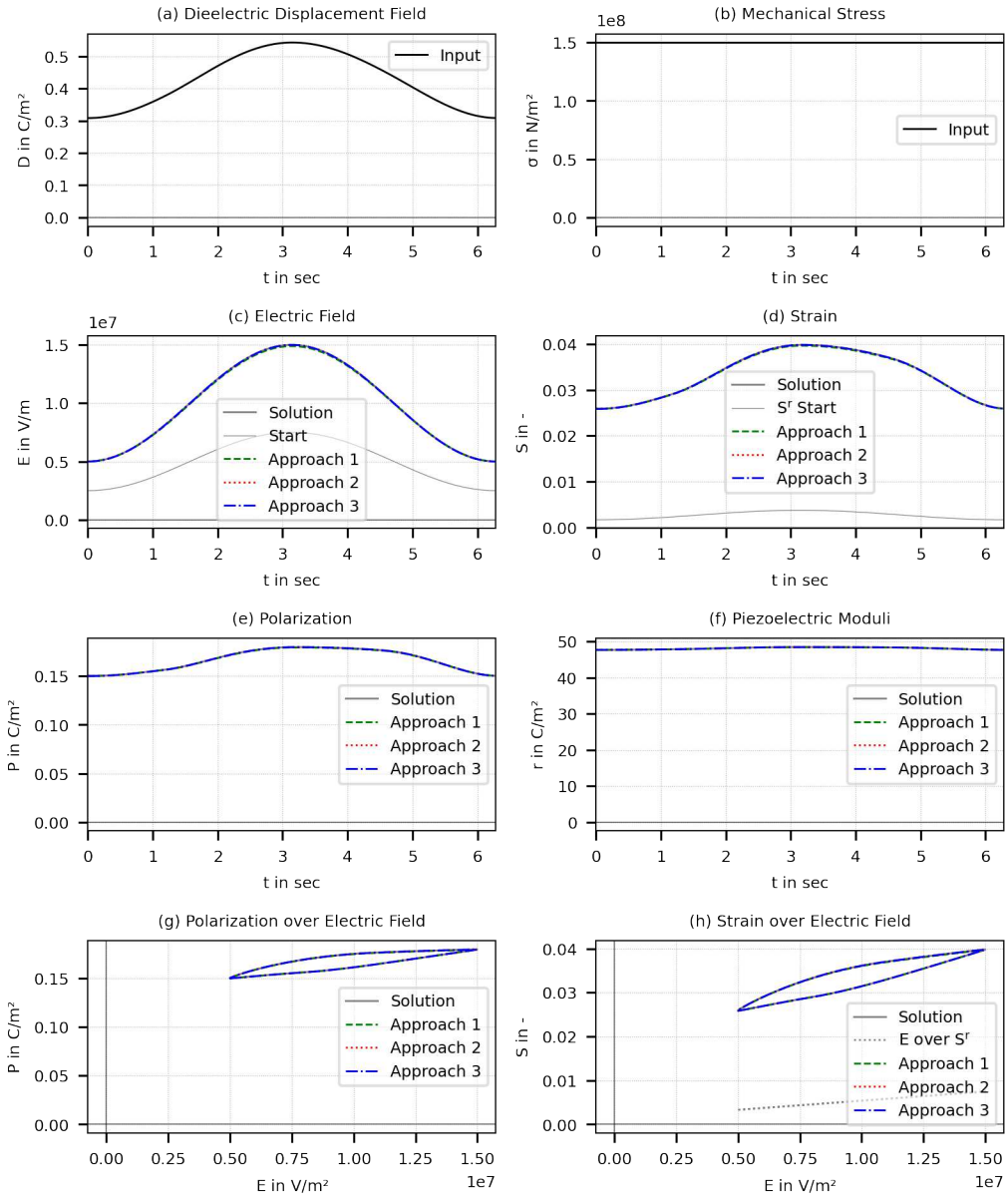

Figure A.13: Case 2: Comparison of all three approaches after 25 iterations. All three approaches converging to the same result and only minor deviations are visible.

Die approbierte gedruckte Originalversion dieser Diplomarbeit ist an der TU Wien Bibliothek verfügbar.
The approved original version of this thesis is available in print at TU Wien Bibliothek.

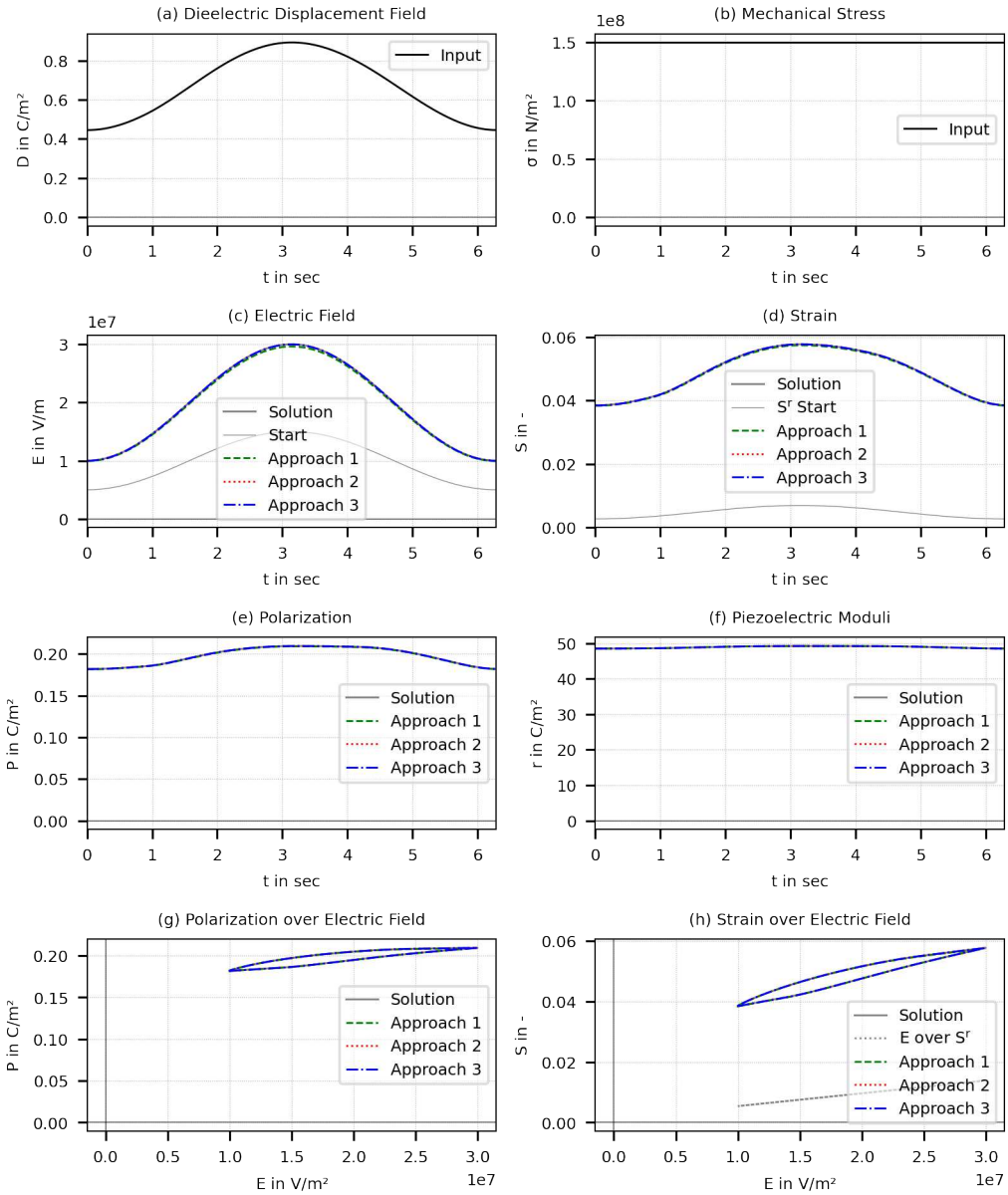

Figure A.14: Case 3: Comparison of all three approaches after 25 iterations. All three approaches converging to the same result and only minor deviations are visible.

Die approbierte gedruckte Originalversion dieser Diplomarbeit ist an der TU Wien Bibliothek verfügbar.
The approved original version of this thesis is available in print at TU Wien Bibliothek.

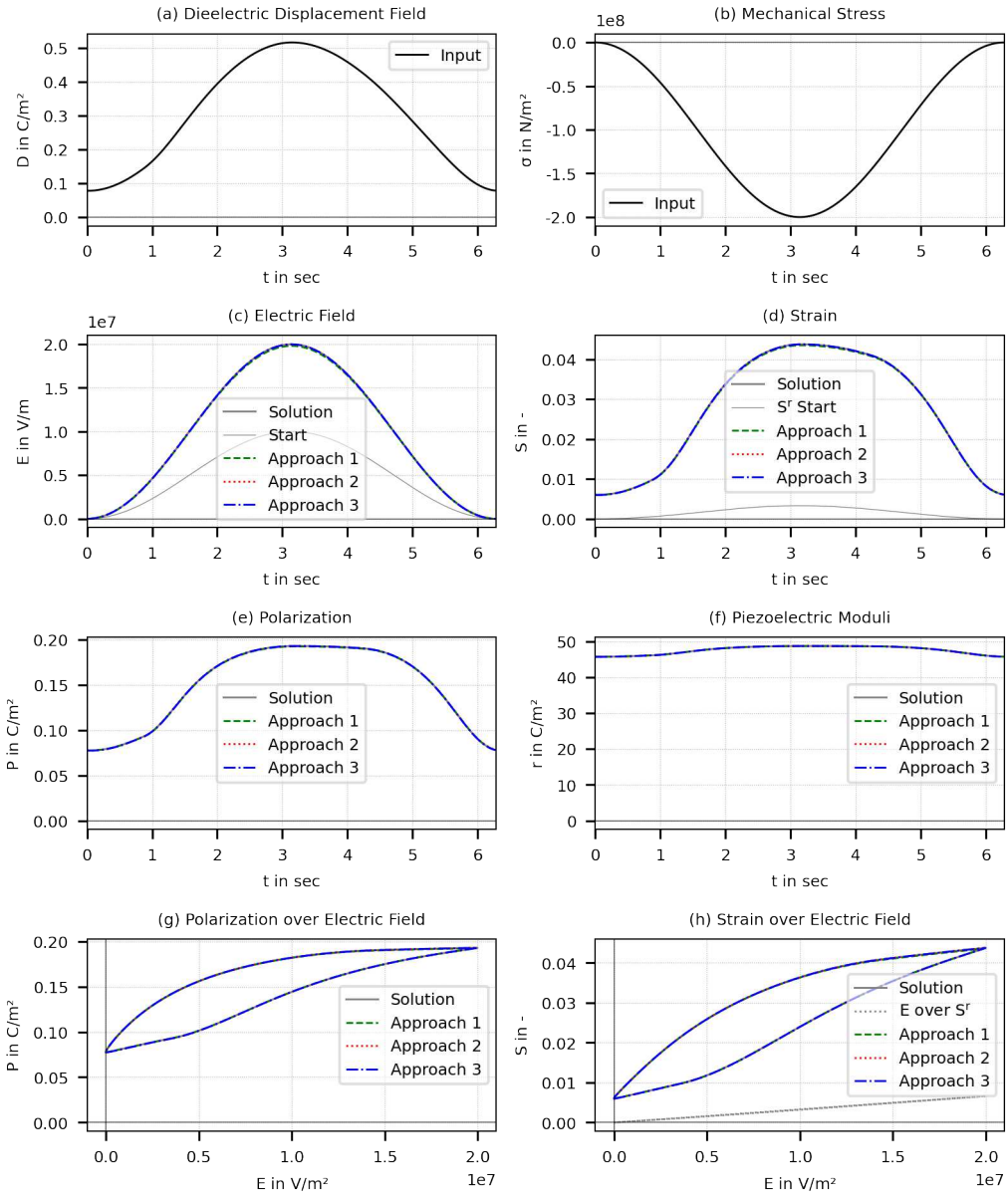

Figure A.15: Case 4: Comparison of all three approaches after 25 iterations. All three approaches converging to the same result and only minor deviations are visible.

Die approbierte gedruckte Originalversion dieser Diplomarbeit ist an der TU Wien Bibliothek verfügbar.
The approved original version of this thesis is available in print at TU Wien Bibliothek.